2009-12-15

Passive Earth Pressures on a Pile Cap with a Dense Sand Backfill

Robert Ashall Marsh
Brigham Young University - Provo

Passive Earth Pressures on a Pile Cap

with a Dense Sand Backfill

Robert A. Marsh Jr.

A thesis submitted to the faculty of
Brigham Young University
in partial fulfillment of the requirements for the degree of

Master of Science

Travis M. Gerber, Chair
Kyle M. Rollins
Paul W. Richards

Department of Civil and Environmental Engineering

Brigham Young University

April 2010

ABSTRACT

Passive Earth Pressures on a Pile Cap

with a Dense Sand Backfill

Robert A. Marsh Jr.

Department of Civil and Environmental Engineering

Master of Science

Pile groups are often used to provide support for structures. Capping a pile group further adds to the system's resistance due to the passive earth pressure from surrounding backfill. While ultimate passive earth pressure under static loading conditions can be readily calculated using several different theories, the effects of cyclic and dynamic loading on the passive earth pressure response are less understood.

Data derived from the full-scale testing of a pile cap system with a densely compacted sand backfill under static, cyclic, and dynamic loadings was analyzed with particular focus on soil pressures measured directly using pressure plates. Based on the testing and analyses, it was observed that under slow, cyclic loading, the backfill stiffness was relatively constant. Under faster, dynamic loading, the observed backfill stiffness decreased in a relatively linear fashion. During cyclic and dynamic loading, the pile cap

gradually developed a residual offset from its initial position, accompanied by a reduction in backfill force. While the pile cap and backfill appeared to move integrally during static and cyclic loadings, during dynamic loading the backfill exhibited out-of-phase movement relative to the pile cap.

Observed losses in backfill contact force were associated with both cyclic softening and dynamic out-of-phase effects. Force losses due to dynamic loading increased with increasing frequency (which corresponded to larger displacements). Losses due to dynamic loading were offset somewhat by increases in peak force due to damping. The increase in contact force due to damping was observed to be relatively proportional to increasing frequency. When quantifying passive earth forces with cyclic/dynamic losses without damping, the Mononobe-Okabe (M-O) equation with a 0.75 or 0.8 multiplier applied to the peak ground acceleration can be used to obtain a reasonable estimate of the force. When including increases in resistance due to damping, a 0.6 multiplier can similarly be used.

ACKNOWLEDGMENTS

This thesis was completed through the support and assistance of several people. I personally wish to express my gratitude to Dr. Travis M. Gerber for the counsel and experience he willingly and patiently offered. The other members of the committee also contributed their time to supplying feedback to this thesis for which I am appreciative.

The research presented in this thesis was supported by the National Science Foundation under Award Number CMS-0421312 and the George E. Brown, Jr. Network for Earthquake Engineering Simulation (NEES) which operates under NSF Award Number CMS-0402490. Additional support was provided via a pooled-fund study led by the Utah Department of Transportation (UDOT) under Contract No. 069148 "Dynamic Passive Pressure of Abutments and Pile Caps" with participation from the Departments of Transportation of California, Montana, New York, Oregon, and Utah. Daniel Hsiao was the project manager for UDOT. The support provided by these organizations is gratefully acknowledged. The views, interpretations, and recommendations expressed in this thesis are those of the author and do not necessarily reflect those of the research sponsors.

Lastly, I am fortunate to have such a wonderful sweetheart who spent many hours at my side, often earlier in the morning than reasonable. To my Natalie, thank you.

TABLE OF CONTENTS

LIST OF TABLES

LIST OF FIGURES

1 Introduction

1.1 Background

Piles are a deep foundation system that mitigates the effects of poor soil or extreme loading conditions. A pile's capacity is dependent on the contact friction between its surface and the surrounding soil in addition to the bearing strength of the soil at the pile's base. A concrete pile cap connects a group of piles providing additional stiffness and support. Pile caps primarily resist lateral movement by pushing against surrounding backfill soil.

Lateral resistance from the backfill develops as passive earth pressure. Passive pressures form as the pile cap encroaches into the backfill as opposed to active pressures which develop as the structure moves away from the soil. Passive and active static earth pressures are generally calculated using one of three theories: Rankine, Coulomb, and logarithmic spiral. These methods predict the theoretical ultimate passive pressure and can be coupled with hyperbolic displacement relationships to account for variable pressure as displacement increases, or constitutive relationships can be used directly in finite element/difference analyses.

Dynamic forces, such as vibrations from an earthquake, change the static soil pressures that have developed between the pile cap and backfill soil. The dynamic

contribution to the already present static force has often been modeled as an additional thrust force on the pile cap. One method which is used to calculate this dynamic or pseudo-static loading is the Mononobe-Okabe (M-O) equation.

The M-O equation, developed in the mid 1920's, was one of the first standardized methods for calculating dynamic soil pressures. This equation supplies engineers with a guide for designing soil retaining walls which will adequately withstand a seismic event. The basis for the M-O equation is the Coulomb theory. To derive the M-O equation, a horizontal seismic force is inserted into Coulomb's equations of active and passive soil pressure. Thus, the M-O adaptation of Coulomb's equations approximates pseudo-static loading by combining a static force with a seismic force.

Since Mononobe and Okabe's research, several studies have been conducted either to validate or expand the M-O equations results or to find alternative ways to design for dynamic loads. For example, the M-O equation provides a resultant force but does not describe the location of the resultant force. Research has been conducted to explain the changing pressure distribution during dynamic loading and to locate where the resultant force acts upon a retaining structure. In addition, M-O equation input factors, such as the horizontal acceleration coefficient, are often ambiguous relying on engineering judgment.

1.2 Description and Objective of Research

The research presented in this thesis is part of a combined effort to quantify passive dynamic soil pressure acting on a concrete pile cap. This includes deriving a reasonable inertial coefficient for the M-O equation to be used in the design of pile caps

by engineers. In addition, field passive forces will be validated in this thesis using calculations independent of the M-O equation. This will verify that the M-O equation reasonably estimates field-tested dynamic forces with appropriate M-O coefficients. These outcomes will be arrived at by first performing full-scale dynamic testing and then analyzing and interpreting the field results.

1.3 Organization of Thesis

This thesis is organized into chapters outlining applicable research, methods of testing, methods of analysis, test results, and interpretation of results.

In Chapter 2, a literature review of published research, previous Brigham Young University theses and reports, and other pertinent articles are briefly summarized. Included in this section is a more detailed discussion of the M-O equation. This includes parameters and limitations of the M-O equation.

Chapter 3 begins with an overview of the site and test set-up used to load a pile cap and activate the passive pressure of the backfill soil. Previous site specific research is referenced as well as modifications to the site in preparation for this new series of tests. The testing equipment will be explained in detail. Chapter 3 concludes with a description of the general test procedures followed to load the pile cap-backfill system.

Field measurements and values are outlined in Chapter 4. This includes dynamic passive pressure at different frequencies and different pile cap displacements. Likewise, accelerations and displacements of the pile cap and backfill are reviewed and reduced in preparation for further observation and results. The concluding chapters will organize the reduced data into different analyses and conclusions to meet the objectives of this thesis.

2 Literature Review

This chapter will provide a brief overview of other research which relates to the topics explored in this thesis. These related research methods and results are placed in an order which parallels the body of this thesis. First, pertinent soil properties, site specific layouts, and test procedures (referenced in other Brigham Young University theses and reports) will be presented. Then this chapter will outline analytical reports that focus on cyclic loading conditions. Lastly, methods for predicting dynamic passive earth pressures will be reviewed.

2.1 Site or Loading Specific Research

2.1.1 Cummins (2009)

The research analysis produced by Cummins is directly connected with this thesis. The scope of his work involved comparing data according to the following pile cap-backfill conditions: without backfill, with densely compacted clean sand backfill, and with loosely compacted clean sand backfill. Full-scale testing of these conditions was part of a larger series of tests operated during 2007. Table 2-1 displays a complete list of all of these tests. The basis for this thesis is the data collected specifically on May 25, 2007 whereas Cummins compares data from May 18, 25, and 29 of 2007.

Table 2-1 Breakup of testing performed (Cummins 2009)

Test Number	Test Date	Backfill Condition
1	18-May-07	Free Response (Condition Cap)
2	25-May-07	Densely Compacted Clean Sand
3	29-May-07	Loosely Compacted Clean Sand
4	1-Jun-07	0.91-m wide Gravel Zone with Loosely Compacted Clean Sand
5	1-Jun-07	No Backfill (Free Response)
6	4-Jun-07	1.83-m wide Gravel Zone with Loosely Compacted Clean Sand
7	6-Jun-07	Loosely Compacted Fine Gravel
8	11-Jun-07	Densely Compacted Fine Gravel
9	18-Jun-07	Mechanically Stabilized Earth (MSE) Wall with Densely Compacted Clean Sand
10	21-Jun-07	Loosely Compacted Coarse Gravel
11	21-Jun-07	No Backfill (Free Response)
12	26-Jun-07	Densely Compacted Coarse Gravel

Since the site set up, soil properties, and test procedures for Cummins' thesis are identical to this thesis, a discussion of these points will be postponed until Chapter 3. However, several analytical observations derived by Cummins are pertinent to the results contained in this thesis. Therefore, this section will include a brief description of these key findings.

Contact pressure at the pile cap-backfill interface was recorded in two separate loading conditions, cyclic and dynamic. The details of these two loading cases will be discussed in Section 3.3, Test Procedures. The pressure results heavily depend on which loading condition was operated first. Figure 2-1 shows a typical cyclic load-displacement chart. When cyclic loading was operated after dynamic loading, shown in the first image (a), each series cycle reached the same approximate load and displacement. However, virgin loading the soil resulted in a residual offset, shown in the second image (b). With each ramp-up, the pile cap displacement increased and maximum load decreased.

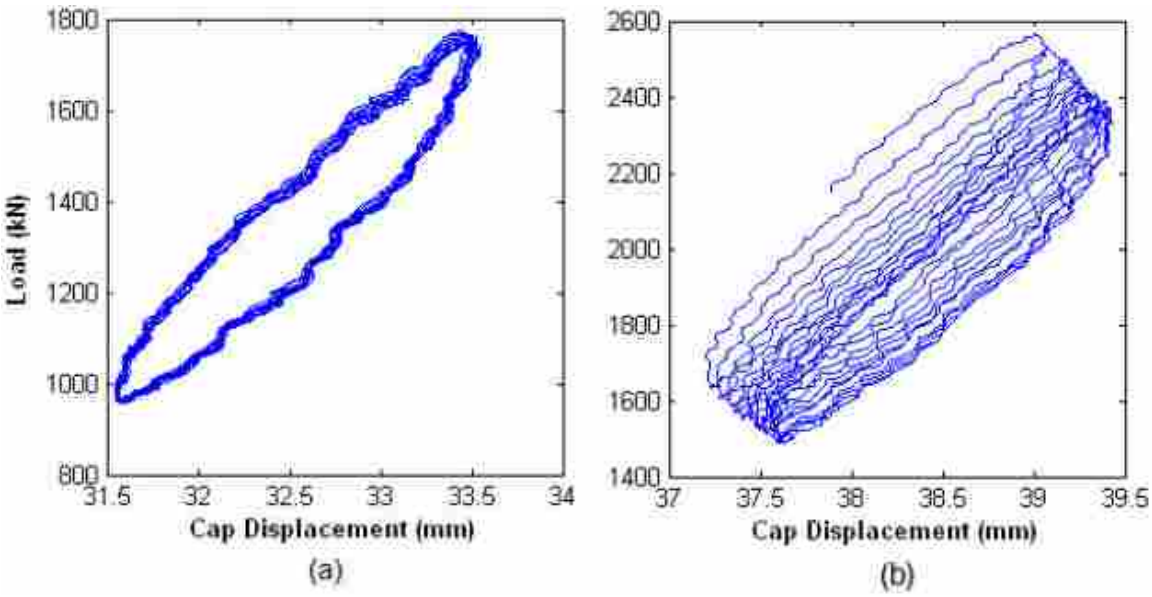

Figure 2-1 Typical load-displacement loops during cyclic loading when the actuators loaded the pile cap (a) after and (b) before the dynamic loading (Cummins 2009)

Similarly, dynamic loading which preceded cyclic loading produced different load-displacement diagrams than those that followed cyclic loading. In Figure 2-2, the first set of load hysteresis decrease in load with increasing frequency; this is the typical response when dynamic loading is operated first. In the second image (b), the general trend is an increase in pressure and displacement with an increase in frequency. However, toward 9 and 10 Hz, this trend slowly disintegrates.

These trends are consistent throughout all 11 displacement intervals of the pile cap. Figure 2-3 shows the displacement, stiffness, loop area, and damping ratio during cyclic loading on May 25, 2007. Notice that every odd-numbered point (a test where the soil was first cyclically loaded prior to dynamic loading) has a slightly lower maximum displacement. This matches the observation from Figure 2-1. Other significant pile cap-backfill trends include the following:

- System stiffness increased as the pile cap was displaced into the backfill
- System stiffness was greater when cyclic preceded dynamic loading
- Load-displacement hysteresis generally increased with forcing frequency
- Damping ratio generally remained constant with pile cap displacement

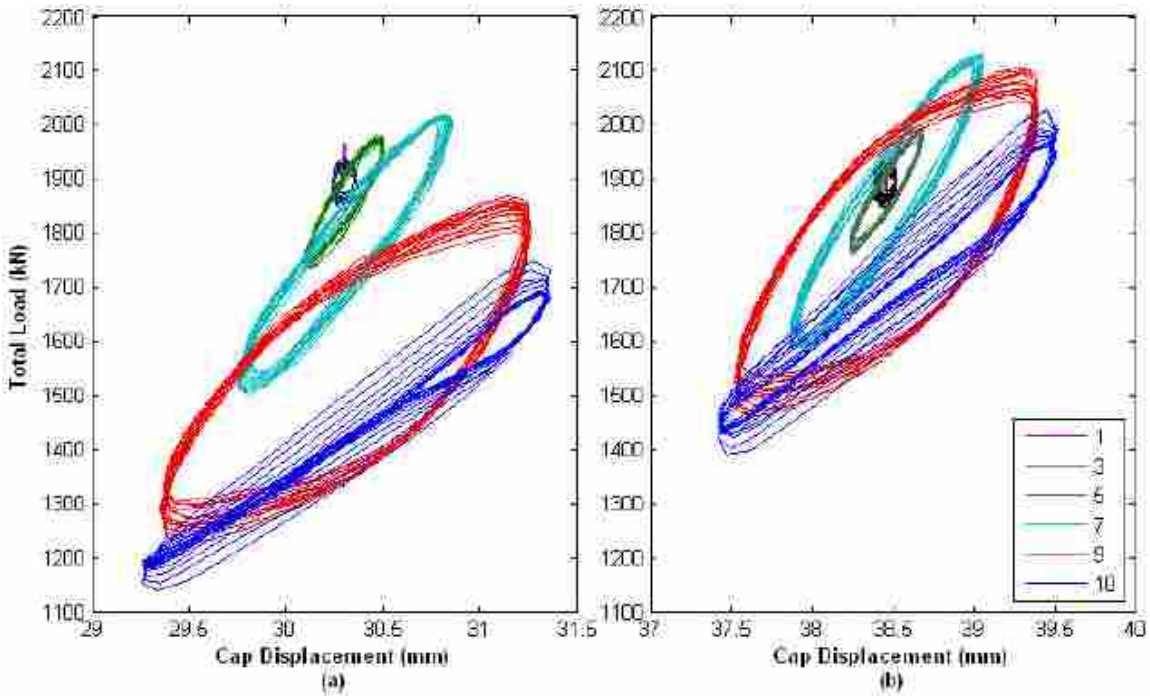

Figure 2-2 Typical load-displacement loops during dynamic loading when the shaker loaded the pile cap (a) before and (b) after the cyclic loading (Cummins 2009)

Figure 2-4 displays the displacement, stiffness, and damping during dynamic loading. Here Cummins compares these dense backfill parameters to the dynamic forcing frequency. In the second column of the figure, stiffness and damping are shown with respect to displacement. The trends from these figures support the relationships of similar parameters (force, displacement, stiffness, and damping) observed in the data for this thesis.

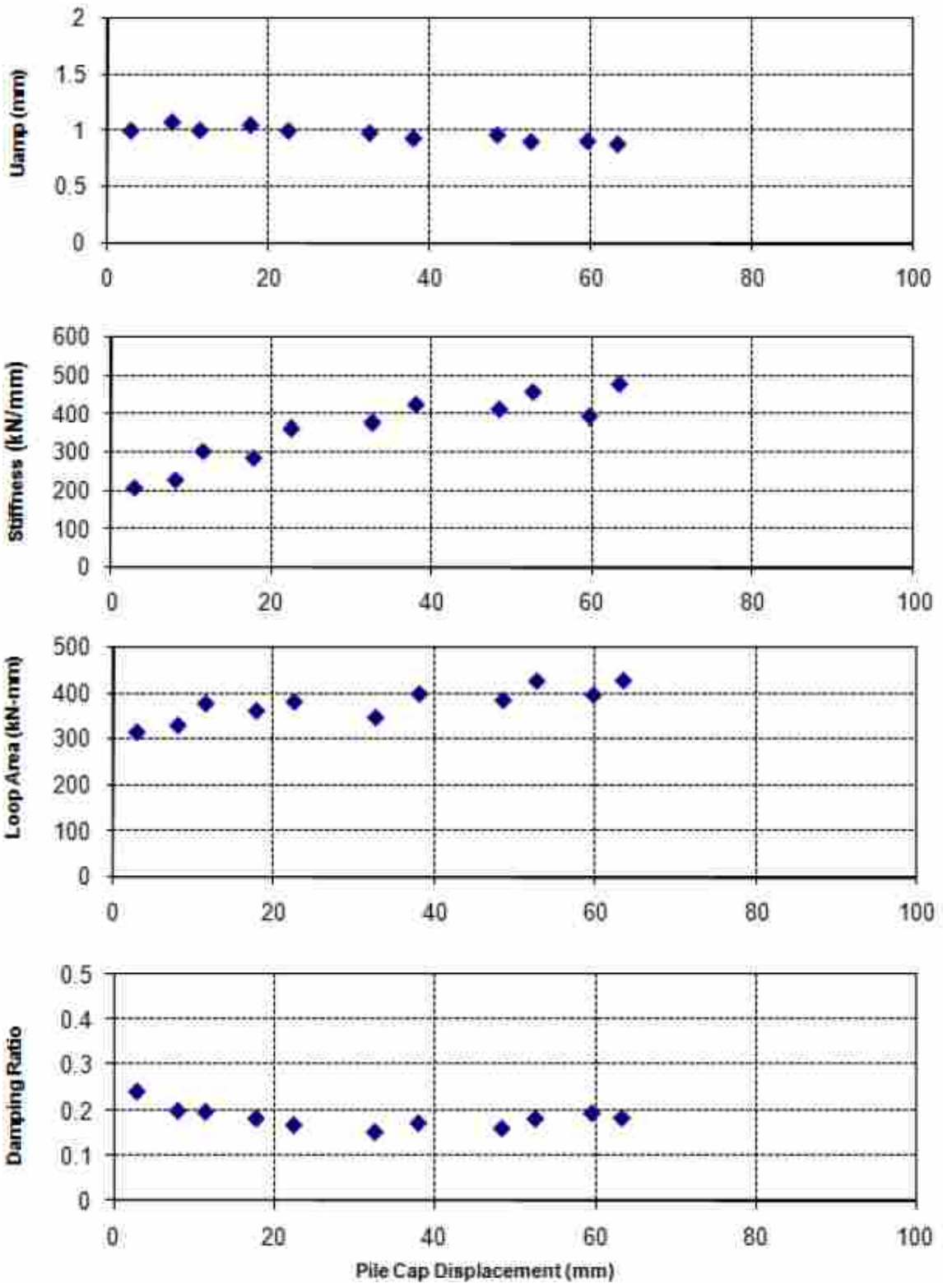

Figure 2-3 Cyclic displacement amplitude, stiffness, loop area, and damping during loading of densely compacted sand backfill (Cummins 2009)

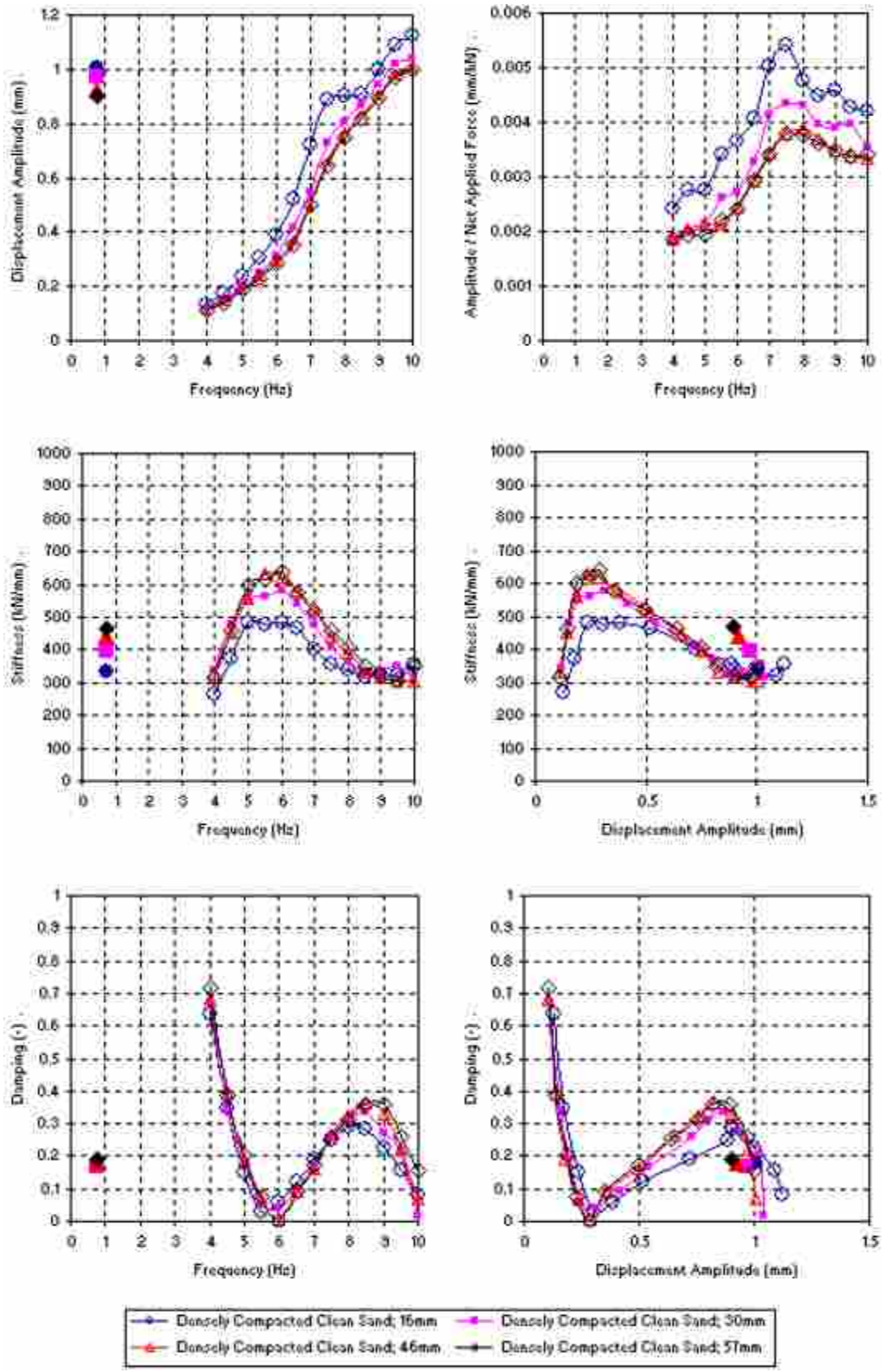

Figure 2-4 Dynamic parameters related to both frequency and displacement during loading of densely compacted sand backfill (Cummins 2009)

Other key components of Cummins research include the following calculations:

- Damped natural frequency of the pile cap-backfill system was 7.5 Hz for the densely compacted sand backfill
- Log-spiral method with shape correction was the best predictor of load versus displacement
- Stiffness of the pile cap system doubled with a loose sand backfill and quadrupled with a dense sand backfill when compared to the same system without any backfill in place

2.1.2 Runnels (2007), Valentine (2007)

Runnels (2007) and Valentine (2007) used actuators, a mass shaker, and a pile cap system to model full-scale cyclic and dynamic loading. The pile cap-backfill system was comprised of silty sand backfill which, when abutted against the pile cap, nearly doubled the dynamic resistance of the cap to loading. The difference between Runnels' and Valentine's test setup was the degree the backfill was compacted. Runnels analyzed a loose silty sand backfill while Valentine analyzed a dense silty sand backfill. Runnels calculated that 22% of passive earth resistance was due to the presence of the silty backfill. Valentine concluded that backfill stiffness reduction was the cause of a 10-15% loss in soil resistance.

The process of analyzing Runnels' and Valentine's test data included: analyzing the dynamic response of the pile cap with the backfill; calculating baseline relationships without any backfill; and lastly, evaluating the backfill contribution by finding the difference of the previous steps. The method of integrating accelerometer accelerations

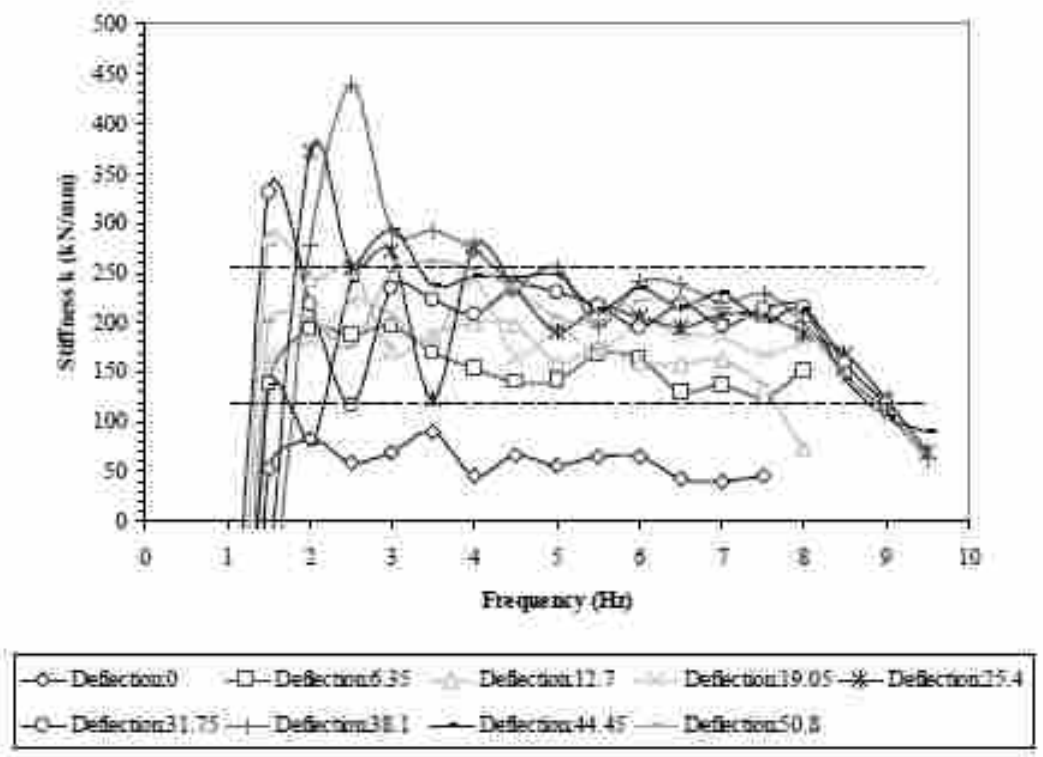

Figure 2-5 Dense silty sand stiffness versus forcing frequency (Valentine 2007)

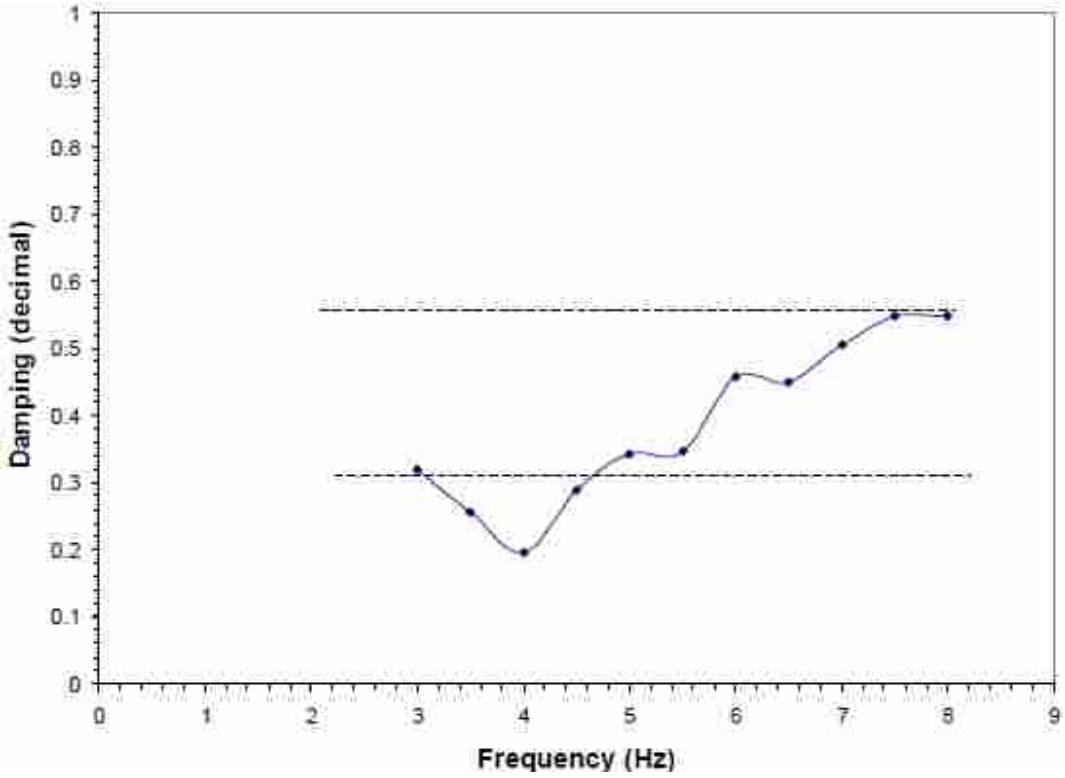

Figure 2-6 Loose silty sand damping versus forcing frequency (Runnels 2007)

(which was adopted into this thesis and will be explained in Section 4.1.1.2.1) was the primary source for retrieving accurate dynamic displacements. Similar to the test set-up for this thesis, string potentiometers were installed, but their readings were skewed during shaker testing due to dynamic vibrations.

Correlations produced by Runnels (2007) and Valentine (2007) validate the trends realized in this thesis. Backfill stiffness was observed to generally decrease with increasing frequency. This relationship is shown in Figure 2-5 at various pile cap displacement intervals. As the pile cap is dynamically loaded, stiffness of the pile cap-backfill system generally decreases after the stiffness is fully activated which occurs between 1 to 3 Hz. Inversely, damping increased with increasing frequency. Figure 2-6 shows this comparison from Runnels (2007).

2.2 Static and Cyclic Passive Earth Pressure

2.2.1 Duncan and Mokwa (2001)

Duncan and Mokwa (2001) loaded an anchor block in both the site's native soil and a denser compacted gravel. The block was horizontally loaded into an excavation in single minute increments. A scarp and bulge were physically observed when the block pushed against the natural soil and gravel fill, respectively, signifying failure. This visual is displayed in Figure 2-7.

The passive pressure measured during the anchor block loading was compared to Rankine, Coulomb, and Log Spiral methods for calculating passive earth pressures. In addition the log spiral approach was also corrected for the shape of the block using a

method produced by Brinch Hansen (1966) based off of research performed by Ovesen (1964). This correction considers a 3D shape effect on mobilizing pressure.

In Table 2-2 these four methods for computing passive pressure are compared to the actual measured pressure. The Coulomb theory and Log Spiral method are similar in their associated passive pressure results. However, the 3D corrected log spiral approximates the earth passive pressure closer to the pressures measured by Duncan and Mokwa than any other method reviewed.

Duncan and Mokwa concluded that passive pressure is dependent on the displacement of a structure, the backfill stiffness, and the structure-backfill interface friction and adhesion. In addition, accounting for the shape of the structure more accurately estimates the calculated passive pressure.

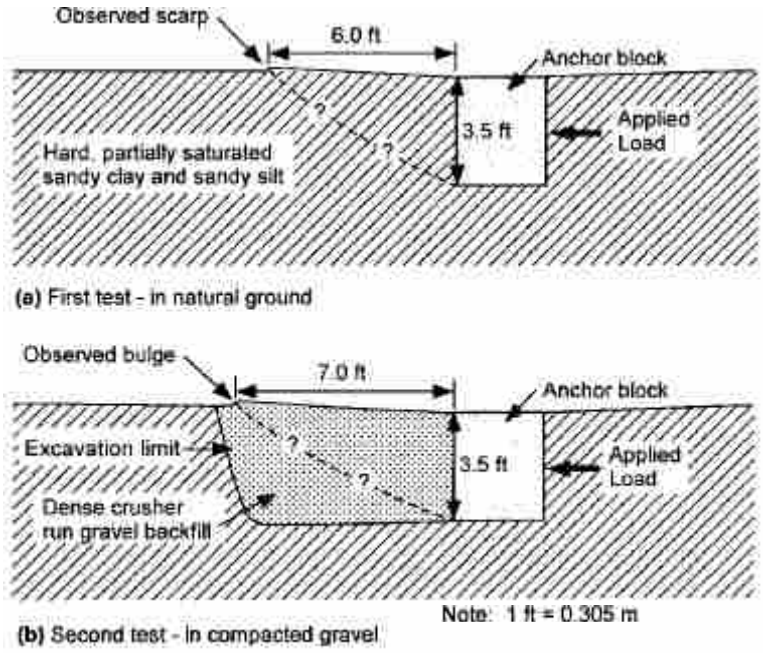

Figure 2-7 Soil failure type during testing various backfill conditions (Duncan and Mokwa 2001)

Table 2-2 Comparison of passive resistances (kips) (Duncan and Mokwa 2001)

Method (1)	Natural Soil			Gravel Backfill		
	High (2)	Low (3)	Aver-age (4)	High (5)	Low (6)	Aver-age (7)
Rankine	110	94.8	102	43.9	35.4	39.6
Coulomb	119	103	111	59.0	49.4	54.2
Log Spiral, without 3D correction	120	102	111	58.0	48.4	53.3
Log Spiral, with 3D correction	173	139	156	104	82.3	93.2
Measured	—	—	138	—	—	91.7

Note: 1 kip = 4.45 kN; high computed using high strengths in Table 5; and low computed using low strengths in Table 5.

2.2.2 Cole (2003), Cole and Rollins (2006)

Several theories analyzing the maximum displacement necessary to fully mobilize passive earth resistance were compiled by Cole and Rollins. One objective of their research was to derive a method for calculating the maximum passive pressure fully mobilized behind a pile cap. Four backfill materials were used: clean sand, silty sand, fine gravel, and course gravel. Cole and Rollins suggest that displacements ranging 3.0 to 5.2% of the pile cap height will allow the maximum passive earth pressures to develop.

Sources, namely the U.S. Navy (1986), Caltran (2001), and Duncan and Mokwa (2001), produced original methods and models to contrast passive force versus deflection. The comparison between these sources is displayed in Figure 2-8. The hyperbolic model produced by Duncan and Mokwa (2001) most closely aligned with the pressure measured by Cole and Rollins (2006). However, generally these three methods underestimated the measured passive resistance.

During cyclic loading, passive force at the pile cap-backfill interface decreased. This reduction stemmed from a gap which formed between the backfill and the pile cap.

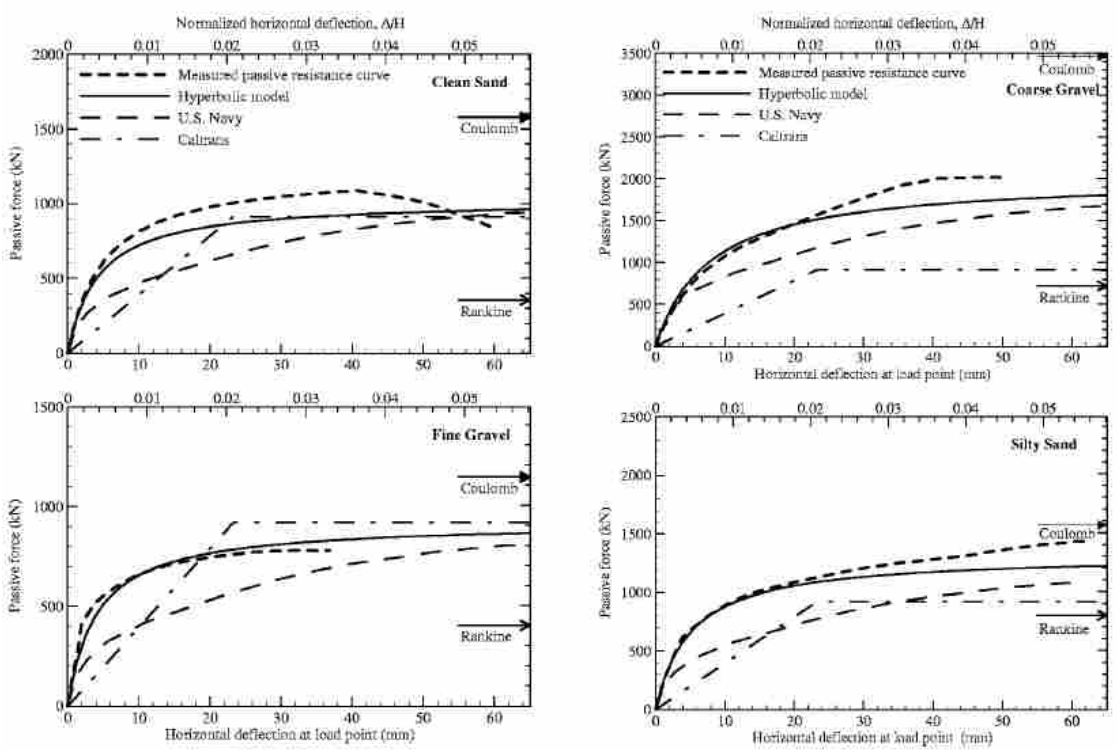

Figure 2-8 Backbone passive resistance comparisons (Cole and Rollins 2006)

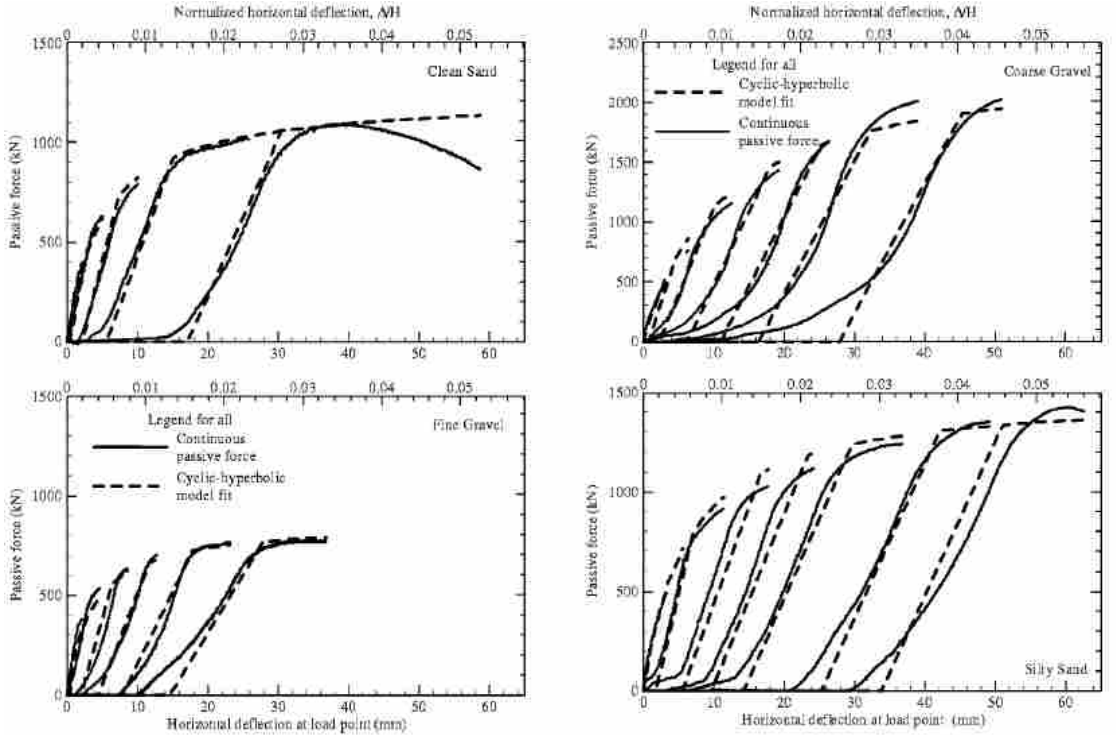

Figure 2-9 Passive resistance using cyclic-hyperbolic model (Cole and Rollins 2006)

In addition, cyclic loading reduced the stiffness of the backfill. Therefore, Cole and Rollins proposed a cyclic-hyperbolic model to calculate passive pressure as a function of displacement. The results of this model account for the reductions of gap formation and backfill stiffness loss and are illustrated in Figure 2-9. The backbone curve by combining these load-deflection charts estimates the measured cyclic pressure closer than methods which do not account for cyclic reductions.

Cole and Rollins validate the contact pressure loss observed in this thesis that has been attributed to cyclic loading.

2.3 Dynamic Passive Earth Pressure

2.3.1 Kramer (1996)

Considering the seismic design of yielding retaining walls, Kramer (1996) sited the widely used Mononobe-Okabe (M-O) equation. Mononobe (1929) and Okabe (1926) evolved Coulomb's theory of active and passive pressure by introducing parameters to account for the soil thrust during seismic activity. The passive earth pressures derived by the M-O equation are calculated using the following expression:

$$P_{PE} = \frac{1}{2} K_{PE} \gamma H^2 (1 - k_v) \qquad \textbf{(2.1)}$$

where:

P_{PE} = passive earth pressure

K_{PE} = dynamic passive earth pressure coefficient (see Equation 2.2)

$\gamma =$ unit weight of soil

$H =$ height of the retaining wall

$k_v =$ vertical acceleration seismic coefficient

This equation is the Coulomb theory for passive pressure with the addition of a dynamic passive earth pressure coefficient (K_{PE}) and a vertical acceleration seismic coefficient (k_v). K_{PE} may be further defined by the following equation:

$$K_{PE} = \frac{\cos^2(\phi + \theta - \psi)}{\cos\psi \cos^2\theta \cos(\delta - \theta + \psi)\left[1 - \sqrt{\frac{\sin(\delta + \phi)\sin(\phi + \beta - \psi)}{\cos(\delta - \theta + \psi)\cos(\beta - \theta)}}\right]^2} \quad \textbf{(2.2)}$$

where:

$\phi =$ backfill friction angle

$\theta =$ inclination of structure measured from vertical

$\psi =$ seismic inertia angle

$\delta =$ interface friction angle

$\beta =$ slope inclination angle

The equivalent from these two equations is a single resultant force representing both the static and dynamic force contributions. The forces resulting in an equivalent passive resultant are shown in Figure 2-10 as a free body diagram. The M-O equation

implies that the resulting force acts at the same height along the retaining wall as the resultant height under static conditions.

Since M-O is based off of the Coulomb theory, it is limited by the same assumptions. Likewise, the M-O equation, like Coulomb, will over estimate passive thrust especially when the interface friction angle is greater than half of the soil friction angle. Therefore, the interface angle should be carefully selected and limited when using the M-O equation to calculate pseudo-static forces.

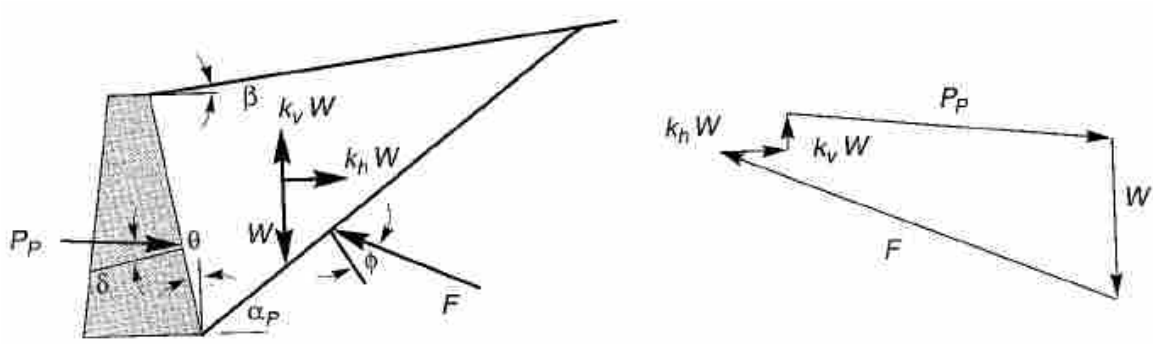

Figure 2-10 Mononobe-Okabe forces acting on a passive soil wedge (Kramer 1996)

2.3.2 Seed and Whitman (1970)

Seed and Whitman (1970) reviewed the two main sources of dynamically loading retaining structures: earthquakes and explosions. For this study, only dynamic earthquake loads on retaining structures above the water table are applicable.

Seed and Whitman began with a study of the M-O equation. Mononobe and Okabe generated perhaps the earliest model for calculating dynamic forces acting on a retaining structure. The M-O equation makes the following assumptions:

- Retaining structure is above the water table
- Backfill is a homogenous, dry, cohesionless material
- Retaining wall yields enough to fully mobilize active and passive pressures
- Backfill acts as a rigid body such that seismic accelerations are consistent
- Resultant force acts at the same height as the static resultant force

In the M-O equation, the horizontal force is extremely sensitive to several terms which, therefore, must be accurately determined. For example, the soil friction angle will increase the horizontal force acting on the retaining wall by 50 percent in only a 10 degree shift. Another condition which largely affects the horizontal force on the wall is the backfill slope. In comparison with static horizontal force calculated by Coulomb, the dynamic horizontal force is sometimes three times higher with a similar backfill slope.

Other variables, such as the vertical acceleration coefficient (k_v), do not largely affect the calculated dynamic force. According to Seed and Whitman, this k_v factor may be neglected for seismic analysis.

Seed and Whitman cited the efforts of Jacobsen (1939) and Matsuo (1941) in verifying their calculated M-O forces. In both of these reports, the resultant force was described as acting on the retaining structure a distance of 2/3 the wall height from the base of the wall.

2.3.3 Richards and Elms (1979)

Richards and Elms (1979) discussed gravity retaining walls during seismic activity calling the review of Seed and Whitman (1970) "misleading and

unconservative." They cite investigatory observations following the 1968 Inangahua, New Zealand earthquake. From the observed damages, estimates of the driving force to wall resistance ratio were determined as 3.5 to 4.5 times the normal static conditions. Mononobe-Okabe, as referred to in Seed and Whitman, would predict only 2.5 times the static condition.

When reviewing the M-O equation, Richards and Elms (1979) concurred with Seed and Whitman (1970) on several levels. Insignificant factors include the wall friction angle and the vertical seismic acceleration. As seismic intensity increases, the contribution of both of these terms becomes negligible. Critical parameters include the backfill slope and the soil friction angle. Richards and Elms differ from Seed and Whitman by assuming a uniform pressure distribution during seismic activity. Thus, the resultant force would act at a height ratio H/2 from the base of the wall as opposed to Seed and Whitman's proposed 2H/3 ratio.

As Richards and Elms continued their discussion, the importance of including the weight of the resisting structure was recommended. By combining the M-O equation and Newmark's sliding block analogy, this study derived an allowable displacement approach. Included in this approach is a maximum wall displacement with an associated vertical acceleration limit.

During shaking when passive conditions exist, Richards and Elms write "the wall and the soil undoubtedly act together since the threshold acceleration for relative motion at the base would be very large indeed" (Richards and Elms 1979). This thesis finds observations contrary to that statement.

2.3.4 Whitman (1990)

Whitman (1990) reviewed the M-O equation in an effort to simplify the design of gravity retaining walls. In addition, the use of the allowable permanent displacement method by Richards and Elms was discussed (1979).

The article began with a review of the M-O equation. The M-O equation is based off of several assumptions. Inherent to the Coulomb equations for pressure, the backfill must deform thus mobilizing the interface shear resistance. Another assumption is that the soil must be uniform. The backfill must also propagate accelerations consistently and evenly.

Whitman then transitioned into a discussion on gravity retaining structures. He concluded that simple walls less than 30 ft (9.14 m) and that are not restrained from outward movements may be effectively designed using the M-O equation.

2.3.5 Ostadan and White (1997)

The objective of Ostadan and White's report was to develop a method for calculating lateral seismic pressure for building foundations. Criticizing the overuse of the M-O equation with its several limitations, the reports says, "The M-O method is one of the most abused methods in geotechnical practice"(Ostadan and White 1997). For building foundations, the M-O equation would be inappropriate. Thus a model for estimating seismic pressures was developed which matched the following conditions:

- Building walls are non-yielding and are confined to displacements
- Design motion is fully considered not just a single peak ground acceleration

- Material damping, Poisson's ratio, soil density, and shearwave velocity are considered
- Soil nonlinearity may be considered
- Soil-building interactions are taken into account by analyzing foundation rocking motion, embedment, and soil motion and geometry

Ostadan and White divide their approach into two fundamental categories: firm soil layer foundation and deep soil sites. The later takes into account the rocking motion of a structure. Each situation was modeled by the Computer Program SASSI. During the firm layer analysis, a vertical propagating shearwave was induced at the rock layer. Pressure amplification was observed as the frequency of the system matched the soil column's natural frequency. In every variation of Ostadan and White's analysis, the maximum amplification of the pressure was at this natural frequency.

At shallow depths the soil tends to soften during dynamic motions. This occurs due to the relatively low confining pressure on the soil material. For this thesis softening of the soil is a significant parameter in calculating soil pressures. Since this thesis studies a single pile cap, all of the backfill may be considered shallow and, therefore, subject to softening.

Ostadan and White developed a polynomial equation to represent the soil distribution acting on the structure. This equation, represented in terms of y, is the following:

$$p(y) = -.0015 + 5.05y - 15.48y^2 + 28.25y^3 - 24.59y^4 + 8.14y^5 \quad \textbf{(2.3)}$$

where:

$y = Y/H$

Y = distance from bottom of the wall

H = height of the wall

The simplified method purposed by Ostadan and White, which output is Equation 2.3, was compared to the computer model from SASSI. This new method yields a range of results largely dependent on the input frequency.

2.3.6 Chandrasekaran (2009)

Chandrasekaran (2009) focused on lateral effects when pile groups are loaded in clay. Laboratory testing was performed in the form of modeling single pile and group effects using static, cyclic, and dynamic loading conditions. Embedded length, clay properties, and pile numbers were adjusted to observe various results.

One analysis procedure performed by Chandrasekaran is also executed in this thesis. Harmonic-like waves were produced during loading both as measured forces and measured displacements. When these response waves were compared, the alignment of peak force to peak displacement shifted throughout testing. At low frequencies, the waves generally aligned as shown in Figure 2-11a. However, when the system's natural frequency was matched by the forcing frequency, the peak displacement lagged behind the peak force. Figure 2-11b shows the out-of-phase relationship at resonance. Chandrasekaran observed a phase angle of 38 degrees before resonance and a 90 degree phase angle during resonance.

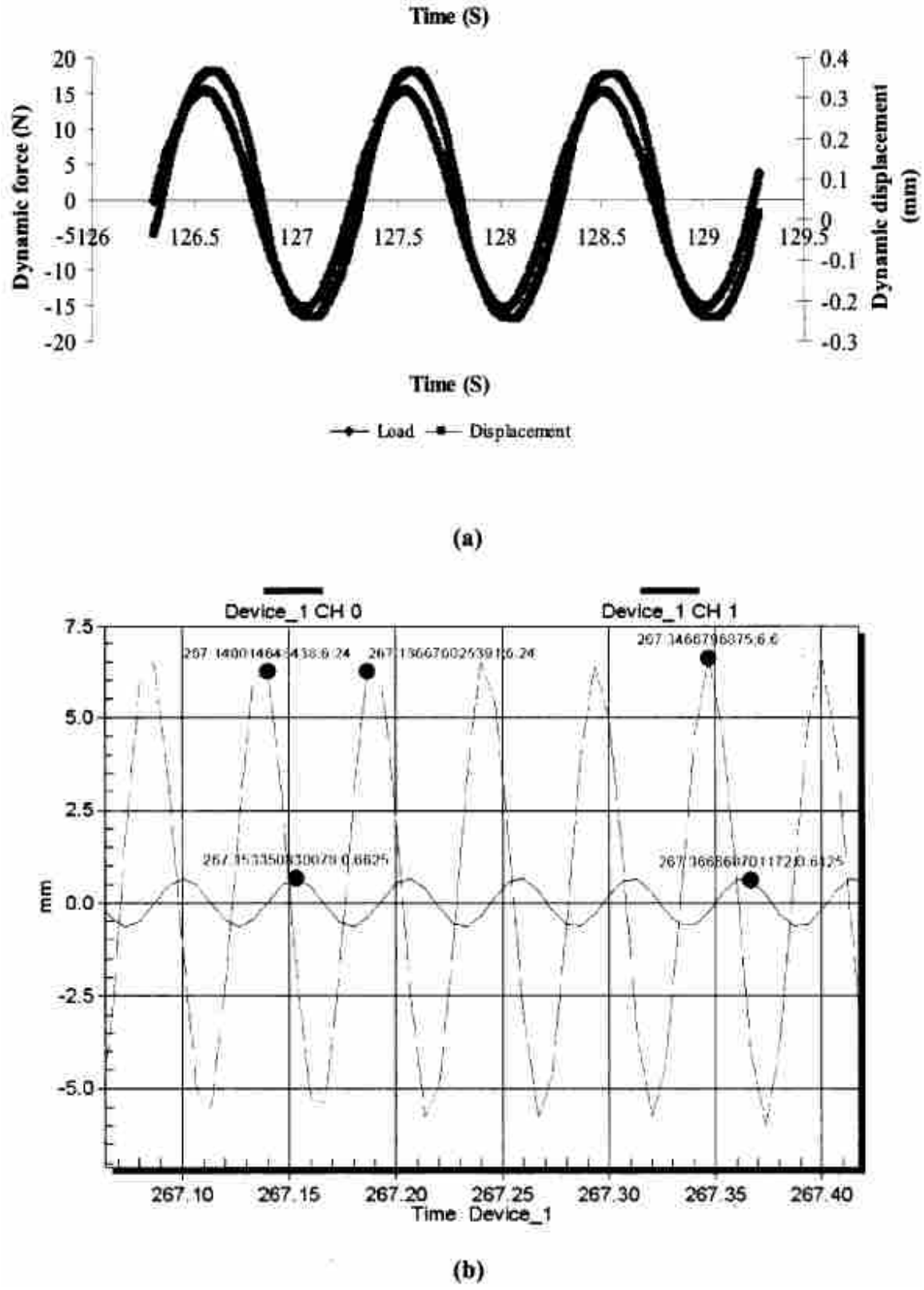

Figure 2-11 Phase lag between force and displacement (a) before resonance (b) after resonance (Chandrasekaran 2009)

The method by which these phase angles were derived is used later in this thesis. Two harmonic waves are first compared during similar time interval. The time interval between peaks is then calculated and divided by the time wavelength of either harmonic wave. This proportion multiplied by 360 degrees yields the phase angle offset between the comparable harmonic measurements.

3 Methods of Testing

The testing for this thesis was part of a larger group of tests performed during May and June of 2007. Some on-site structures were constructed in previous years in connection with other research testing. Likewise, subsurface conditions were explored in prior years. All of the test data analyzed in the following chapters was recorded on May 25, 2007. This chapter specifically outlines methods for retrieving data on the 25th of May and relevant data compiled from previous research.

3.1 Site Characterization

For this research, testing was performed at a site located 300 m north of the control tower at the Salt Lake City International Airport, in Salt Lake City, Utah. Figure 3-1 displays a satellite image of the testing site in relation to the Salt Lake City International Airport.

The site, generally open and flat, is covered by approximately 1.5 m of imported clayey to silty sand and gravel fill. Exploration of subsurface material was primarily conducted in 1995 by Peterson (1996). Testing included Cone Penetration Tests, Pressuremeter Tests, and laboratory tests. The locations of subsurface tests at the site are illustrated in Figure 3-2. Figure 3-3 displays an idealized soil profile formulated using these investigatory tests. The test site may be generally described as silt and clay layers

occasionally interrupted by sand layers. For a more detailed review of the site and its subsurface characteristics reference Peterson (1996), Rollins et al. (2005a, 2005b), Christensen (2006), and Taylor (2006). Because this research is independent of the surrounding native soil, the subsurface conditions will not be belabored.

During testing, the water table on site was less than 10 m below the ground surface. Pumps were used throughout the testing process to keep the water level at this depth – beneath the pile cap and backfill.

Figure 3-1 Arial view of the site plan located 300 m north of the SLC Airport Control Tower

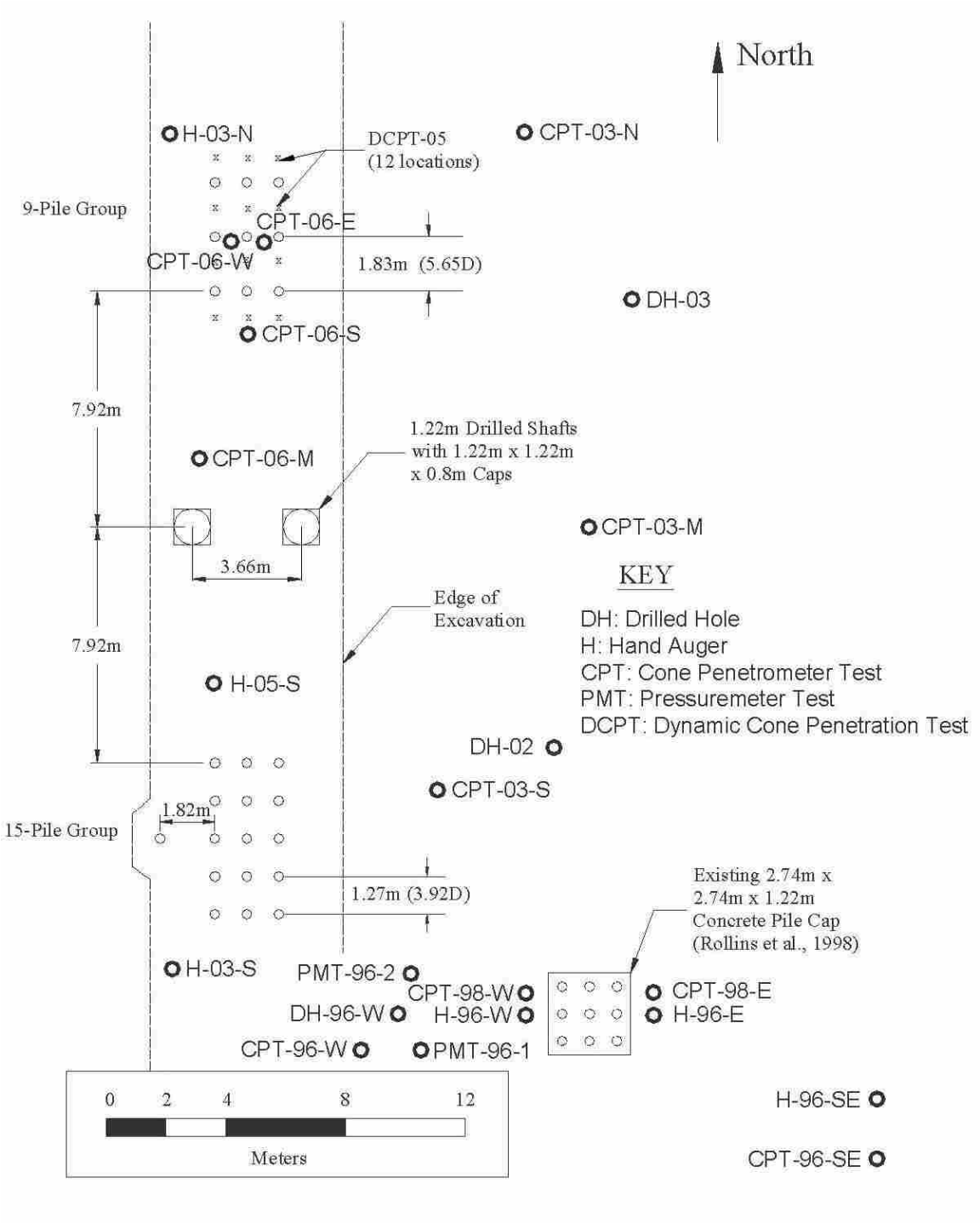

Figure 3-2 Test site referencing the location of subsurface test (Christensen 2006)

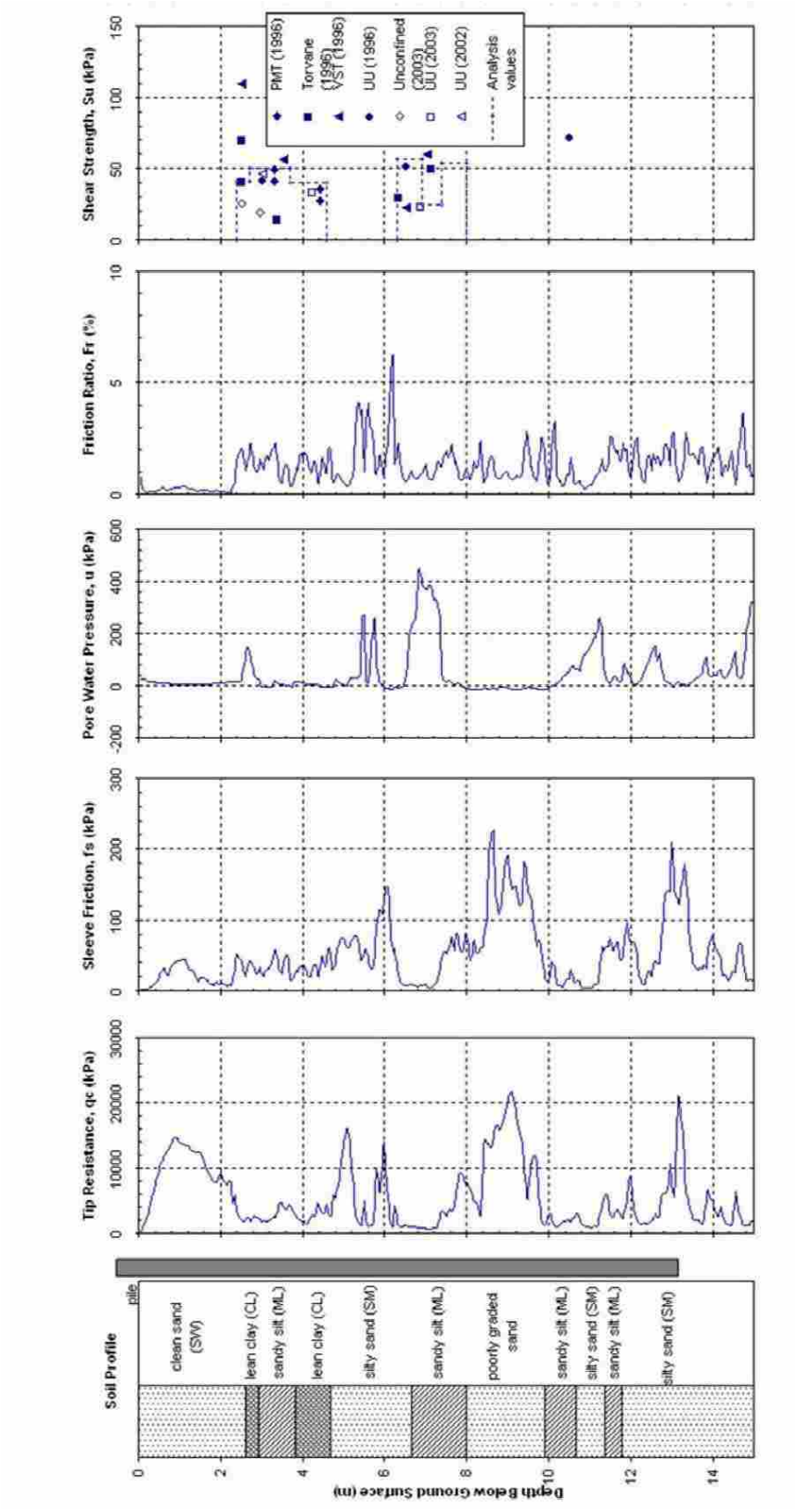

Figure 3-3 Idealized soil profile with CPT (Christensen 2006)

3.2 Test Components

Testing for this research includes the setup of a pile cap, backfill, loading equipment, and a reaction foundation. The loading equipment consists of two actuators and an eccentrically loaded mass shaker. Figure 3-4 shows a plan and profile view of the test layout. Aligning photographs of the setup are displayed in Figure 3-5.

3.2.1 Pile Cap Foundation

Constructed previously on the site was a nine-unit steel pile group which protruded out of the ground. The piles were oriented in a three by three grid arrangement. Each pile was closed end driven to a depth of 13 m. An outside diameter of 324 mm coupled with a wall thickness of 9.5 mm composes a single pile. The piles were specified as ASTM A252 Grade 3 steel having a yield strength of 310 MPa.

In preparation for summer 2007 testing, the three center row piles were removed. This created a clear span between the north and south rows of 3.66 m on center. The remaining piles were then cut and filled with concrete. The concrete had a compressive strength of 41 MPa. The north and south center piles were each equipped with an inclinometer tube extending lengthwise through the pile.

A pile cap was constructed on top of the six remaining steel-concrete piles. The cap dimensions are 1.68 m tall by 4.57 m long by 3.55 m wide. Pile cap reinforcing was designed in a double grid: one layer at the top and one layer at the bottom. Each layer consists of #19 rebar at 203 mm on center in both the longitudinal and transverse direction.

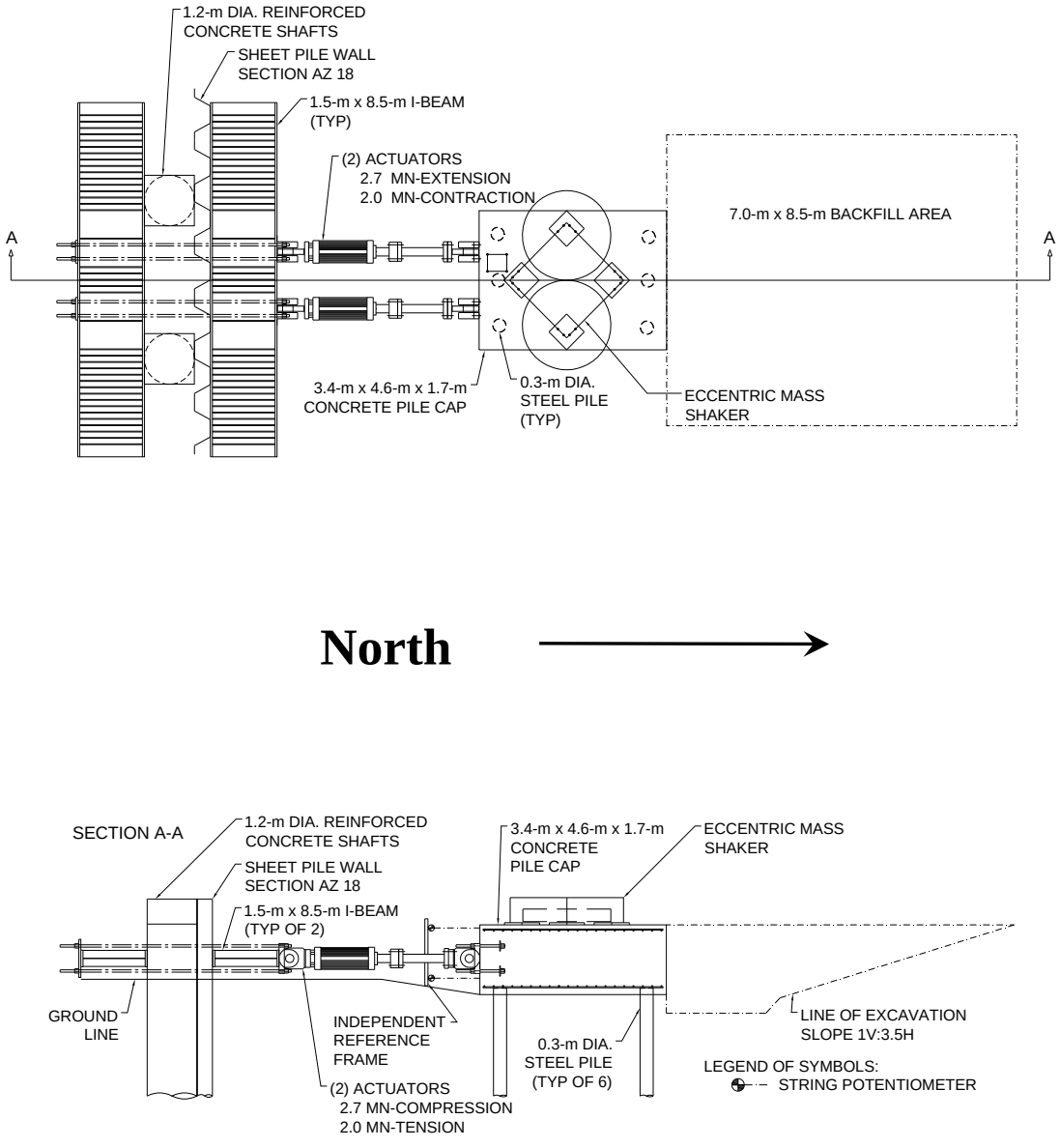

Figure 3-4 Plan and profile views of the test layout

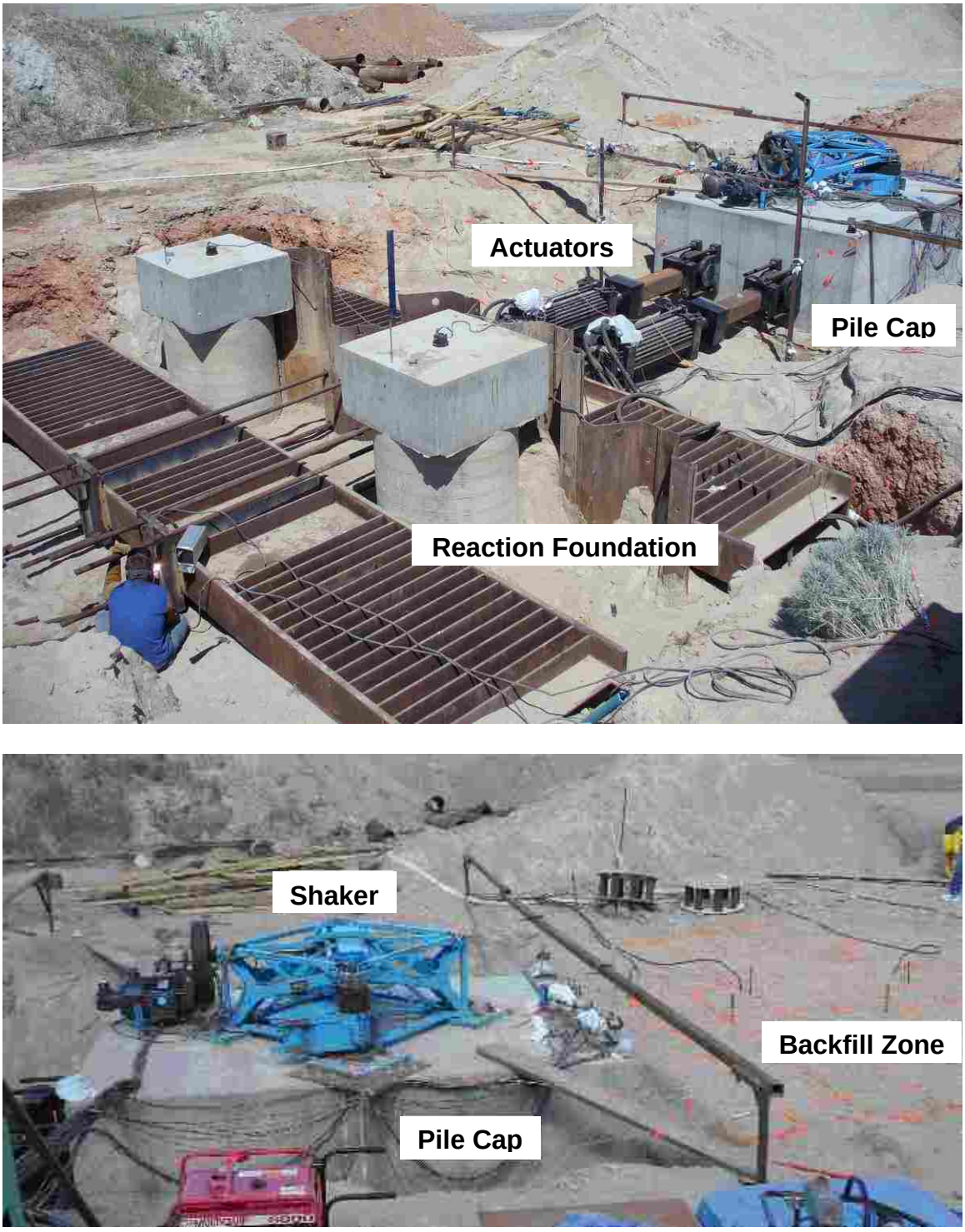

Figure 3-5 Photographs of the test layout

The pile cap encompasses the top 150 mm of each of the six remaining piles. A 5.49-m rebar cage connects the pile cap to each of the piles. The cage extends 1.47 m into the cap and 4.02 m into each pile. Cage reinforcing is comprised of (6) #25 vertical rebar encompassed by a 152 mm pitched #13 spiral rebar restraint. Incased by the pile and pile cap, this cage ensures a rigid connection. The pile and pile cap now act as a single, integral unit. Other connections extruding from the pile cap will be discussed in Section 3.2.4 Loading Equipment.

3.2.2 Backfill

An excavation surrounded the pile cap. The excavation continued north of the pile cap 5.2 m wide and 8.5 m long. Heavy equipment accessed the excavation via a construction ramp with a vertical/horizontal slope of 1.0/3.5. This slope began 2.44 m north of the pile cap. Between the slope and the pile cap, the excavated area was a constant 2.16 m deep.

The excavation was filled with soil north of the pile cap. The backfill rested against the northern face of the pile cap. For this thesis, well graded sand (SW), designated using the Unified Soil Classification System (USGS), was used as backfill. The sand was installed using 10-cm layers. Between each level, the backfill was compacted.

Classifying the backfill as a well graded sand is illustrated in Figure 3-6. The gradation curve, shown by a solid line, gradually and smoothly decreases generally passing through the restraints for a well graded sand. The index properties for the backfill are also presented in Table 3-1.

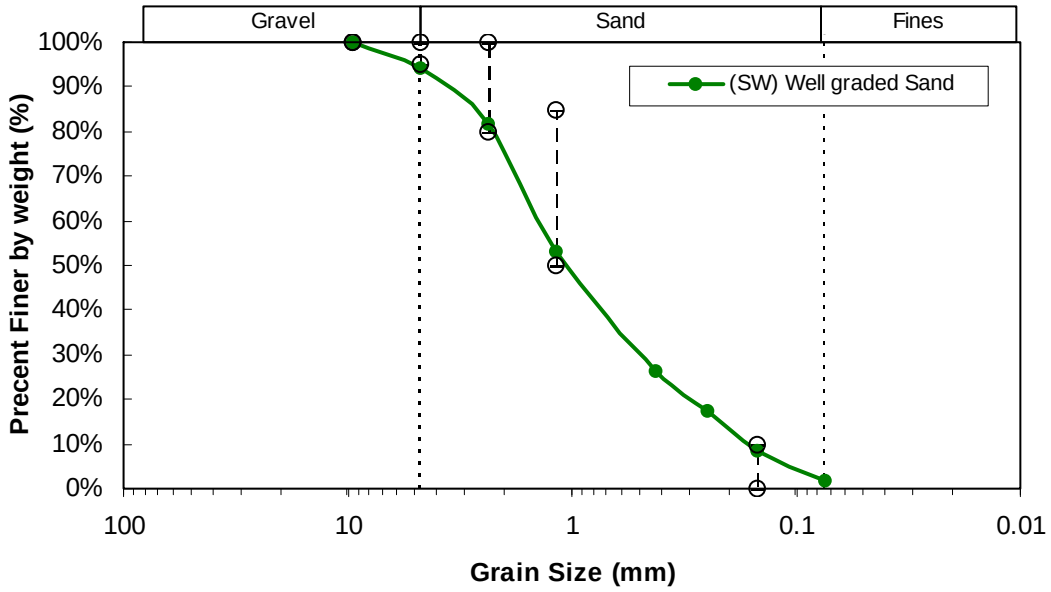

Figure 3-6 Particle size distribution with qualifying limits for clean sand backfill material

Table 3-1 Index properties for clean sand backfill material

Backfill Type	Gravel (%)	Sand (%)	Fines (%)	D_{60} (mm)	D_{50} (mm)	D_{30} (mm)	D_{10} (mm)	C_u	C_c
Clean Sand	6	92	2	1.50	1.11	0.56	0.17	8.7	1.2

The backfill was densely compacted as the sand was layered behind the pile cap. Compactors, such as a vibrating drum compactor, a vibrating plate compactor, and a jumping jack compactor, were operated to obtain a desired compaction. Compaction dependent soil characteristics, shown in Table 3-2, describe the optimum moisture content and the dry unit weight of the sand during both the standard and modified effort. Nuclear density gage testing verified these parameters after each compaction. Figure 3-7 is a histogram of the backfill density distribution. Table 3-3 organizes the soil parameters obtained from the nuclear density gage. The backfill has an average dry density of nearly

96% of the Modified Proctor maximum dry density and an average moist unit weight of 18.3 kN/m^3.

Table 3-2 Compaction characteristics of clean sand backfill

Backfill Type	USCS	Standard Effort		Modified Effort	
		w_{opt} (%)	γ_d (kN/m^3)	w_{opt} (%)	γ_d (kN/m^3)
Clean Sand	SW	17	16.5	15	17.4

Table 3-3 Average in-situ unit weight properties for clean sand backfill

Backfill Type	$\gamma_{d,avg}$ (kN/m^3)	w_{avg} (%)	$\gamma_{m,avg}$ (kN/m^3)	Relative Compaction
Densely Compacted Sand	16.8	9.1	18.3	95.9% of modified

Testing of soil properties also included lab tests performed in the Brigham Young University soil mechanics laboratory. To evaluate the clean sand's shear strength, direct shear testing was performed in general accordance with ASTM D 3080. The resulting peak and ultimate friction angles were 43.3 and 40.5 degrees, respectively.

Along with the normal direct shear tests, a series of modified tests were performed to quantify the interface friction angle (δ) between the concrete and the densely compacted clean sand. The interface friction angle was determined by placing a concrete sample of comparable roughness to the face of the pile cap into the bottom half of the shear box, filling the top half of the box with fine gravel compacted to the appropriate density, and shearing the composite sample under the same normal stress range as the internal friction angle tests. The interface friction angle determined from the

ultimate stress points was 29 degrees for densely compacted clean sand against concrete. The δ/φ ratio based on ultimate value results is about 0.72, which generally agrees with the value of 0.77 determine by Cole and Rollins (2006) for a similar sand material.

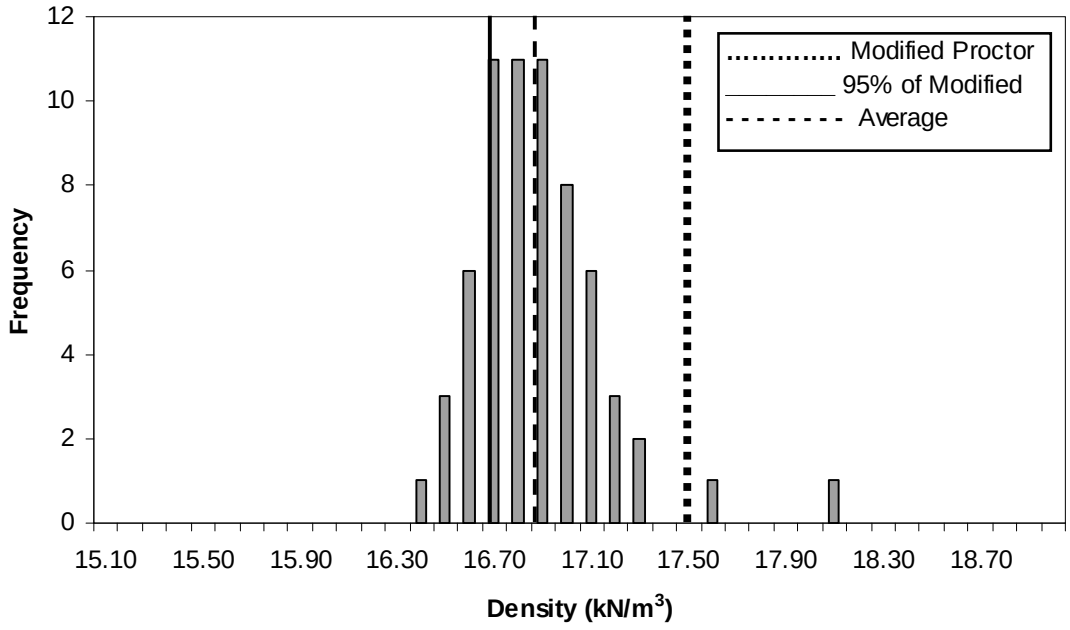

Figure 3-7 Density distribution of densely compacted clean sand backfill

3.2.3 Reaction Foundation

Constructed to the south of the pile group and backfill (refer to Figure 3-4), a reaction foundation provided bearing for loading the pile cap. The reaction foundation consisted of two drilled shafts and a sheet pile wall compressed between two I-beams. This foundation, significantly stiffer than the pile group, was used as an anchor for loading the pile cap and backfill throughout testing.

The drilled shafts were constructed prior to this series of tests. The shafts, each 1.2 m in diameter, are separated 3.66 m on center. Orthogonal to the north-south

direction of testing, these shafts are the structure behind static and dynamic loading of the pile cap. When constructed, the two shafts were capped with a 1.22 m by 1.22 m by 0.61 m concrete cap. Beneath the cap the west shaft extends downward a length of 16.82 m. The east shaft was constructed to 21.35 m deep. Each shaft was reinforced using #36 bars with #16 spiral stirrups. From the top to 10.67 m deep, (18) #36 reinforcement bars were installed with the stirrups on a 75-mm pitch. At 10.67 m half of the rebar was discontinued and the stirrup pitch increased to 300 mm. A 120-mm clear cover was maintained between the surface of the concrete and the outermost steel reinforcement. The concrete compressive strength is 41-MPa for both shafts.

An AZ-18 sheet piling was installed flush to the drilled shafts. This wall, 12.2 m in height, provides additional stiffness to the drilled shafts. The sheet pile wall was made from ASTM A-572, Grade 50 steel, and was pushed to a depth of 10.24 m to 10.85 m below the excavation's surface using a vibratory hammer.

Two steel I-beams pinch the sheet pile wall to the existing drilled shafts. Each beam extends 8.53 m running parallel to the sheet pile wall in an east-west direction. The beams, 1626 mm by 406 mm, lay flat on either side of the shaft-sheet pile system. The beams web stiffeners, groups of 16 on each end and a group of 8 in the center, protect the beam from crippling.

The two steel beams, sandwiching the drilled shafts and sheet pile wall, are strapped to each other by (8) 64-mm high-strength, treaded bars. After post tensioning to 45 kN, the entire reaction foundation acts as an amalgamated unit 1.22 m south of the pile-pile cap system.

3.2.4 Loading Equipment

Between the pile cap and the reaction foundation, two hydraulic actuators were oriented north to south. Each actuator has the capacity to produce up to 2.7 MN of horizontal force as it expands and contracts. The actuators were attached to the center of the south face of the pile cap using four treaded bars which protruded from the concrete cap at the time of construction. This connection was designed so that the actuator would perform as an integral unit with the pile cap. The south end of the actuator was attached to the reaction foundation at the four treaded post-tensioned ties discussed above. Rotational joints on the actuator heads ensured moment free connections. Extension arms were added to the actuator so that the loading equipment could span between the reaction foundation and the pile cap system.

Dynamic loading on the pile cap was stimulated using an eccentrically loaded mass shaker. This mechanism imitates earthquakes through quick rotations of an off-balanced weight. Steel blocks may be added to the shaker in 0.08-kN increments to increase the force produced by the shaker. Adjusting the placement of these weights will also modify the force exuded by the shaker. The further away the weight is from the center of rotation the greater the shaker force. This offset distance is referred to as the eccentricity. The force the shaker produces is directly related to both the weight and its eccentricity in addition to the number of rotations per time. This equation may be written as follows:

$$F = 0.04016 \cdot (WR) \cdot f^2 \qquad \textbf{(3.1)}$$

where:

F = force produced by shaker, kN

WR = moment, weight multiplied by the its eccentricity, kN-cm

f = frequency, Hz

The term 0.04016 is an empirically derived factor specific to the model of shaker used. For this research, the shaker climbed to a maximum frequency of 10 Hz with weights offset to produce a 110.97 kN-cm moment. This configuration generated a maximum force of 446 kN. This force acted in the north-south direction, perpendicular to major supports and parallel to loading from the actuator.

The shaker's attachment to the pile cap was similar to the actuator's connection to the cap. In this case, treaded bars were positioned in the pile cap protruding from the top, centered. The shaker was supported directly on top of the cap and bolted in place. Thus, the shaker acted integral with the pile cap.

3.2.5 Instrumentation

An independent reference frame was constructed to provide an unmoving datum. Steel beams spanning the excavation were anchored in concrete unaffected by the actuator. The reference frame dissected the space between the pile cap and the stiff reaction frame directly above the actuators. Tension guide cables were used to stabilize the frame from any movement. However, during dynamic loading the ground in which the independent reference frame was anchored vibrated thus invalidating the measurements of instruments attached to the frame.

Mounted on the independent reference frame attaching to the pile cap face were four string potentiometers. Sting potentiometers measure real-time displacements by gauging the expansion or retraction of a cable connecting the potentiometer to the object under observation. In this manner, relative displacements could be evaluated during testing. Seven additional string potentiometers were attached to the pile cap and staked into the backfill.

Attached to the top of the pile cap in the corners, the center, and along the northern edge were triaxial accelerometers. These instruments measure accelerations in real-time. Accelerometers were independent from the reference frame which is critically important during dynamic loading when the reference frame began to vibrate. Accelerometers were also strategically positioned in the backfill at 0.61, 1.83, and 3.66 m north of the pile cap.

Earth pressure cells were used to measure contact pressures between the pile cap and the backfill. The Geokon Model 3510 Earth Pressure Cell was chosen for its ability to accurately measure dynamic soil pressures. This stainless steel, circular model was designed with two plates, a thick back plate and a thin upper plate. The thick back plate is designed to be in direct contact of the structure (ie. pile cap) and resist flexure through the earth cell induced by the dynamically loaded structure. This back plate protects against erroneous point loads from being measured by the pressure cell. The thin plate responds to the change in pile cap-backfill interface pressure. A depiction of the Geokon Model 3510 is shown in Figure 3-8. The pressure plates were also designed with a semi-conductor pressure transducer, as opposed to a vibrating wire transducer, to accurately measure pressures during dynamic loading.

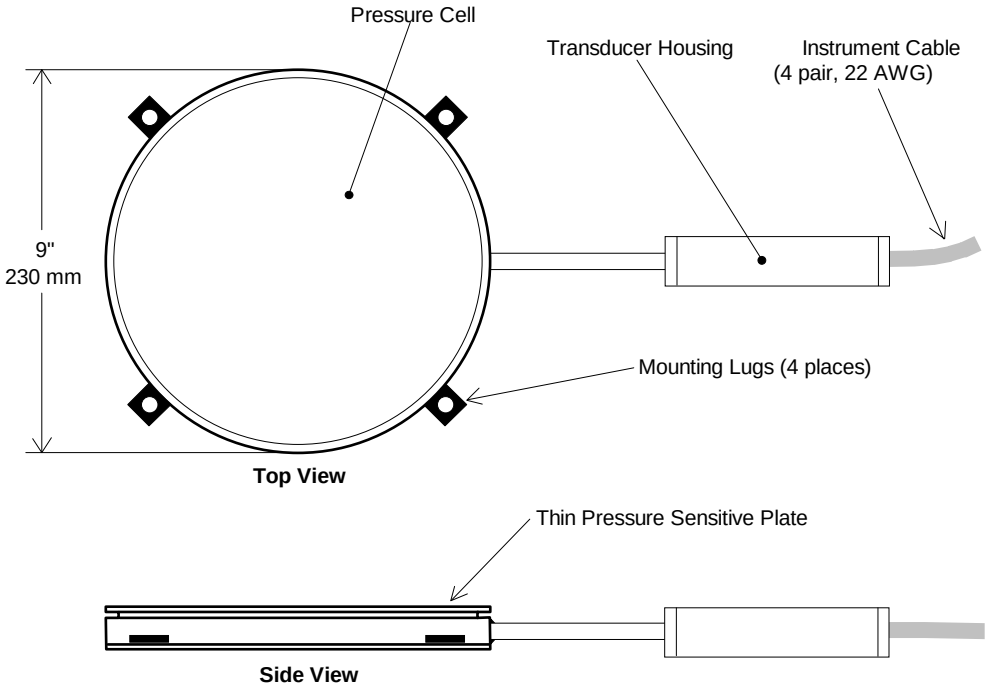

Figure 3-8 Geokon Model 3510 contact pressure cell (Geokon 2004)

Figure 3-9 Pressure plates constructed on the north face of the pile cap

Six Geokon 3510 Earth Pressure Cells were wet set flush into the north face of the pile cap during construction. The pressure plates were staggered within the central portion of the pile cap face located at depths of 0.14, 0.42, 0.7, 0.98, 1.26, 1.54 m from the top of the cap. Figure 3-9 shows the northern face of the pile cap with the pressure plates in position before the backfill was in place.

Lastly, a painted grid was outlined on the top of the backfill's surface after the backfill was in place and compacted according to specifications. The grid, spaced with 0.61-m square nodes, provided a means for visual inspection. The vertical displacements at each node were measured using traditional surveying methods and equipment.

3.3 Test Procedures

The pile cap with densely compacted sand backfill in place was loaded statically, cyclically, and dynamically. Each type of loading was completed according to the testing procedures described in this section.

After placement of backfill materials, the hydraulic load actuators were used to load and displace the pile cap to its initial target displacement level. After a several-second pause to manually record verification data, the actuators were used to apply 15 small amplitude displacement cycles (typically on the order of 2 mm (single amplitude) at 0.75 Hz). After returning the actuators to their starting pre-cycling positions, the lengths of the actuators were fixed, causing each actuator to act as a strut between the reaction and test foundations. The shaker was then activated and a dynamic stepped-ramp loading was applied. The ramped loading consisted of dwelling on a specified frequency for 15 cycles and then ramping as fast as possible to the next dwell frequency.

The dwell frequencies ranged from 1 to 10 Hz, in 0.5 Hz increments. Afterwards, the shaker was allowed to ramp back down. The duration of shaker operation was typically about 3½ minutes, which includes the ramp up and the ramp down to the stopped position.

Figure 3-10 displays a typical shaker frequency verses time relationship during dynamic loading. The dwelling periods are illustrated as the plateaus between increasing frequencies. As the frequency increases, the cycles occupy less time; therefore, the plateau lengths decrease as dynamic loading progresses. Noise at the beginning and ending of the dynamic loading are mechanical and ignored in the analysis.

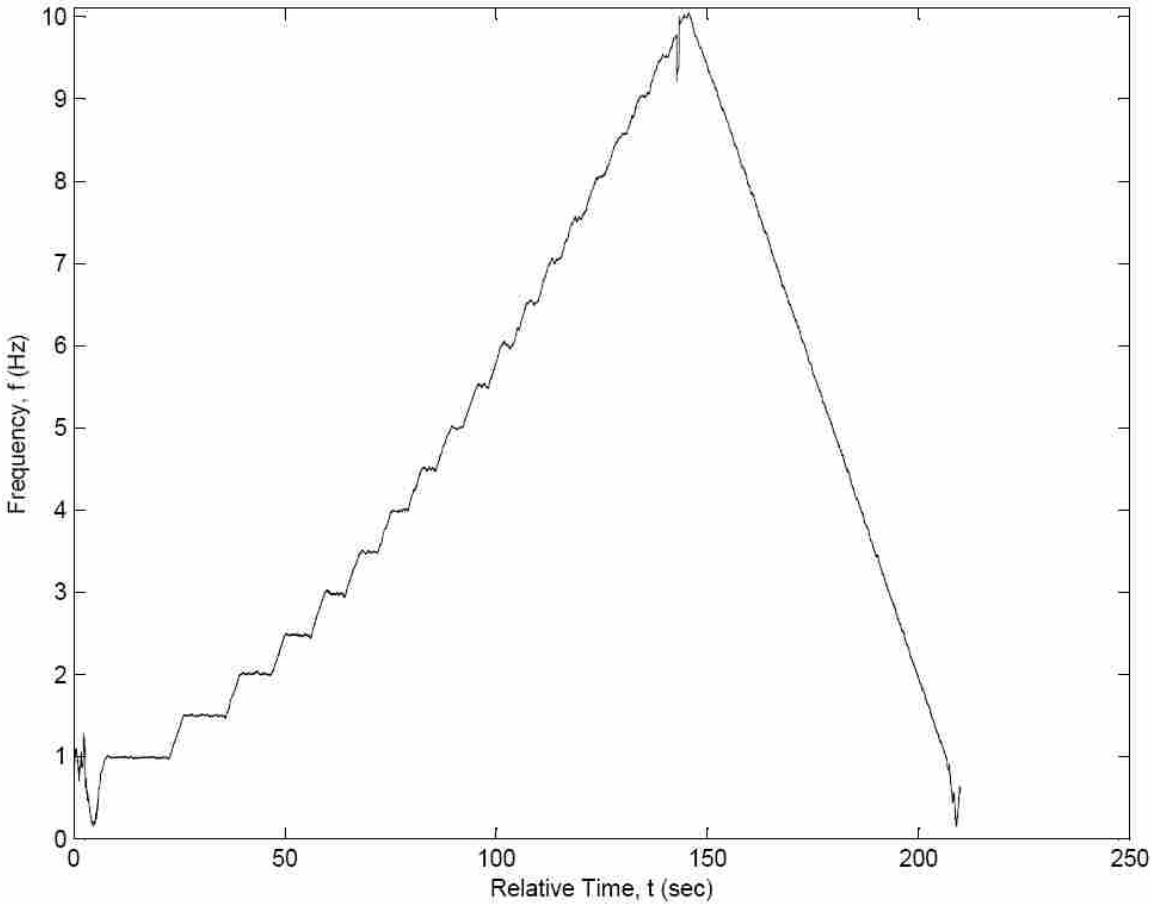

Figure 3-10 Typical forcing frequency verses time during dynamic loading

After cyclic and dynamic loading were completed the backfill was visually inspected, the actuators were extended again to push the pile cap to the next displacement level. Upon reaching the target displacement level, rather than having the actuators cycle first as was performed previously, the shaker was used with the actuator lengths fixed. Dynamic shaker loading was operated with the same prescribed frequencies as before.

After the shaker loading was completed, the actuators applied their cyclic loading as previously described. Hence, the use of cyclic actuator loads and dynamic shaker loads was alternated between each target displacement level throughout the testing program until the maximum target displacement was reached.

This process was repeated, expanding the actuator arms and then loading the pile cap with the actuators and shaker (alternating loading order at each pile cap displacement interval), for 11 displacement intervals. Throughout the entire test, data was continually being recorded. Measurements were made with a computer data acquisition system at a sampling rate of 200 samples per second (sps). The test data is organized under one of two categories. Notation for data during the dynamic loading is classified as a "Shake" followed by the pile cap displacement interval. The cyclic loading measurements are categorized as "Series" followed by the pile cap displacement interval.

Table 3-4 displays the organization of data in categories of Series and Shakes according to various pile cap displacements. For example, if backfill accelerations were recorded during dynamic loading while the actuators were locked in place at 16 mm, then these accelerations would be categorized as results in Shake 4. The fourth displacement interval encompasses all results from both Shake 4 (dynamic loading) and Series 4 (cyclic loading).

Table 3-4 Sequence of testing for each push

Displacement Interval	Displacement (mm)	Actuator Loading	Shaker Loading
1	2.8	First	Second
2	6.6	Second	First
3	11	First	Second
4	16	Second	First
5	22	First	Second
6	30	Second	First
7	37	First	Second
8	46	Second	First
9	53	First	Second
10	57	Second	First
11	64	First	Second

4 Methods of Analysis

This chapter describes the measurements collected from the lateral load test performed on the pile cap with dense sand backfill in place. The methods used to reduce measured data will be discussed, and the analytical methods used to interpret the reduced data will also be presented. The details of the testing procedure were presented previously in Section 3.3. Subsequent chapters will discuss the interpreted results.

Focus has been placed on pile cap displacement interval eight and nine for two primary reasons. First, previous research has concluded that displacements of 2 to 5% of the pile cap height are required to fully mobilize soil passive earth pressures (NCHRP 2008). For this pile cap (1.68 m deep), 2 and 5% equate to displacement levels of 33.6 and 84 mm. Push 8 and Push 9 begin at a pile cap displacement level of 46 mm (2.7%) and 53 mm (3.15%), respectively. In this case, inspection of the load-displacement curve by Cummins (2009) determined that passive pressure was fully mobilized at a displacement-to-pile-cap-height ratio of approximately 0.03, which corresponds to a displacement of about 50 mm. Hence, the displacement levels associated with the eighth displacement interval and subsequent displacement intervals are in the range where passive earth pressures are expected to be fully mobilized. At lower displacement levels, passive pressure is largely a function of displacement, and cyclic and dynamic loading effects are difficult to separate. Additionally, even and odd numbered displacement

intervals reflect different loading conditions. During the even-numbered displacement intervals, the dynamic loading from the shaker is performed first as opposed to the odd-numbered displacement intervals during which the cyclic loading from the actuator is performed first. Because of this alternating order, data obtained during the second half of the loading sequence (cyclic loading if even and dynamic loading if odd) are based off of non-virgin (i.e., previously loaded and affected) soil conditions.

4.1 Data Reduction

4.1.1 Pile Cap Displacements

The data collected by string potentiometers during cyclic loading conditions will be reviewed first followed by displacements collected by string potentiometers during dynamic loading conditions. In addition, accelerations measured by accelerometers were reduced into displacements. The reduction and importance of these acceleration based displacements will be presented.

With respect to sign convention, the string potentiometer data has been adjusted such that positive pile cap displacement values represent northward displacements, in the direction of the actuator thrust during static loading. When accelerometer data was recorded, positive values represented accelerations in the north direction. After integrating these accelerations to determine displacements, positive values likewise represented displacements in the north direction. However, positive displacements measured by string potentiometers at first represented displacements in the south direction. String potentiometer signs were reversed to make the displacements compatible with the accelerometer data (the relationship between accelerations and

displacements will be explained at a later point in this section). To assure the correctness and consistency of the displacement data from both string potentiometers and accelerometers, the pressure plate data was examined during the static pushes as well as the slowly applied cyclic loadings. During the slow actuator loadings, dynamic effects are expected to be minimal and the measured pressures should increase as the pile cap moves northward into the soil backfill.

Figure 4-1 displays a sample of measured pressures during cyclic loading. This sample does not include any adjustments to either the string potentiometers or the pressure plates. The general trend in contact pressure is to increase with increasingly negative displacements. Since pressure should increase with northward pile cap movement, displacements measured by string potentiometer originally measured northward pile cap displacements as negative.

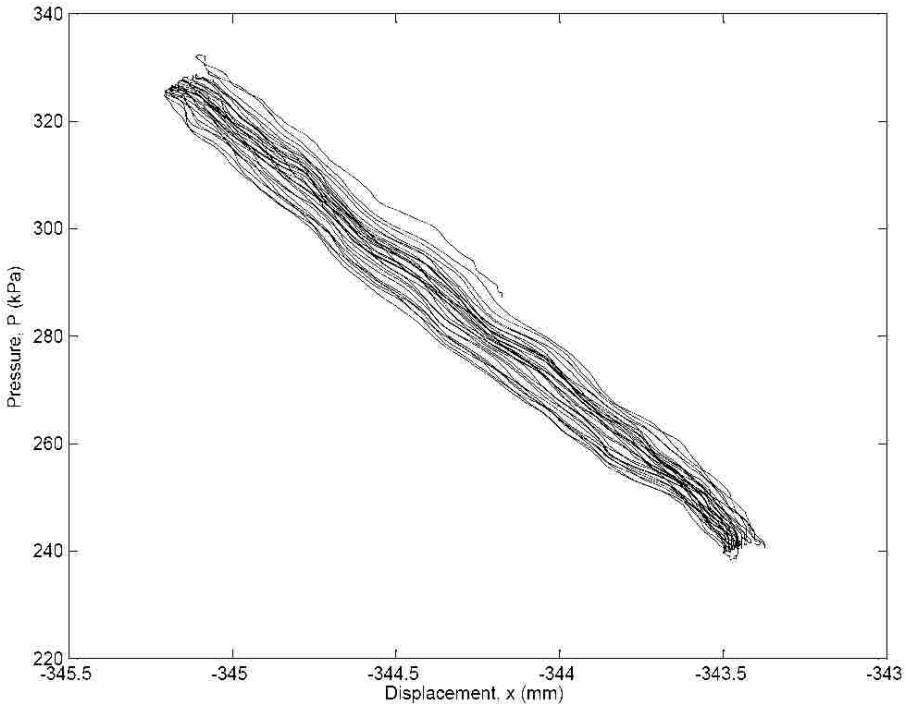

Figure 4-1 Pressure verses string potentiometer displacements during cyclic loading

When the string potentiometer displacements were reversed to display northward movement as positive, the string potentiometer displacements generally aligned with displacements measured by other means. For example, Figure 4-2 compares reversed string potentiometer measured displacements to double integrated acceleration displacements throughout the duration of a cyclic loading test. The reversed string potentiometer displacements peak in a similar trend as the double integrated accelerations displacements.

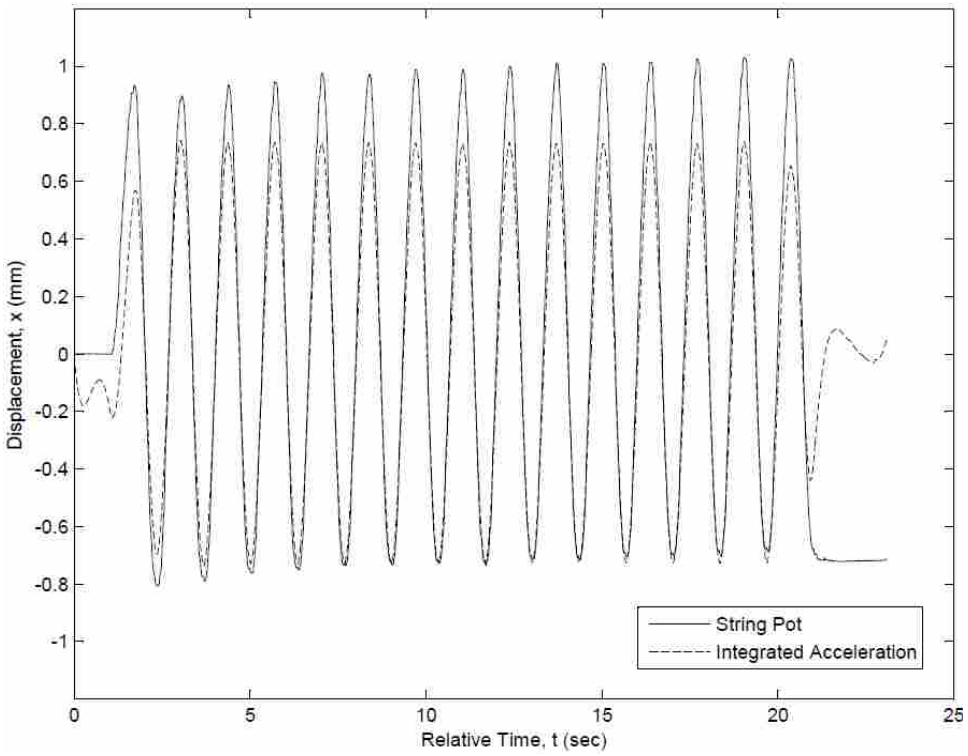

Figure 4-2 Reversed string potentiometer displacements and accelerometer derived displacements during cyclic loading

4.1.1.1 Displacements during Cyclic Loading

Measured displacements during cyclic loading exhibited similar displacement patterns at each pile cap displacement interval. Figure 4-3 and Figure 4-4 display cyclic loading displacements during Series 8 and Series 9, respectively. In each figure, the load series are represented with an initial displacement corresponding to the displacement interval of the pile cap (refer to Table 3-4).

A typical cyclic loaded displacement pattern begins with a brief quiet period. Then the actuators start to expand and retract according to the prescribed test procedure. The actuators cycle 15 times shown as 15 distinct peaks in the corresponding figures. The wavelength between peaks is approximately 1.33 seconds which agrees with the prescribed actuator cyclic frequency of 0.75 Hz. After the actuators have expanded and contracted 15 times the retracted position was held constant before the pile cap was returned to its displacement interval position.

While the general pattern of cyclic displacements remains constant at each pile cap displacement interval, a few distinct differences may be highlighted by the comparison of Series 8 and Series 9. During Series 8 the pile cap displaces between 45.2 and 47 mm north from its unloaded position (prior to the first displacement interval). This is a 1.8 mm spread between the maximum and minimum displacement. During Series 9 the pile cap displacements range from 52.2 to 54.2 mm north of the unloaded pile cap position, a 2 mm spread throughout loading.

The difference between Series 8 and Series 9 displacement spread is largely attributed to the residual offset occurring during each cyclically loaded displacement interval. The pile cap is being displaced further north into the backfill with each actuator

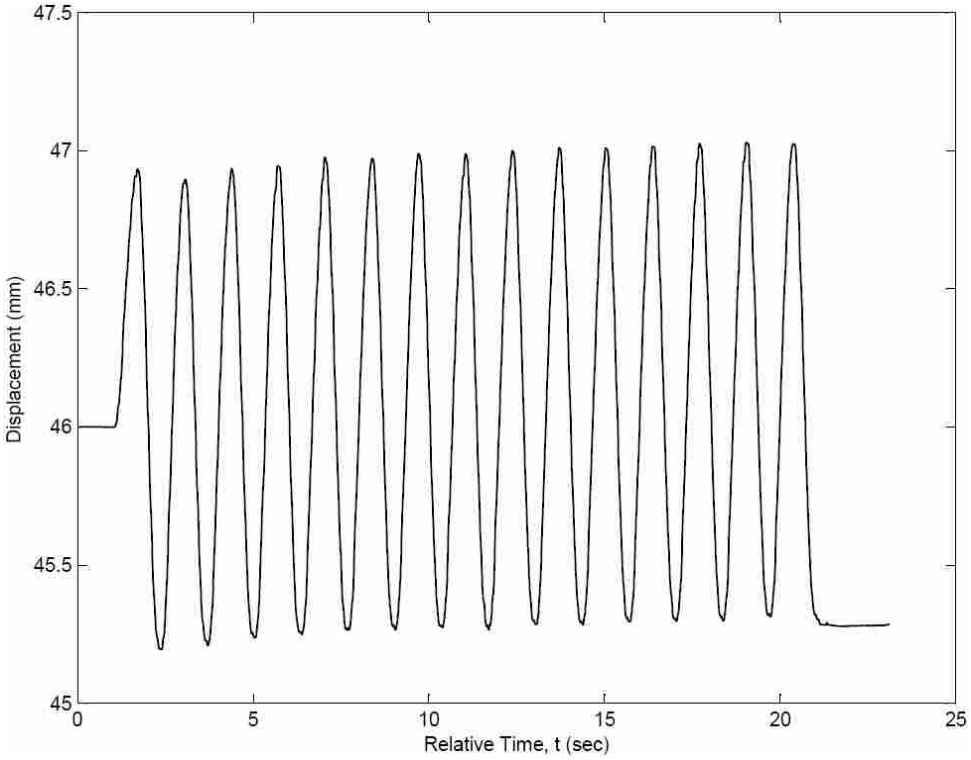

Figure 4-3 Pile cap displacements recorded by string potentiometer, Series 8

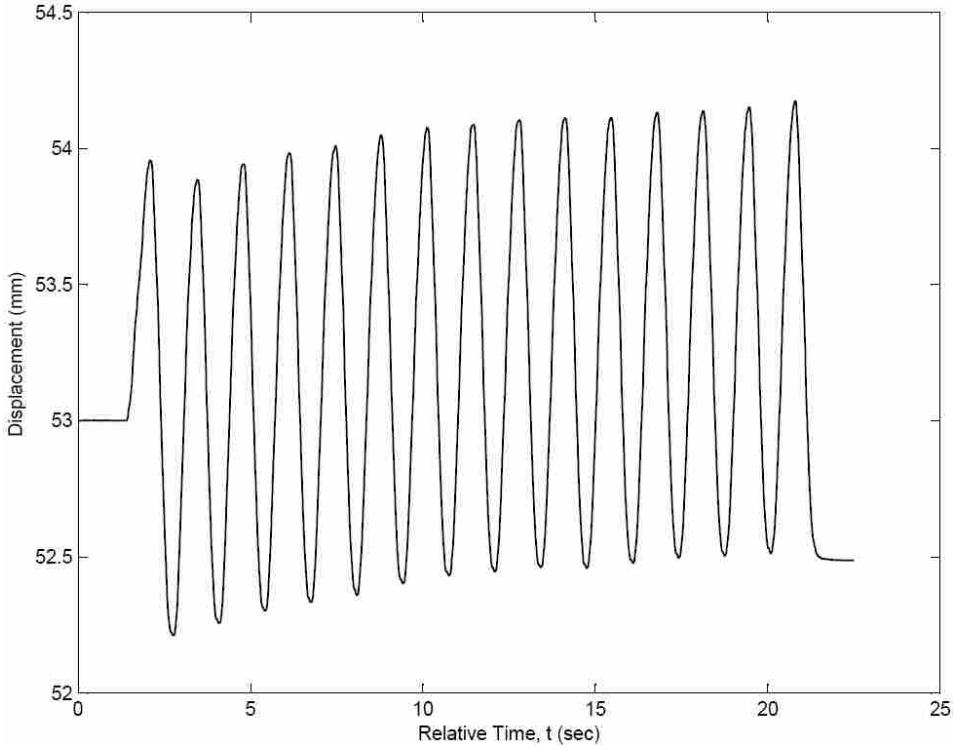

Figure 4-4 Pile cap displacements recorded by string potentiometer, Series 9

cycle. This offset may be observed in both Figure 4-3 and Figure 4-4 as the displacement peaks gradually become increasingly positive. The displacements in Series 8 and Series 9 offset approximately 0.12 and 0.29 mm, respectively. This expected difference originates from the alternating loading sequence for even and odd displacement intervals.

4.1.1.2 Displacements during Dynamic Loading

Like cyclic displacements, typical dynamically loaded pile cap displacements have correlating trends and patterns. Figure 4-5 and Figure 4-6 show a string potentiometer measured displacements during Shake 8 and Shake 9, respectively. The pile cap at the beginning of Shake 8 has previously been displaced 46 mm into the backfill from the unloaded pile cap position. Shake 9 begins at a displacement of 53 mm from the unloaded pile cap position.

As the eccentrically loaded mass shaker began to ramp up, the dynamic forces jerked the pile cap back and forth. At first this motion minimally displaced the pile cap. As the test progressed, the increasing bandwidth (the difference between minimum and maximum displacement at a specific time) on the figures signifies increasing pile cap displacement. Once the shaker began to ramp down, the displacement bandwidth decreased until the dynamic loading concluded.

During dynamic loading, the ground surrounding the excavation shook including the independent reference frame. Since string potentiometers measure the distance between the pile cap and the independent reference frame, erratic peaks and dips in Figure 4-5 and Figure 4-6 are likely caused by the vibratory reference frame position. Therefore, local displacements measured by string potentiometers during dynamic loading at every displacement interval are considered erroneous.

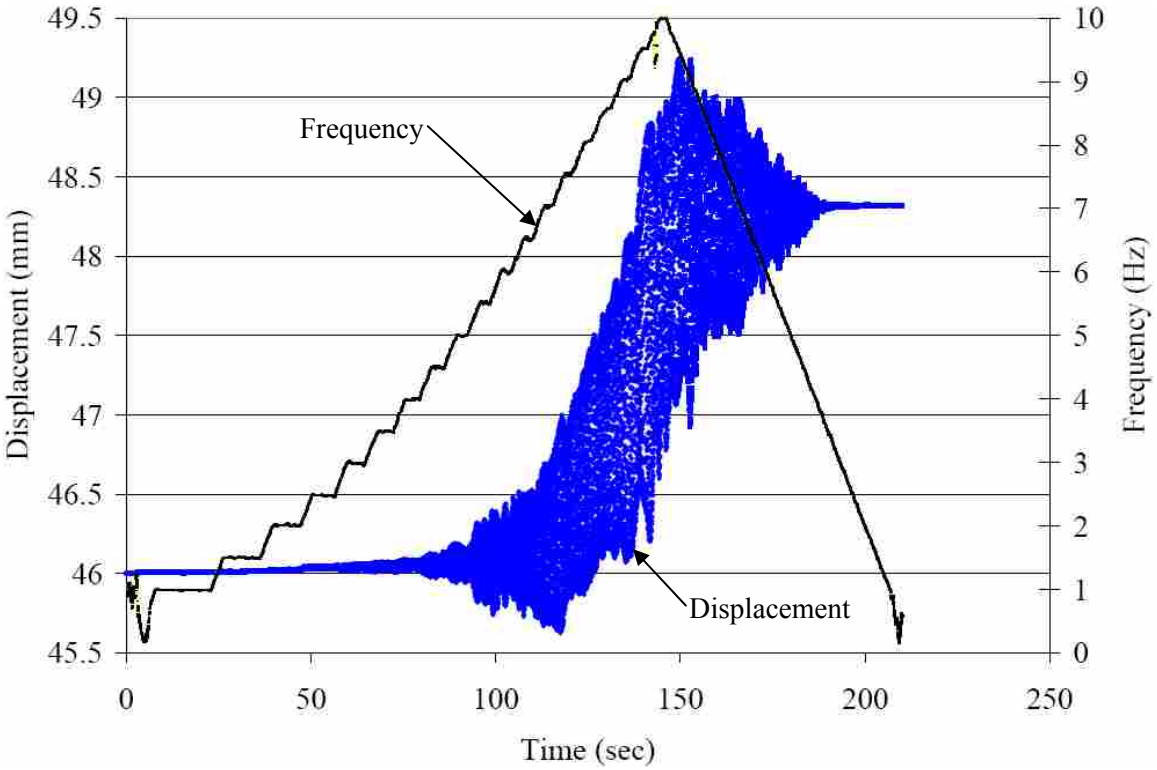

Figure 4-5 Pile cap displacement time history recorded by string potentiometer, Shake 8

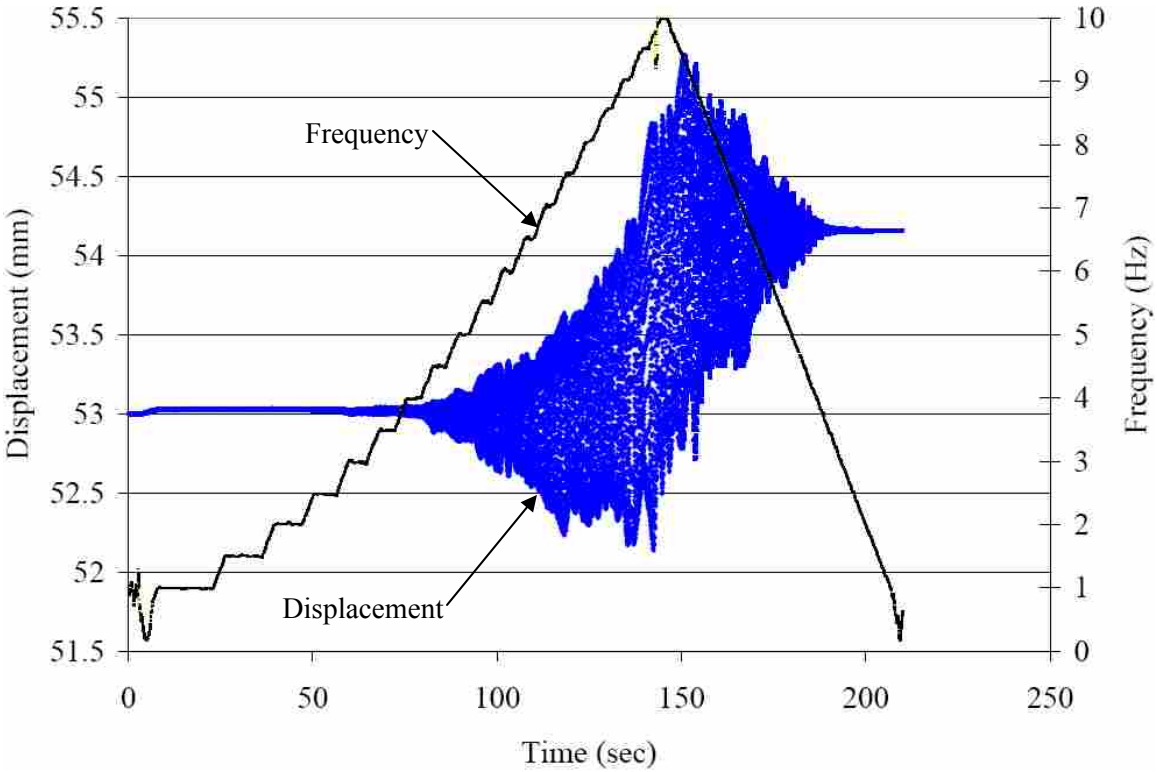

Figure 4-6 Pile cap displacement time history recorded by string potentiometer, Shake 9

One relationship measured from the string potentiometers during dynamic loading that is considered accurate is the total offset of the pile cap throughout dynamic loading. The position of the independent reference frame before and after dynamic loading did not change. However, neither Figure 4-5 nor Figure 4-6 show the pile cap ending in its starting position. Figure 4-5, for example, shows the final pile cap location 48.4 mm north from the unloaded pile cap position despite the pile cap being displaced only 46 mm north at the beginning of the dynamic loading. This means that during Shake 8 the pile cap displaced an additional 2.4 mm north. Likewise, during Shake 9, the pile cap displaced an additional 1.16 mm north.

4.1.1.2.1 Integrating Accelerations

Dynamic accelerations on the pile cap are directly related to the shaker frequency. Figure 4-7 is one example of the pile cap accelerations during dynamic loading. In this figure, the accelerations are symmetrical about the x-axis origin signifying that accelerations induced by the mass shaker were approximately equal in both the north and south direction. The peak acceleration of the pile cap occurs just before 150 seconds which corresponds to the maximum shaker frequency, 10 Hz. The cap maximum acceleration occurs at 10 Hz during dynamic loading at every pile cap displacement interval.

One method to obtain accurate displacements during dynamic loading is to double integrate accelerations. Accelerations were integrated using MatLab programming by the following process:

1. Raw data accelerations taken at 0.005 second intervals (200 sps) were uploaded
2. Accelerations were processed using a forward and backward FIR filter

3. Velocities were derived by summing trapezoidal areas using time periods of 0.005 seconds
4. Velocity units were converted into inches per second
5. Velocities were processed using a forward and backward FIR filter
6. Displacements were derived by summing trapezoidal areas using time periods of 0.005 seconds
7. Data file was exported with displacements in inches

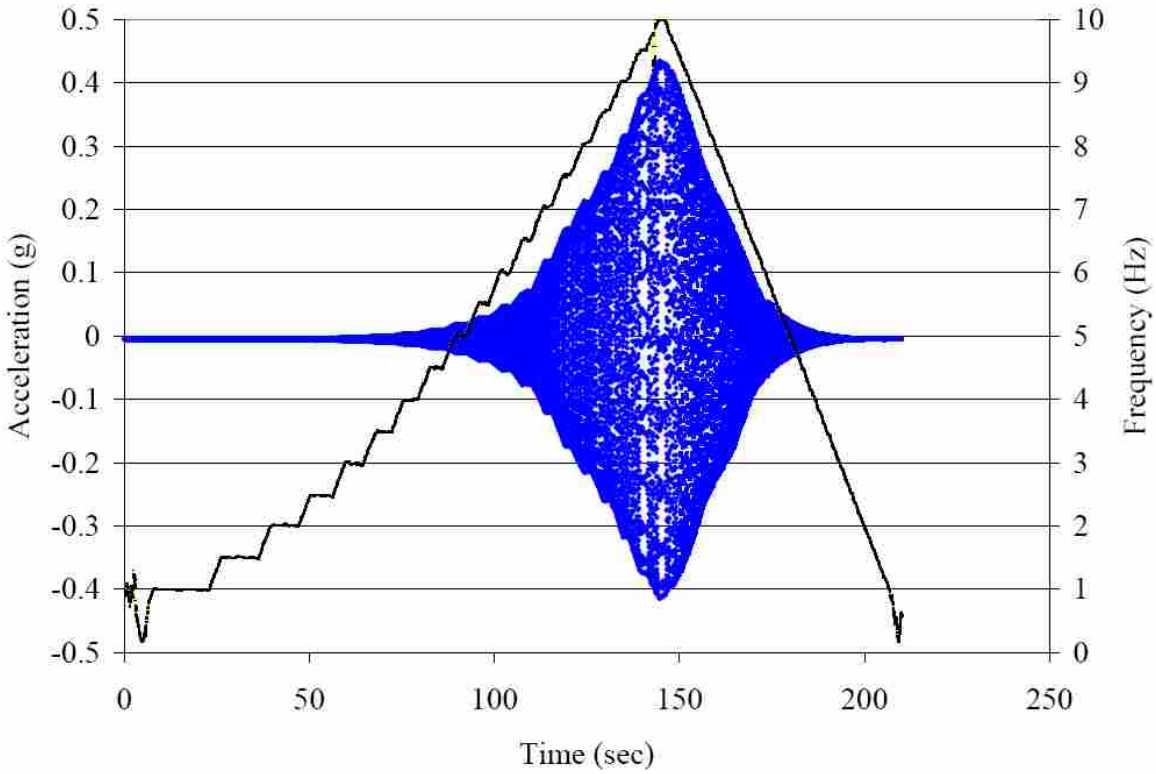

Figure 4-7 Typical pile cap accelerations time history due to dynamic loading, Shake 8

A finite impulse response (FIR) filter was used for its unique ability to filter displacements without shifting the time interval of those displacements. Unlike a typical Butterworth filter which attempts to remove peaks by mathematically flat-lining data, a

FIR filter eliminates potential group delay or phase distortion. Using the FIR filter and the trapezoidal integration method, pile cap accelerometer accelerations were integrated into displacements for all eleven displacement intervals.

A typical plot of integrated acceleration displacements is shown in Figure 4-8. This specific figure was created using displacements calculated by double integrating Shake 8 accelerations. The displacements directly follow the accelerations pattern of the mass shaker which was presented in Figure 4-7. Displacement magnitudes are symmetric about the pile cap position at the beginning of the dynamic loading. Therefore, the acceleration based displacements do not account for any residual offset (i.e., the displacements end at the same position as the displacements begin at the start of the

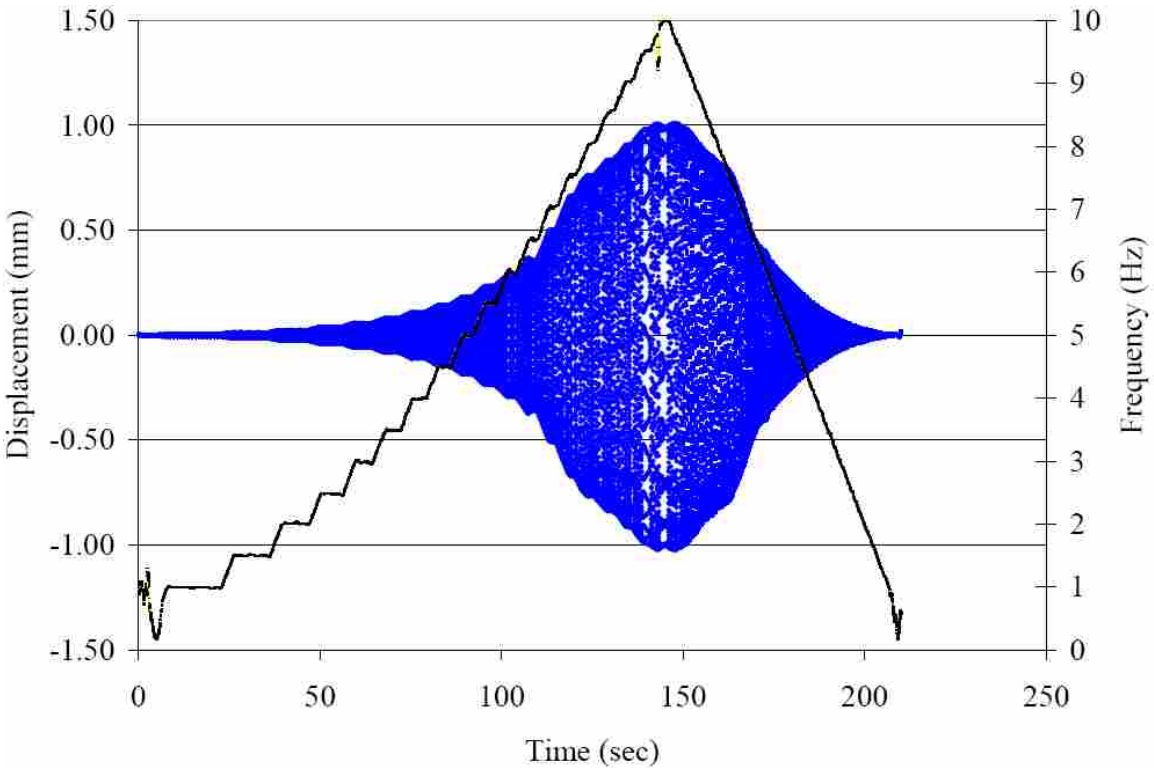

Figure 4-8 Typical displacements calculated from double integration of accelerometer data

dynamic loading). The peak displacement and peak acceleration directly correspond at a forcing frequency of 10 Hz.

Using integrated accelerations for displacements suggests that the dynamic displacements at every pile cap displacement interval are generally the same with a peak value of about 1 mm. As shown during cyclic loading conditions each cycle displaced about the same magnitude regardless of the number of previous cycles or the alternating loading sequence between even and odd displacement intervals. However, overall offset throughout the cyclic loading series did vary between displacement intervals and alternating loading conditions. Therefore, displacements calculated by integrating acceleration are accurate in amplitude but do not account for pile cap offset during dynamic loading.

4.1.1.2.2 Accounting for Residual Offset

Since the string potentiometer displacements accurately account for the overall offset (residual offset) and the acceleration derived displacements produce accurate displacement magnitudes, combining the two displacement groups will result in accurate pile cap displacements induced by the shaker.

The procedures used to superimpose string potentiometer displacements and acceleration based displacements are the following:

1. String potentiometer displacements were forced to start at zero displaying relative displacements
2. String potentiometer displacements were filtered using a FIR filter to produce a single trendline
3. Filtered displacements were added to the acceleration based displacements

To further explain this process the steps will be illustrated, compared, and contrasted during Shake 8 and Shake 9.

Figure 4-9 and Figure 4-10 show the same string potentiometer displacements presented in Figure 4-5 and Figure 4-6. The displacements were translated to initially begin at zero. The same erratic peaks and dips caused by the vibrating independent reference frame still exist. The relative offset remains the same – 2.4 mm during Shake 8 and 1.3 mm during Shake 9.

Figure 4-12 and Figure 4-13 display the second step in determining accurate displacements during the dynamic loading. A FIR filter, depicted in Figure 4-11, was processed through the string potentiometer displacements. The outcome was a single trendline which has a zero phase distortion. At this point in the process the string

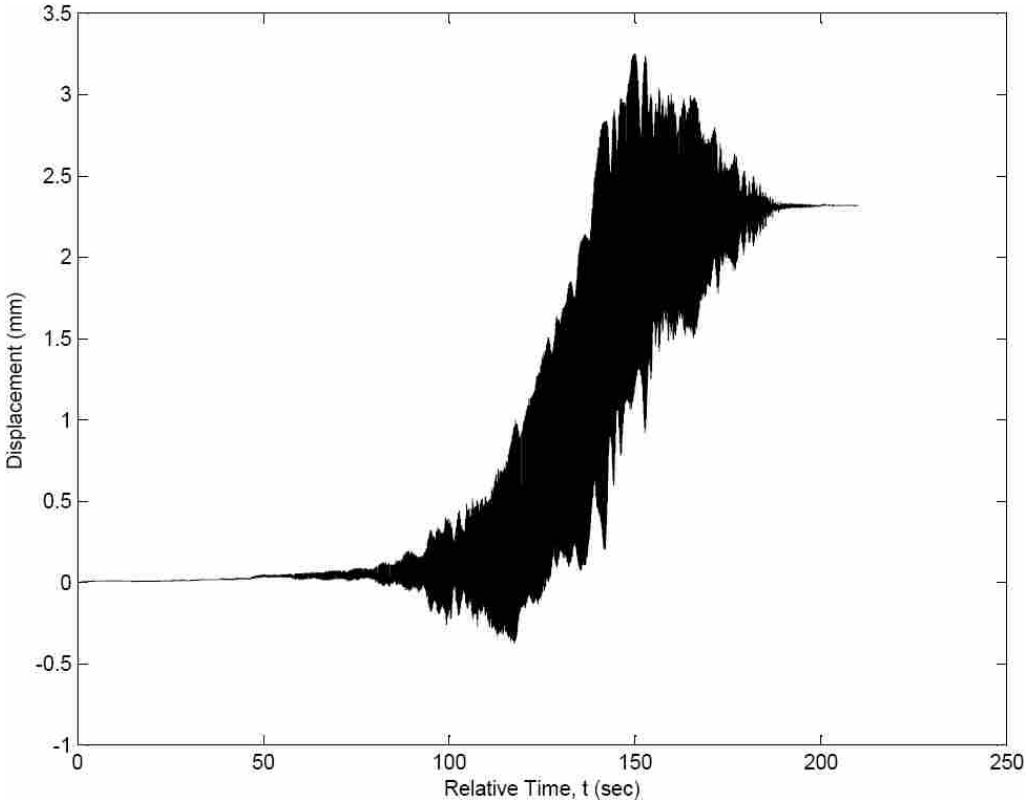

Figure 4-9 Cap displacement time history based on string potentiometer data, Shake 8

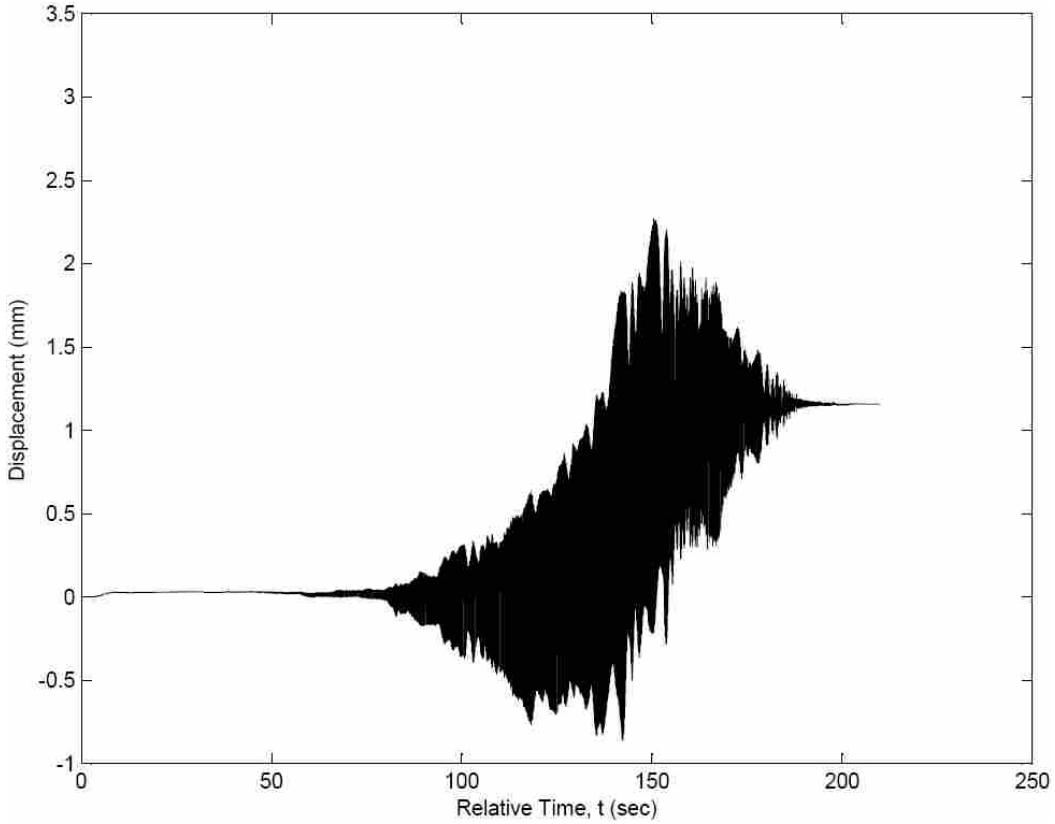

Figure 4-10 Cap displacement time history based on string potentiometer data, Shake 9

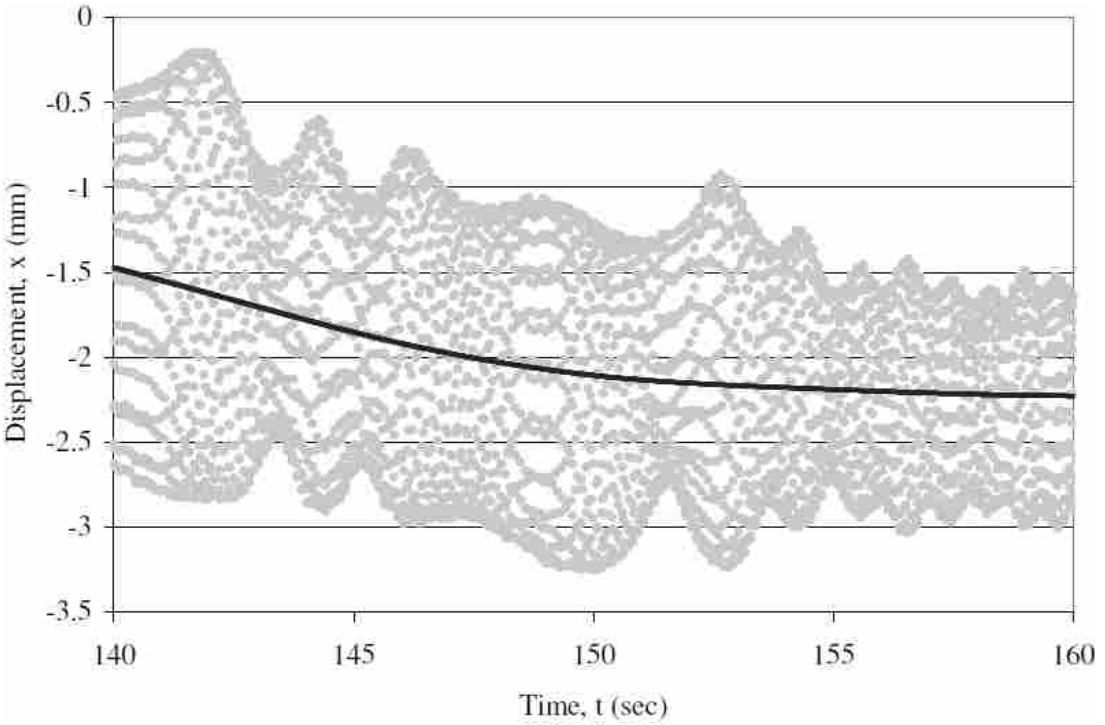

Figure 4-11 Trendline showing overall offset in sample of cap displacement data during dynamic loading

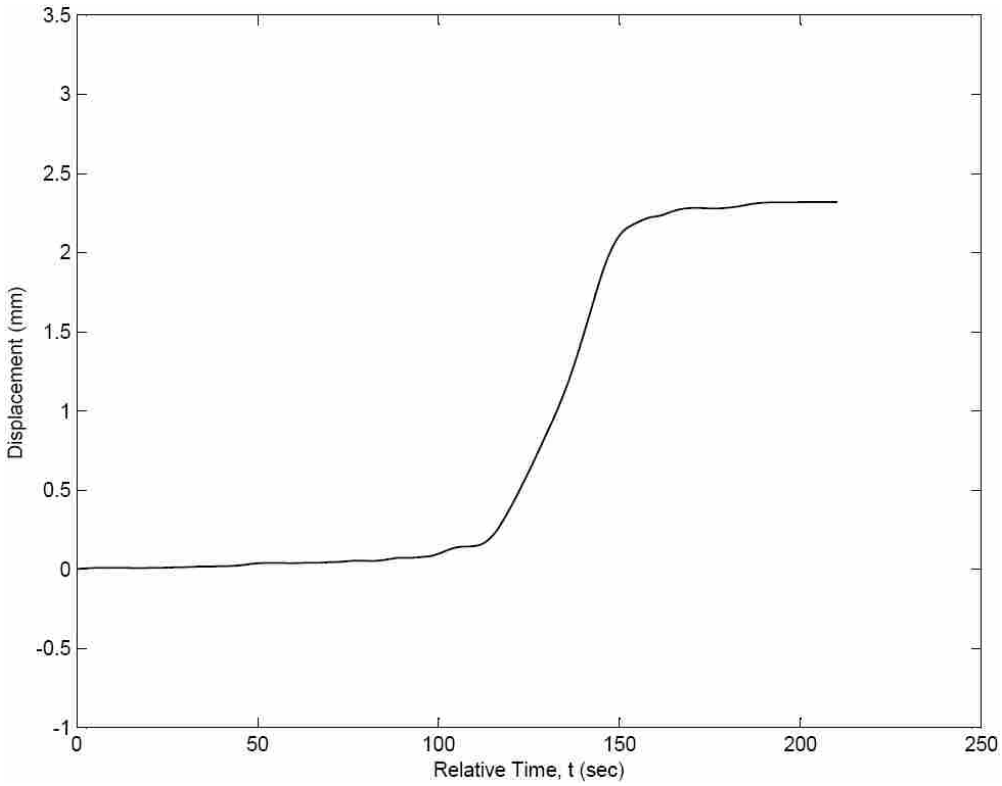

Figure 4-12 Overall trend of displacement data based on string potentiometer data, Shake 8

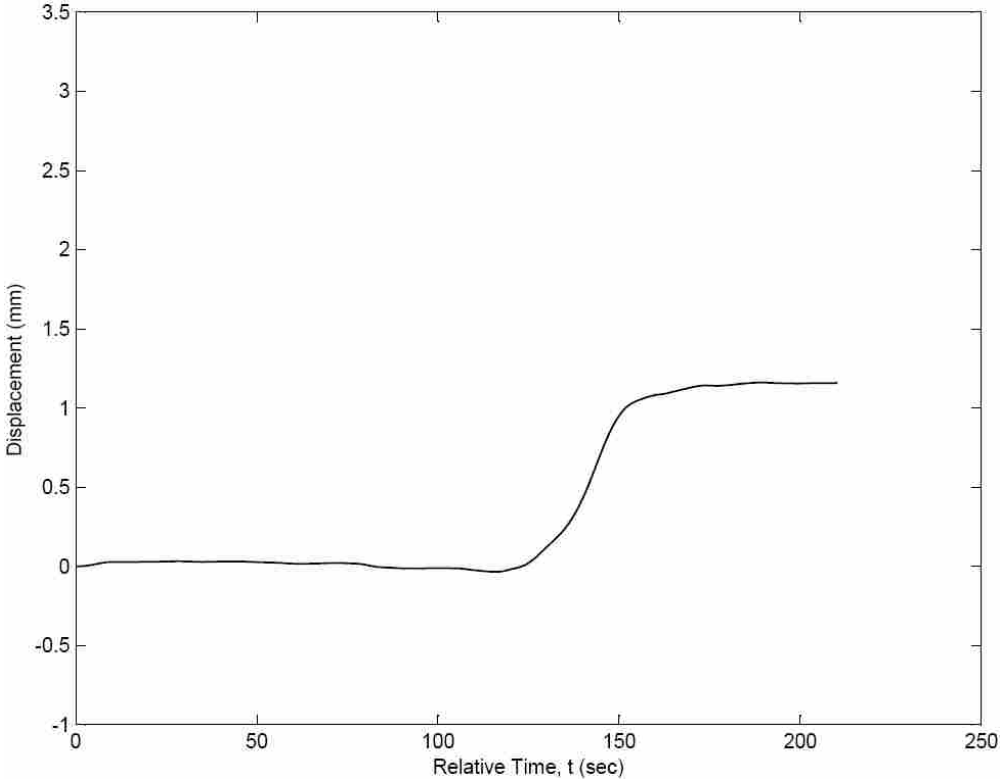

Figure 4-13 Overall trend of displacement data based on string potentiometer data, Shake 9

potentiometer displacements begin at zero displacement, maintain their respective offsets (2.4 and 1.3 mm for Shake 8 and Shake 9, respectively), and are represented as a trendline.

The displacements originating from accelerometer measurements are then combined with the trendline displacements, resulting in the displacement time histories shown in Figure 4-14 and Figure 4-15. These figures resemble the typical displacements shown in Figure 4-8 but now including 2.4 and 1.3 mm offsets between the beginning and ending of the dynamic loading as measured by the string potentiometers during Shake 8 and Shake 9, respectively. These combined displacements represent the pile cap displacements as they are believed to have occurred during testing.

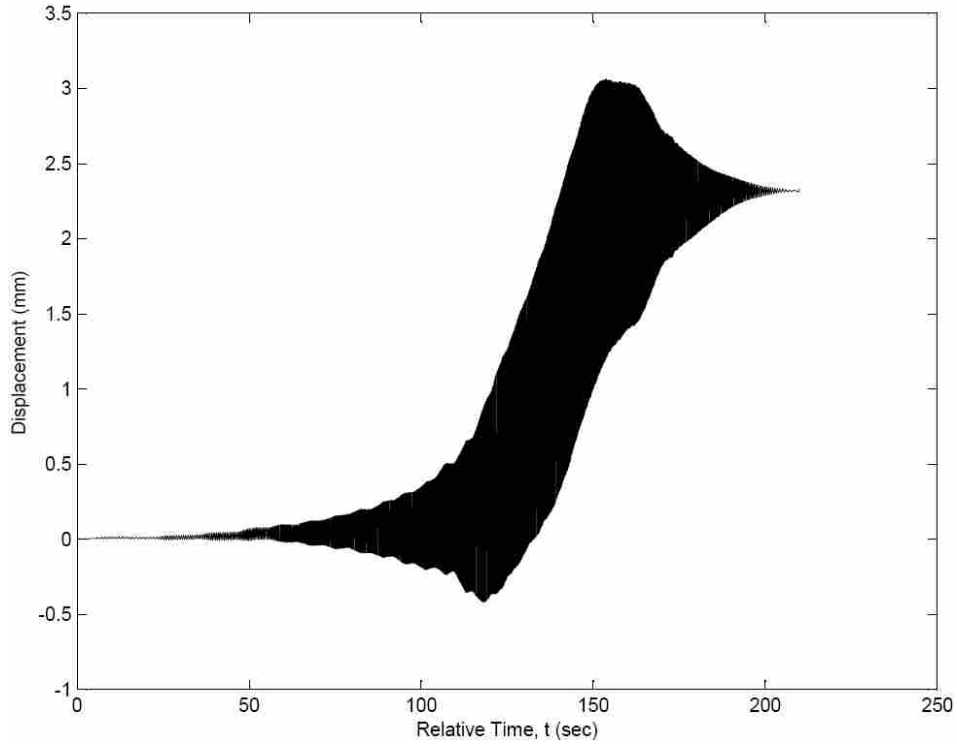

Figure 4-14 Cap displacement time history based on accelerometer-derived displacements corrected for offset, Shake 8

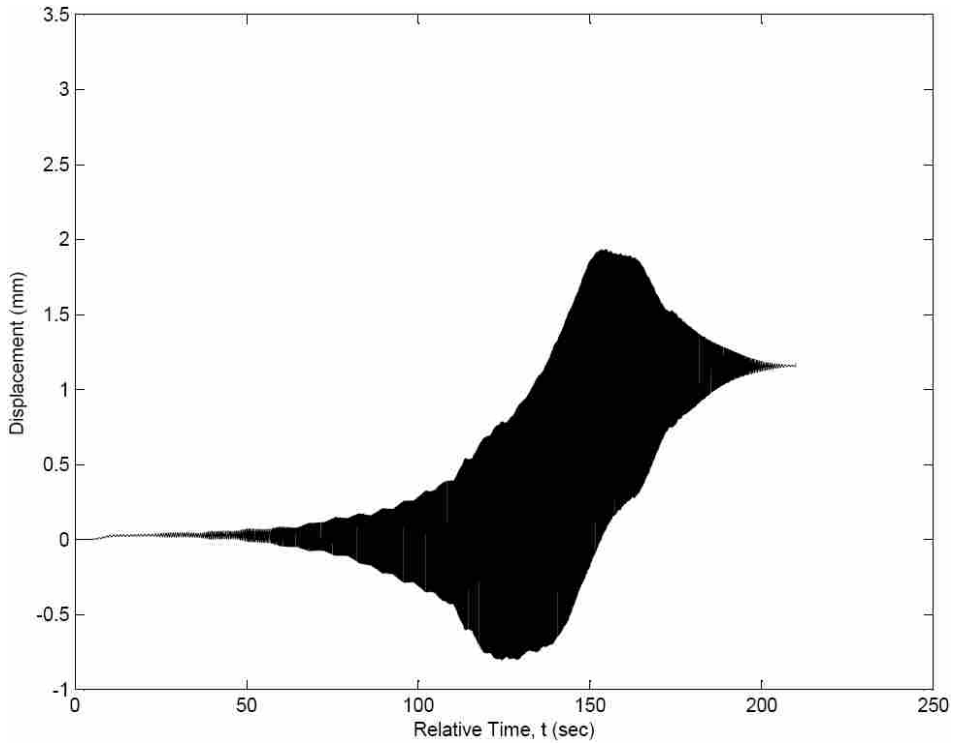

Figure 4-15 Cap displacement time history based on accelerometer-derived displacements corrected for offset, Shake 9

4.1.2 Passive Earth Pressures and Forces

In this research, passive earth pressure develops between the northern face of the pile cap and the backfill soil. This contact pressure is measured by the pressure plates located in the pile cap face. The specifications and layout of the pressure plates were discussed in Section 3.2.4. The plates are referenced in numerical order from Pressure Plate 1 to Pressure Plate 6, starting with the uppermost pressure plate located 0.14 m below the top of the pile cap and continuing with increasing depth. The depth of each pressure plate is shown in Table 4-1.

Static contact pressure was initially introduced as the backfill was placed in the excavation. Once the backfilling operation was completed and the testing started, the

Table 4-1 Depth to pressure plates

Plate Number	Depth (m)
1	0.14
2	0.42
3	0.70
4	0.98
5	1.26
6	1.54

actuators displaced the pile cap into the backfill. With each pile cap displacement interval, static pressure increased. The resulting pressure distributions corresponding to the end of each static push are shown in Figure 4-16. As shown in the figure, the measured pressures generally increased with depth. This aligns with accepted static soil pressure distribution theories. However, the deepest pressure plate (referred to as Pressure Plate 6 in this thesis) does not follow this trend.

A few possibilities may explain the seemingly questionable measurements from Pressure Plate 6. One possibility could be that the backfill was not firmly compacted against the plate. The measured pressure would be unexpectedly low with minimal contact area between the soil and pressure plate. However, since pressures measured by Pressure Plate 6 increase initially (between the first and second pile cap displacement interval) this explanation is not likely. Another explanation for the low pressures might be that the pile cap rotated during loading (the top of the pile cap displacing further into the backfill than the bottom of the pile cap). Douglas and Davis (1964) state that a 0.1° rotation (2.8 mm for this pile cap) would be sufficient for the bottom pressure plate to measure no increase in pressure. However, the observed cap rotation during testing was significantly less than the 0.1° rotation needed to produce such a significant decrease in pressure at the bottom of the pile cap. It is possible, and most probable, that the pressure

cell was damaged in some way or that, being near the location where a pile is embedded into the cap, an interaction between the end of the embedded pile and the concrete of the cap near the cell produced stress on the back side of the pressure cell which led to inaccurate measurements.

The top pressure cell also appears to not entirely follow the trend, reaching a plateau at about 125 kPa at a displacement of about 37 mm, and then decreasing slightly in pressure to 110 kPa during the last four pile cap displacement intervals. The peak value in the top pressure cell generally coincides with the displacement level at which the backfill appears to reach its ultimate strength, with the lower cells (excluding the bottom one) showing progressively smaller gains in pressure with increasing displacement.

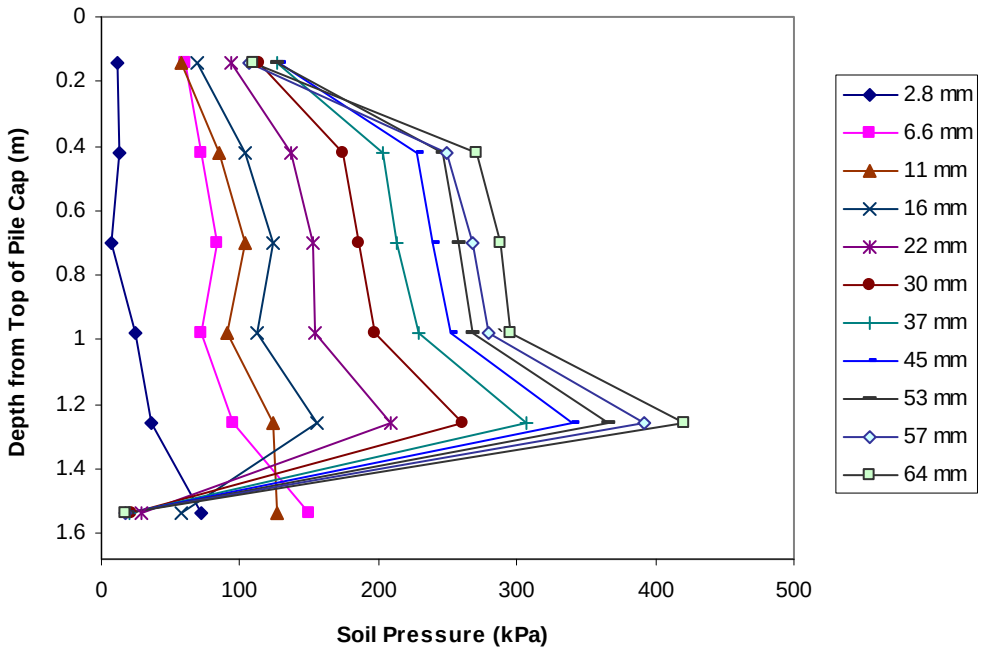

Figure 4-16 Earth pressure distribution as a function of pile cap displacement

In addition to pressures measured under static loadings, pressures were measured during both cyclic actuator loading and dynamic shaker loading. Figure 4-17 and Figure 4-18 show pressures measured by each pressure plate during Series 8 and Series 9, respectively. The pressures, with the exception of those measured from Pressure Plate 6, increase with depth, consistent with the trends observed during the static loadings. The pressures during Series 9 do drift (i.e., decrease) slightly which directly corresponds to the displacement offset observed during Series 9.

Figure 4-19 (Shake 8) and Figure 4-20 (Shake 9) display typical dynamic pressure measured by the pressure plates. As the dynamic loading begins, pressure measurements oscillate sinusoidally in response to the applied load. The pressure spread, the difference between a local maxima and minima, slowly increases as each of the dynamic loading sequences 7 Hz (120 seconds). Nearing 120 seconds there is a shift in the pressure trend. At this point, the maximum pressures begin to decrease and the minimum pressures decrease more rapidly than before. The spread of pressure continues to widen with increasing shaker forcing frequency. For dynamic loading at both pile cap displacement intervals (Shake 8 and Shake 9), the minimum pressure occurs around 150 seconds which equates to a frequency of 10 Hz (the maximum shaker frequency). The maximum pressure, however, does not occur at this point. After the minimum pressure, the spread between maximum and minimum pressures decreases as the mass shaker ramps down. This behavior is more fully examined and discussed in Chapter 6. Shake 8 exhibits significant offset between starting pressures and ending pressures. Shake 9 shows only a slight offset measured only by a few of the pressure plates. Recall that during Push 8 the shaker loaded the pile cap first. Thus, during Shake 8 the pile cap and backfill were

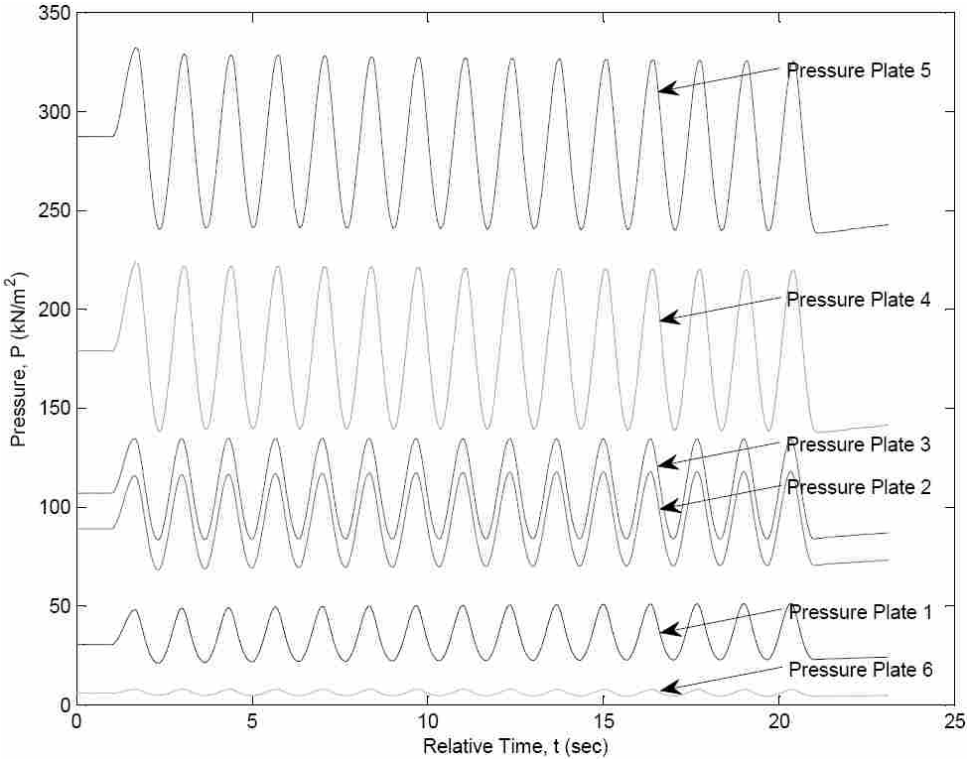

Figure 4-17 Cap pressure time history measurements during cyclic loading, Series 8

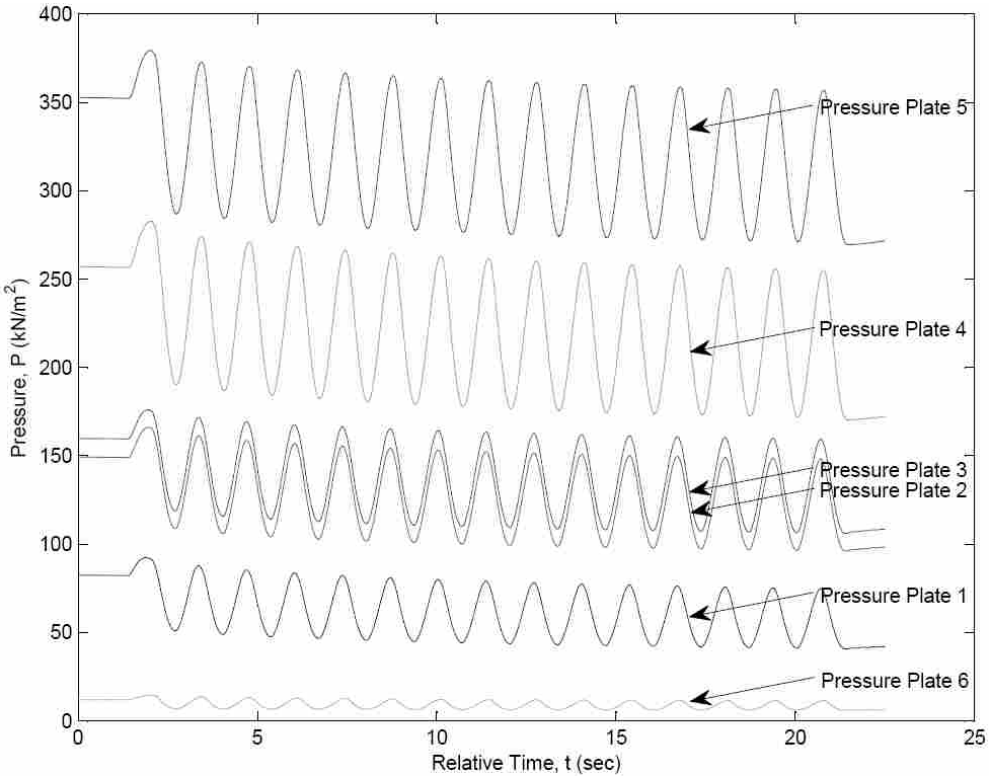

Figure 4-18 Cap pressure time history measurements during cyclic loading, Series 9

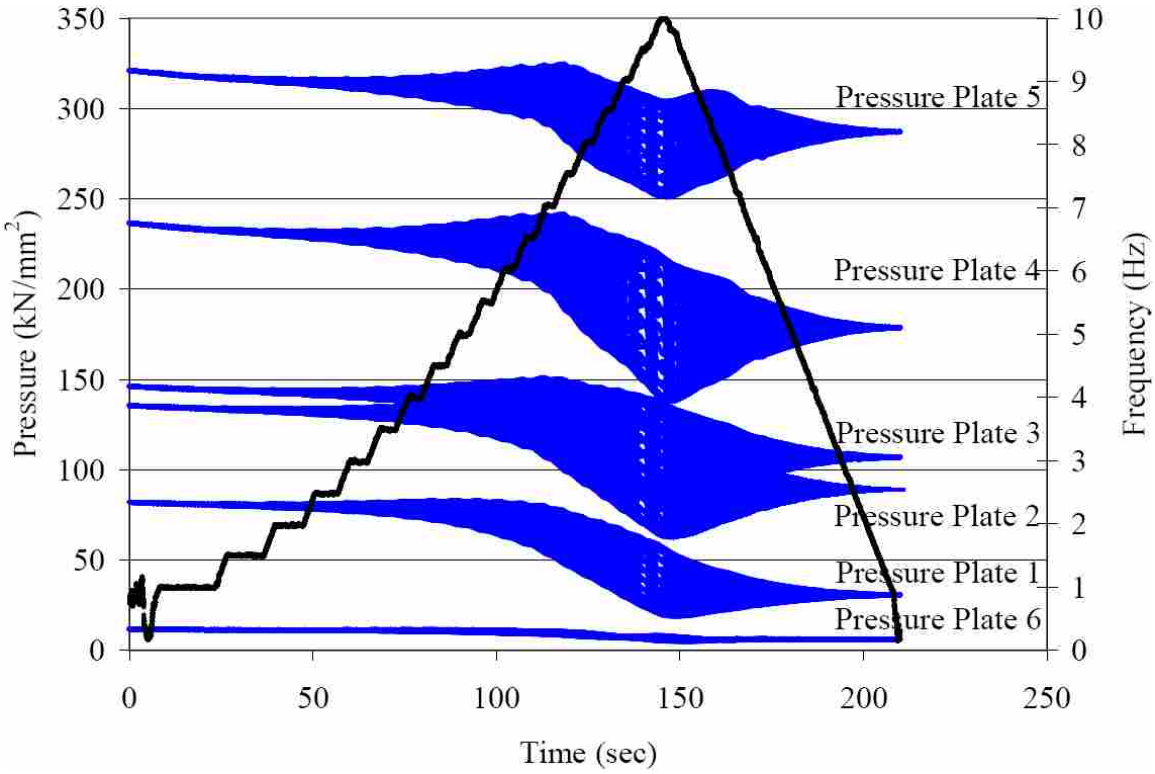

Figure 4-19 Cap pressure time history measurements during dynamic loading, Shake 8

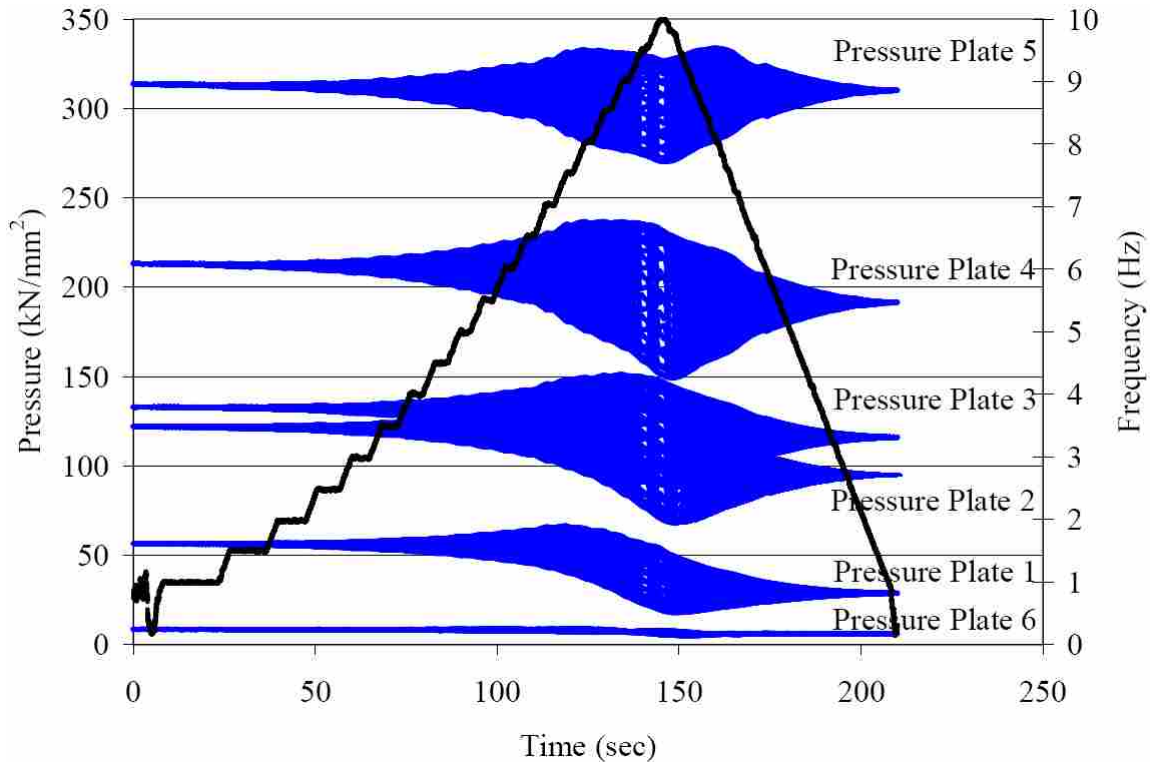

Figure 4-20 Cap pressure time history measurements during dynamic loading, Shake 9

being displaced further than at any other prior time during testing. This was not the situation during Shake 9 when the actuators loaded the pile cap and backfill at that pile cap displacement interval before the shaker.

To facilitate further analyses, the pressures measured from each pressure plate were combined to determine the contact force on the northern face of the pile cap. The pile cap face was segmented into six horizontal strips with one of the pressure cells near the center of each. These strips represent the tributary area of the pile cap face associated with each pressure cell. Each area was multiplied by the pressures at each depth, and the summation of these individual forces is the total pile cap-backfill contact force. However, in an analysis conducted using the pressure-based forces at the beginning of each static displacement interval (before cyclic and dynamic loads were applied) throughout testing with several backfill type, the correlation between pressure cell-based forces and actuator-based forces was found to be approximately 0.6 (i.e., the pressure cell-based measurements accounted for only 60% of the force produced by the actuators). This correlation is shown in Figure 4-21. This correlation is consistent throughout pile cap testing with a densely compacted sand backfill. This behavior is also consistent with elastic pressure distribution equations which typically shown higher pressures occurring near the edges of a foundation and lower pressures near the center. Consequently, forces calculated by multiplying pressure plate pressures by tributary areas were multiplied by 1.67 (the inverse of 0.6). As shown in Figure 4-22, the adjusted pressure cell based passive force computed with a multiplier closely matched the actuator-based passive forces at the beginning of each static displacement interval (Passive Earth Response).

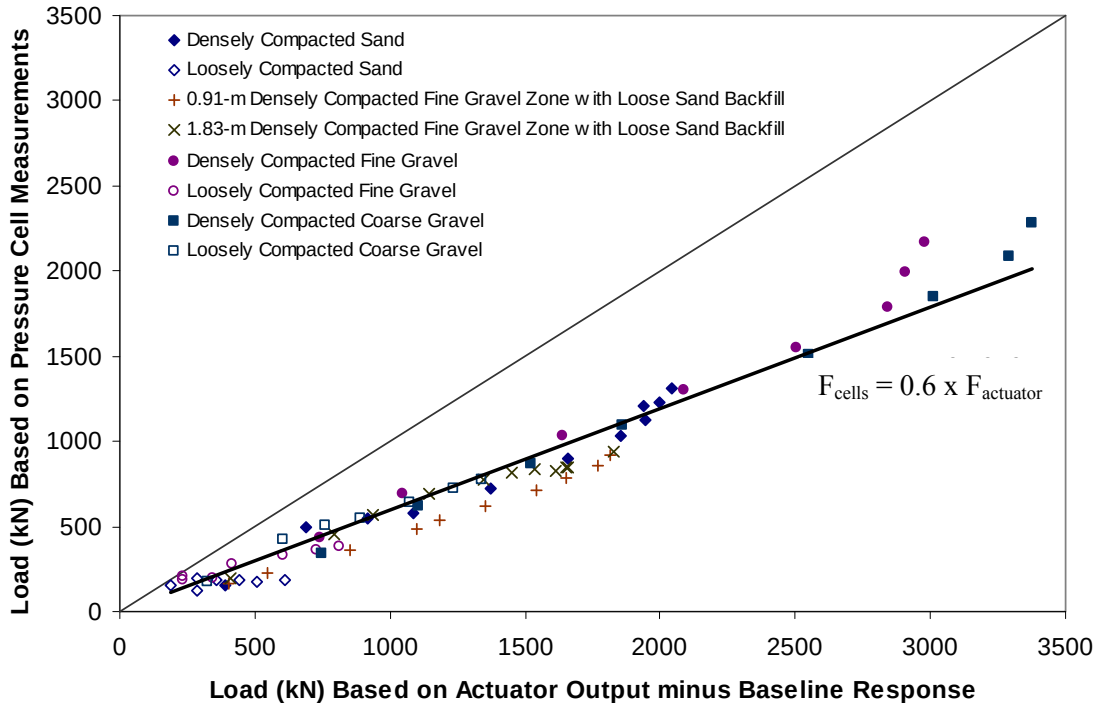

Figure 4-21 Passive earth loads based on pressure cells versus load actuators

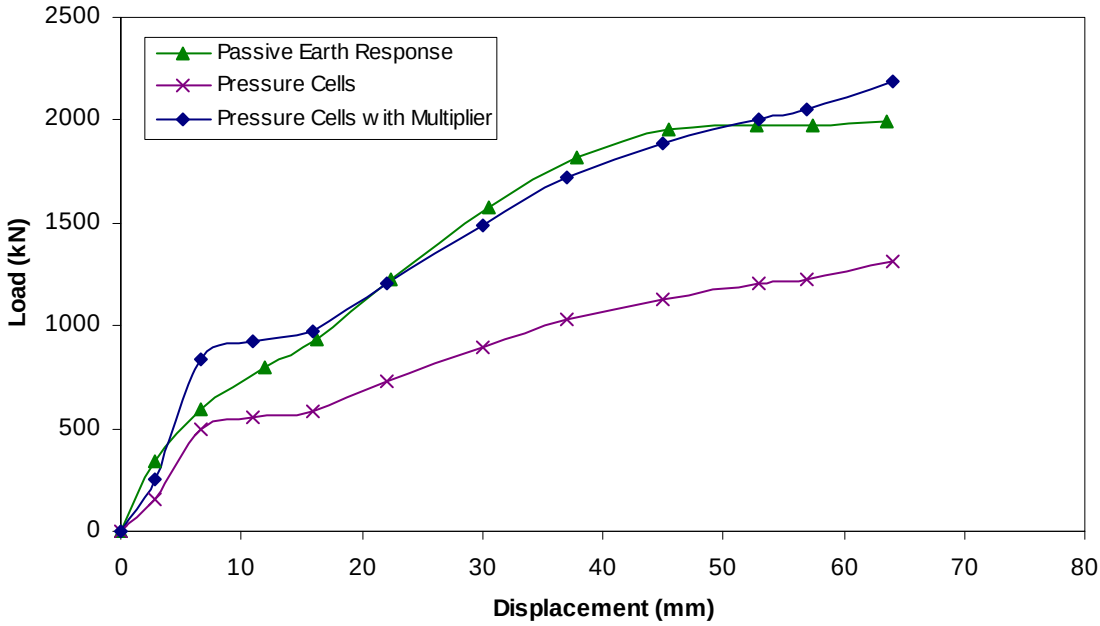

Figure 4-22 Comparison of earth forces based on actuators and pressure cells

4.2 Determination of Parameters

4.2.1 Backfill Stiffness

Stiffness is an inherent material and geometric property which resists external forces. For this research, the pile cap activated the backfill stiffness as the cap was displaced into the backfill. Stiffness may be measured with units of force per displacement. The backfill stiffness may be calculated using the following equation:

$$k = \left(\frac{F_{\max} - F_{\min}}{x_{\max} - x_{\min}} \right)_{cycle} \tag{4.1}$$

where:

k = backfill soil stiffness

F = contact force at maximum and minimum displacements of a cycle

x = maximum and minimum pile cap displacements of a cycle

Since stiffness is dependent on force and displacement, several force-displacement figures are used in this research to identify trends in stiffness. On a force verses displacement plot the slope of a trendline connecting force at minimum and maximum displacements is the backfill stiffness.

4.2.2 Residual Offset

Displacement offset was previously observed during both cyclic and dynamic loadings. During cyclic loading conditions, with each cycle the maximum displacement increased (ie. the pile cap was displaced further north with each cycle). The difference

between displacement maxima during the 15 cycles provides continuous displacement offset. Dynamic loading displacements were converted to a single trendline to show continuous displacement offset (shown in Figure 4-12 and Figure 4-13). The difference between the starting pile cap displacement and the pile cap displacement at the conclusion of the dynamic loading is the total displacement offset or residual offset due to dynamic loading.

Residual offset of the pile cap is directly responsible for partial reduction in passive force between the pile cap and the backfill. During cyclic loading conditions the difference between peak to peak force magnitudes provides continuous losses in force which are at least in part associated with displacement offset. However, during dynamic conditions continuous force losses associated with displacement offset may not simply be computed using a filtered trendline of forces (as was previously done to compute continuous displacement offset during dynamic loading). This is because several different dynamic factors (in addition to displacement offset) contribute to losses in dynamic contact force. Therefore, to isolate the loss in force due to displacement offset that occurs throughout dynamic testing, force loss must be connected to displacement offset.

One method to attribute the force loss due to displacement offset is to estimate the force loss per unit of residual offset. This parameter may then be multiplied by the displacement (relative to the displacement interval of the pile cap) at any time during loading and yield a force loss due to the drifting displacements. The following equation provides such a parameter:

$$\left(\frac{F_{offset}}{x_{offset}}\right)_{Total} = \frac{F_2 - F_1}{x_2 - x_1} \quad \textbf{(4.2)}$$

where:

$\frac{F_{offset}}{x_{offset}}$ = force loss per unit of residual offset

F_1 = beginning measured force at pile cap-backfill interface

F_2 = ending measured force at pile cap-backfill interface

x_1 = beginning pile cap position

x_2 = ending pile cap position

4.2.3 Phase Angle

By definition, a phase angle is a numerical value denoting the degree in which two moving objects are synchronized in motion. A phase angle of zero or 360 degrees signifies that two objects are moving in the same direction at the same time. Inversely, a phase angle of 180 degrees defines movement in opposing directions at similar time.

The relative movement of the backfill in relation to the pile cap during dynamic loading may be observed by the separation of the pile cap and backfill displacement amplitudes in relation to time. The following formula may be used to derive the phase angle between the pile cap movement and the backfill movement:

$$\phi = 360 * \frac{(t_{cap} - t_{soil})_{\max displacement}}{\lambda_{cap}} \quad \textbf{(4.3)}$$

where:

ϕ = phase angle, degrees

t_{cap} = time when maximum soil displacement occurs

t_{soil} = time when maximum soil displacement occurs

λ_{cap} = pile cap wavelength in time

Alternatively, phase angles may be calculated through a comparison with damping ratio. This relationship is introduced in basic structural dynamics (Chopra 2001). The phase angle increases as the forcing frequency surpasses the natural frequency of the system subject to some degree of damping. This relationship is described by the following equation:

$$\phi = \tan^{-1}\left[\frac{2\zeta(\omega/\omega_n)}{1-(\omega/\omega_n)^2}\right] \quad \textbf{(4.4)}$$

where:

ϕ = phase angle

ζ = damping ratio

ω = circular frequency

ω_n = natural circular frequency

However, the relationship between phase angle and damping assumes a linear stiffness. In the analysis section of this thesis, the non-linearity of the backfill stiffness during

dynamic loading will be apparent. Therefore, this method of calculating phase angle was not used.

4.2.4 Damping

A damping ratio may be calculated from load-displacement loops. In this calculation the area of the loop, or dissipated energy, is first determined. A ratio between this area and the area signifying the strain energy is then multiplied by $1/4\pi$. The equation for damping for load-displacement loops is as follows:

$$\zeta = \frac{1}{4 \cdot \pi} \frac{E_D}{E_{So}} \tag{4.5}$$

where:

$\zeta =$ damping ratio

$E_D =$ dissipated energy

$E_{So} =$ strain energy

Figure 4-23 shows the parameters of dissipated energy and strain energy in relation to a load-displacement loop. For this research, Equation 5.2 was rearranged as the following:

$$\zeta = \frac{A_{loop}}{2\pi \cdot k \cdot u_{amp}^2} \tag{4.6}$$

where:

ζ = damping ratio

A_{loop} = inside area of the load-displacement loop

k = stiffness of backfill

u_{amp} = loop displacement single amplitude

These parameters are illustrated in Figure 4-24. The loop area is the region enclosed by increasing and decreasing forces during northward and southward pile cap movement.

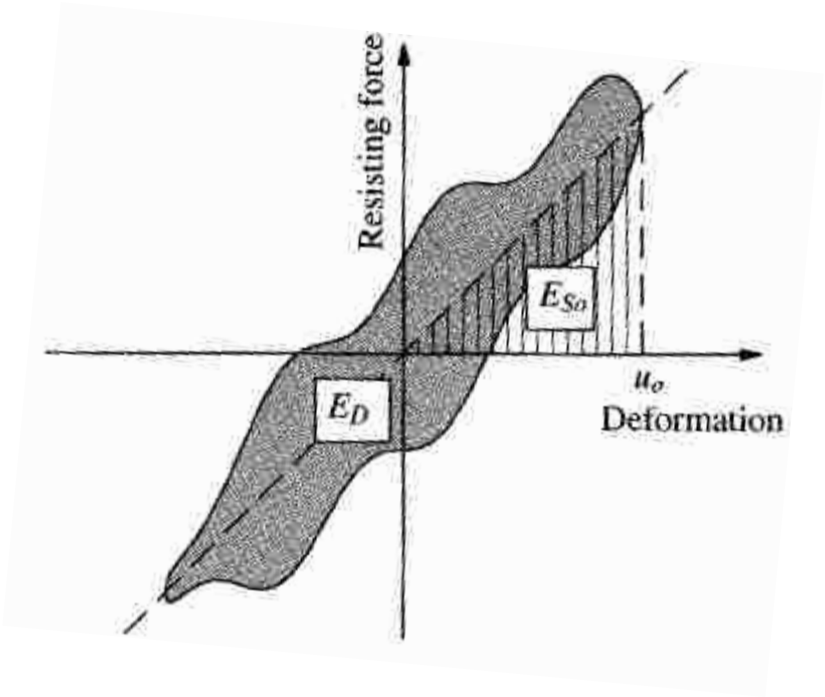

Figure 4-23 Damping calculation parameters displayed on a load-displacement loop (Chopra 2001)

Figure 4-23 shows the maximum and minimum forces almost occurring at the same points as the maximum and minimum displacement. When the maximum forces and displacements do not coincide (as clearly shown in Figure 4-25), it is due to

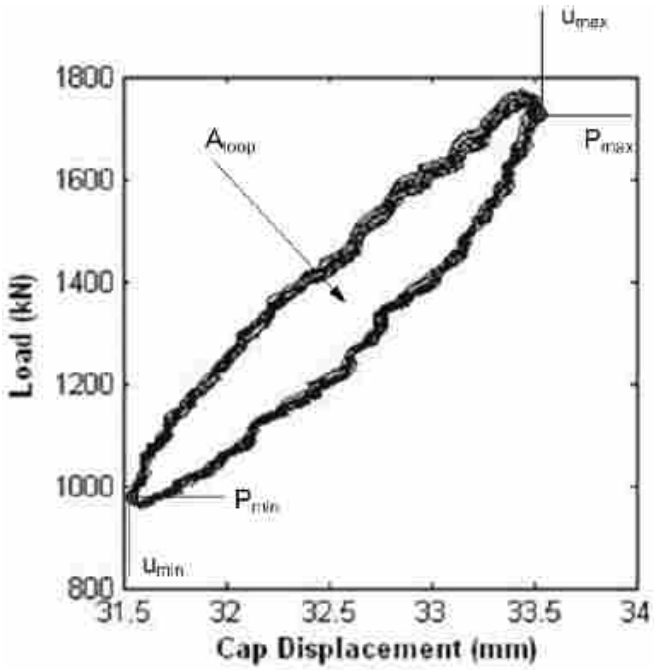

Figure 4-24 Key parameters displayed on a load-displacement loop

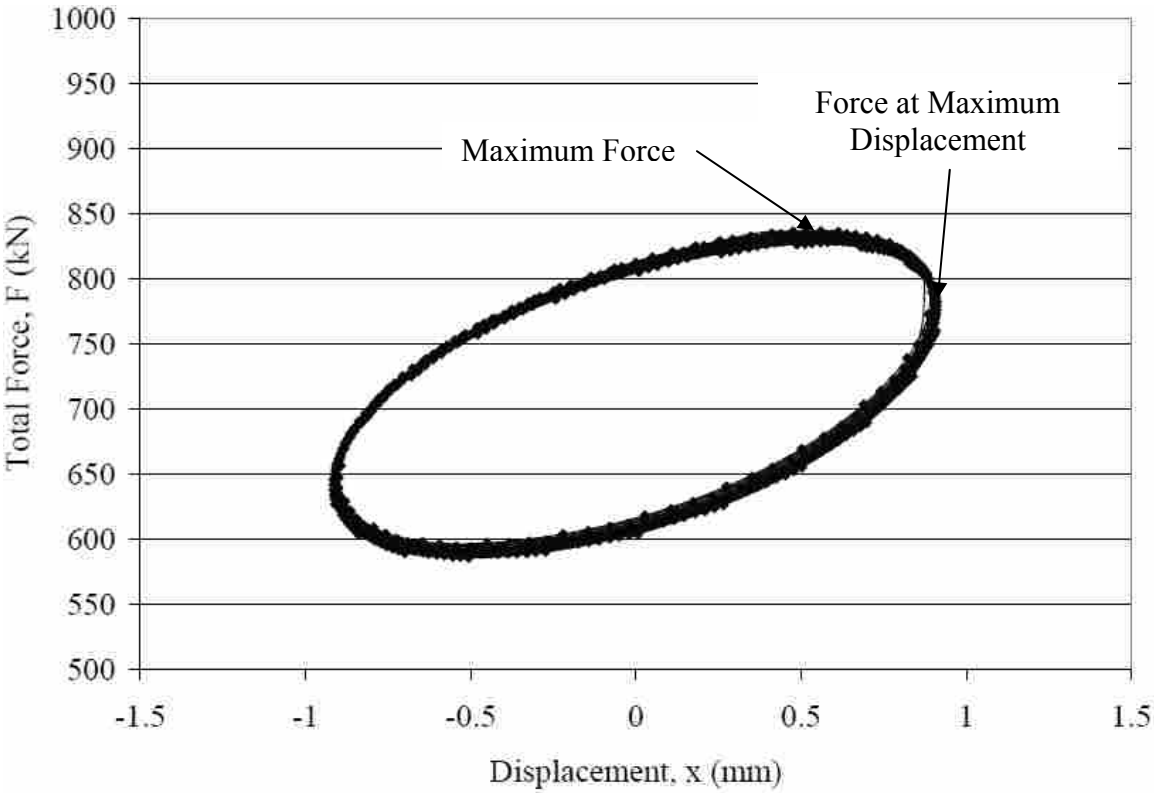

Figure 4-25 Typical load displacement loop during dynamic loading at high frequency

damping. Stiffness (or the slope of the loop) is based on the peak displacements and associated forces and not the peak (i.e., maximum) forces.

Figure 4-26 (after Chopra 2001) illustrates the relationship of viscous damping to the force-displacement hysteresis loop which is a composite of both the damping and stiffness forces. As derived from this figure and shown in the following equation, the damping coefficient for the backfill can be calculated as:

$$c = \frac{f_d}{(\omega \cdot u_{amp})} \quad \textbf{(4.7)}$$

where:

c = damping coefficient

f_d = force of the load-displacement loop at zero displacement

ω = circular forcing frequency (which is the circular frequency of the loop)

u_{amp} = loop displacement amplitude

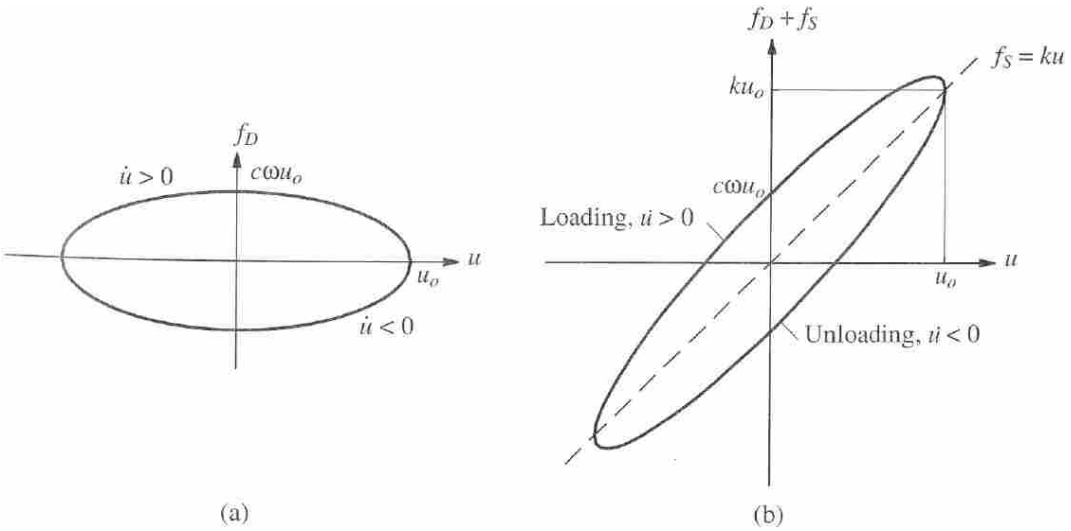

Figure 4-26 Damping component and combined stiffness and damping components (Chopera 2001)

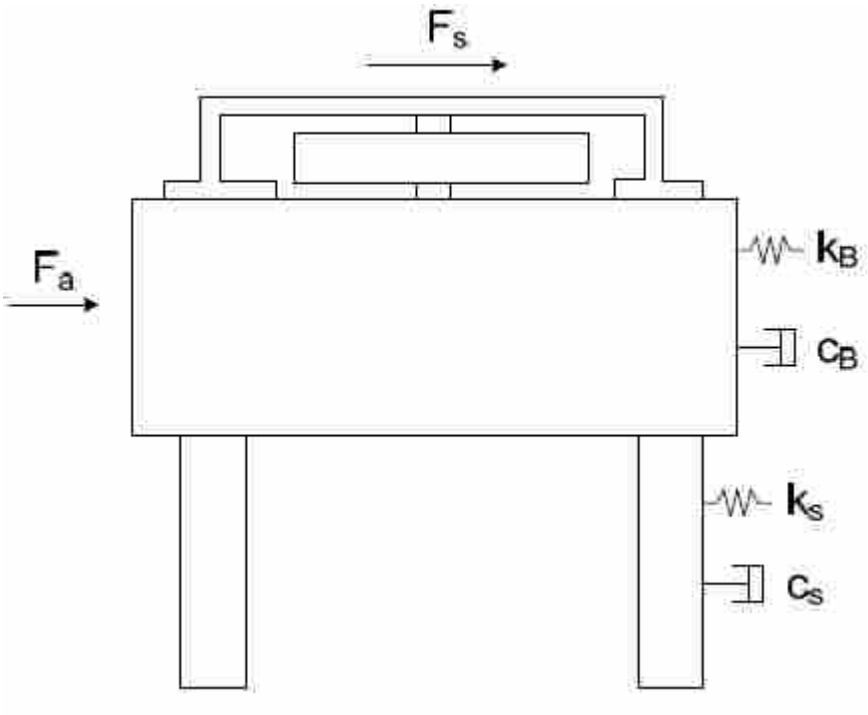

Figure 4-27 Pile cap system showing dynamic parameters of force, stiffness, and damping

For the pile cap-backfill system used in this research, the damping coefficient (as well as stiffness) of the backfill can be combined in parallel with the corresponding damping coefficient and stiffness for the pile cap without any backfill in place to describe the behavior of the overall system. Visually this system is shown in Figure 4-27. The parameters shown are the actuator force (F_a), shaker force (F_s), backfill stiffness (k_B), backfill damping coefficient (c_B), pile-cap-and-pile stiffness (k_s), and pile-cap-and-piles damping coefficient (c_s). The damping ratio can then be calculated as follows using the sum of the backfill and pile-cap-and-piles damping coefficients divided by the critical damping coefficient of the composite system:

$$c_c = 2 \cdot m \cdot \omega_n \qquad \textbf{(4.8)}$$

where:

c_c = critical damping coefficient of the composite system

m = mass of the system

ω_n = natural circular frequency of the composite system

5 Test Results

The development of passive earth pressure at the pile cap-backfill interface is dependent on several factors. Some of these factors include backfill stiffness, cyclic losses, damping, and the relative movement of the cap and backfill. Using the methods discussed in Chapter 4, these parameters and their impact on the backfill soil pressure will be assessed and presented in this chapter.

5.1 Backfill Stiffness

The backfill stiffness values calculated for both cyclic actuator loading and dynamic shaker loading will be presented in this section. These stiffness values represent reloading conditions rather than the initial loading stiffness associated with the static displacement of the pile cap. The methods by which backfill stiffness was determined were previously presented in Section 4.2.1.

Backfill stiffness generally remained constant during cyclic loading associated with each particular displacement interval. This behavior is shown in Figure 5-1 for the eighth pile cap displacement interval, where the force-displacement relationship is linear and consistent during the 15 actuator loading cycles. As the actuator pushes the pile cap into the soil, the cap and the soil are displaced to approximately one millimeter. When this extension is reached, the actuators retract. As the actuators retract, the pile cap force

decreases linearly. As this action of expansion and retraction repeats, contact force reaches a similar maximum force and a similar minimum force with every cycle. However, throughout the actuator cycles the pile cap moves slightly north (just above 0.1 mm). Since the change in displacement is uniform, the general force-displacement slope remains constant. The slope of this relationship approximates the backfill stiffness. In Series 8, the soil resistance is 157 kN/mm.

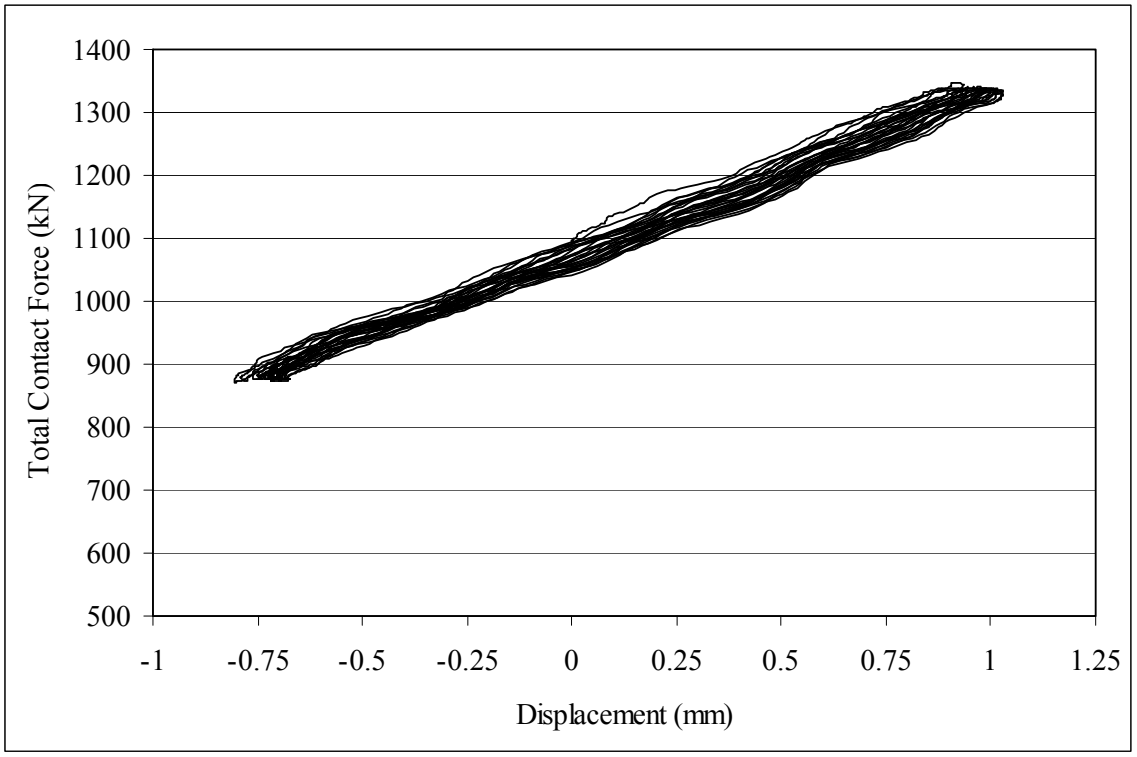

Figure 5-1 Force on backfill varying with cyclic displacement, Series 8

The expected trend for soil stiffness during cyclic loading is to increase with pile cap displacement intervals as more of the ultimate passive force is mobilized. This stiffness increase is displayed in Figure 5-2 which shows backfill stiffness at all eleven pile cap displacement intervals. One reason that the backfill stiffness does not

consistently increase at each displacement interval is the alternation of cyclic and dynamic loading. During the odd displacement interval numbers the pile cap was loaded cyclically before dynamically. During the even displacement intervals the pile cap was loaded dynamically before cyclically. Generally when the pile cap was first loaded dynamically, the backfill stiffness decreased from the backfill stiffness during the previous displacement interval. This trend indicates stiffness loss during dynamic loading.

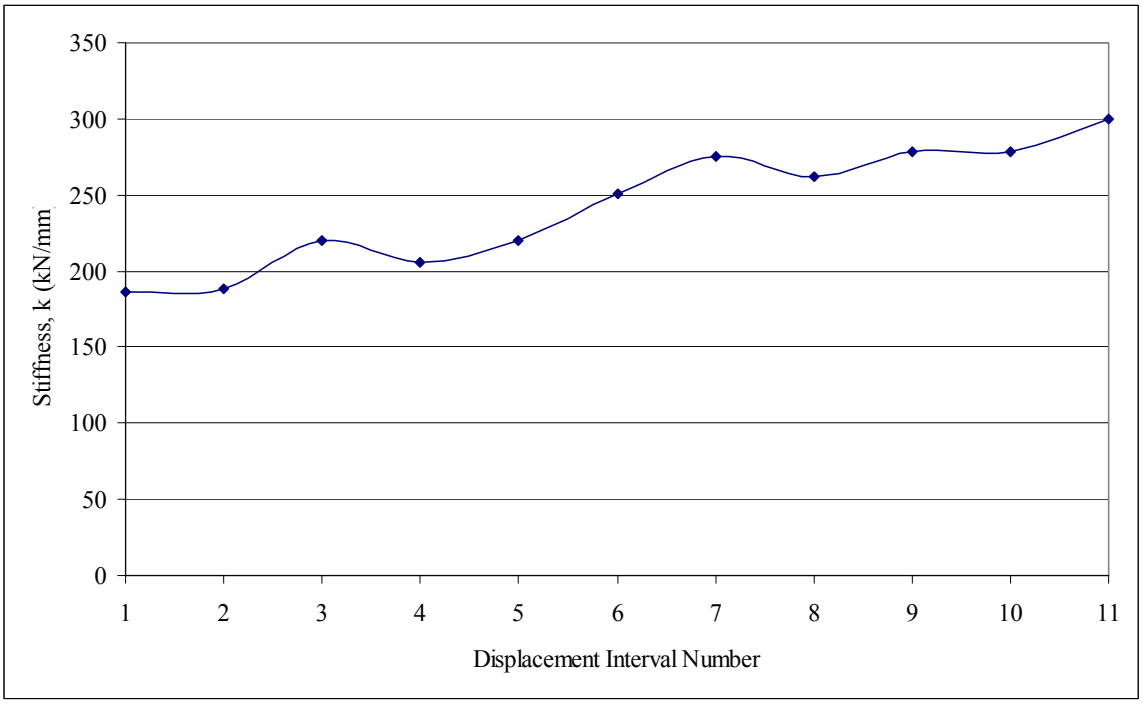

Figure 5-2 Backfill stiffness at each pile cap displacement interval

Stiffness during dynamic loading can be calculated using the same force-displacement relationship presented previously. At low frequencies the force-displacement relationship is linear. However, as frequency increases, the load path

begins to transition from a linear to elliptical shape, with increasing northward movement of the cap occurring from left to right along the upper portion of the ellipse. Figure 5-3 illustrates this behavior as a function of frequency during Shake 8. At 5 Hz the force-displacement relationship begins to form a loop meaning that dynamic backfill stiffness begins to differ from the previously described cyclically loaded backfill stiffness. Even with load-displacement loops, the stiffness for the backfill is still calculated by connecting the forces at minimum and maximum displacements with a linear line. The slope of this line is the stiffness of the soil at that particular frequency.

As frequency increases, the stiffness does not remain constant. This is shown as the linear slope between peak displacement forces slowly decreases and occurs because the change in pile cap displacement is nonlinear to the change in contact force. For this thesis, this dynamic loss in stiffness will be attributed to cyclic effects during dynamic loading.

Shake 8, for example, has a 1 mm spread in displacements at 7 Hz and a 2 mm spread nearing 10 Hz. The difference between forces at peak displacement at 7 Hz is 221 kN and at 10 Hz is 162 kN. Therefore, the backfill stiffness changes from 221 kN/mm to 81 kN/mm from 7 to 10 Hz.

Shake 9 load-displacement loops are shown in Figure 5-4. These loops do not lose the same magnitude of force as displayed in Shake 8. Rather in Shake 9, 1440 kN seems to be a general steady peak force as the frequency increases. This is far different from Shake 8 (dynamic loading first) which has a peak force just under 1500 kN at 7 Hz but by 10 Hz has dropped to a peak loading of 1300 kN. While during each dynamic loading condition the backfill stiffness decreases as the frequency of the mass shaker

increases, the effect is far greater when the eccentrically loaded mass shaker is the first loading device acting on the pile cap at the beginning of a load displacement interval. Therefore, the effects of forcing frequency on stiffness loss should be observed during Shake 8 as opposed to Shake 9.

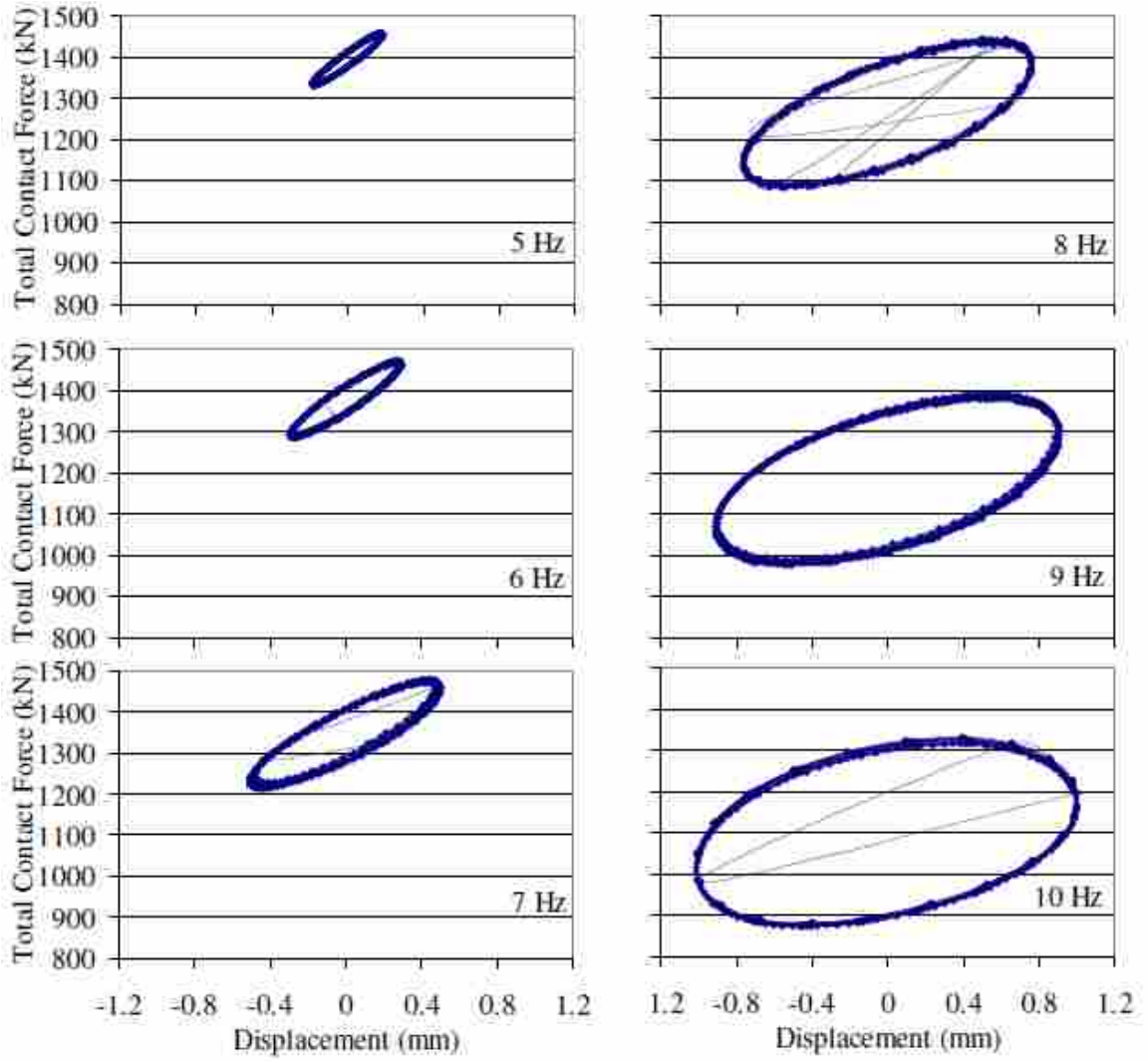

Figure 5-3 Load displacement loops at 5, 6, and 7 Hz (column 1) and 8, 9, and 10 Hz (column 2), Shake 8

In Figure 5-5, Shake 8 backfill stiffness is displayed from 5 Hz to 10 Hz. At 5 Hz the stiffness of the backfill is 321 kN/mm. By 10 Hz, the stiffness has dropped to 80 kN.

A linear relationship connects the data points between these two frequencies. At lower frequencies the stiffness behaves similarly to cyclic conditions.

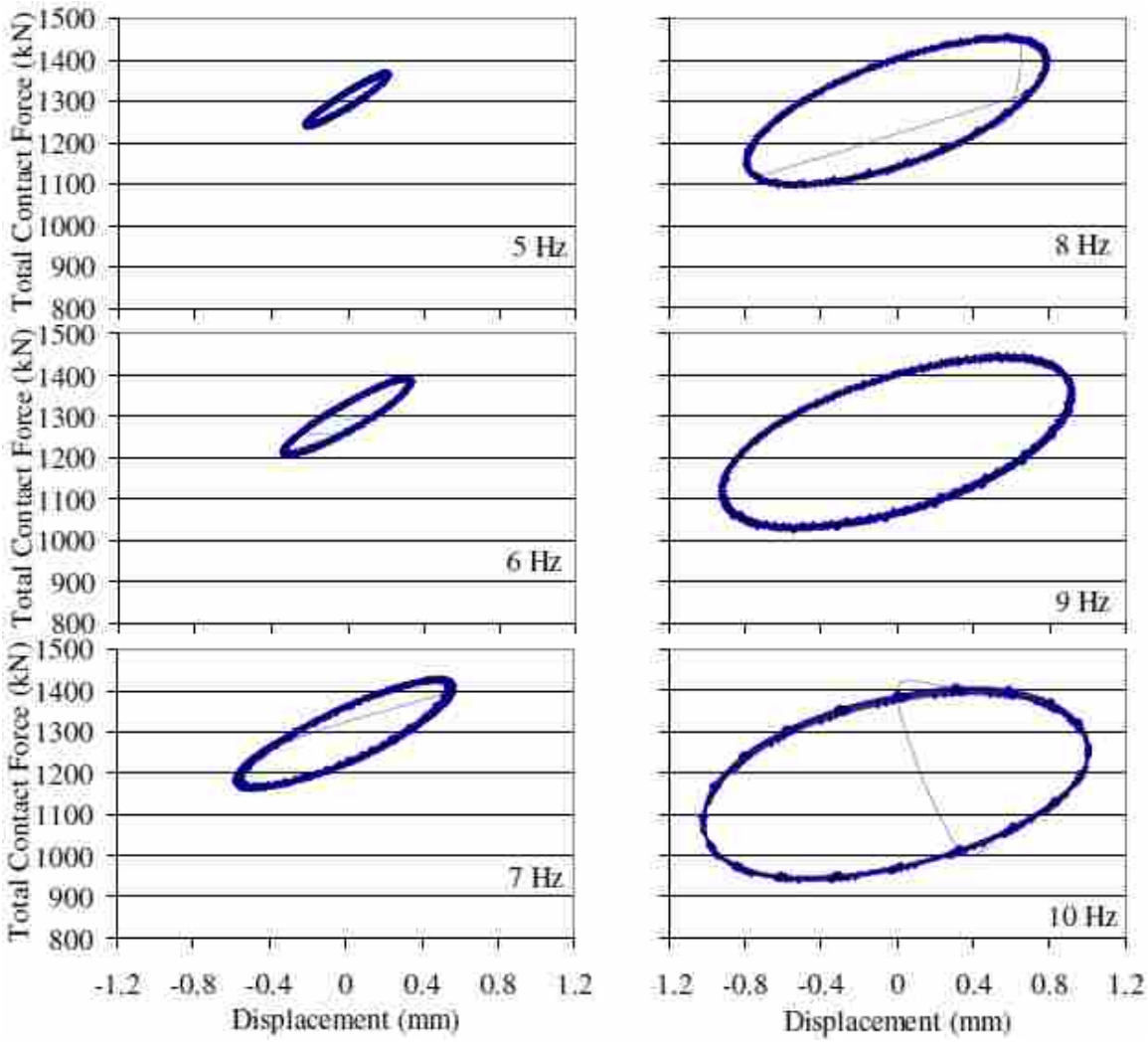

Figure 5-4 Load displacement loops at 5, 6, and 7 Hz (column 1) and 8, 9, and 10 Hz (column 2), Shake 9

5.2 Residual Offset

During dynamic loading, the pile cap displaced further north into the backfill such that at the end of dynamic loading the pile cap was offset from its position at the

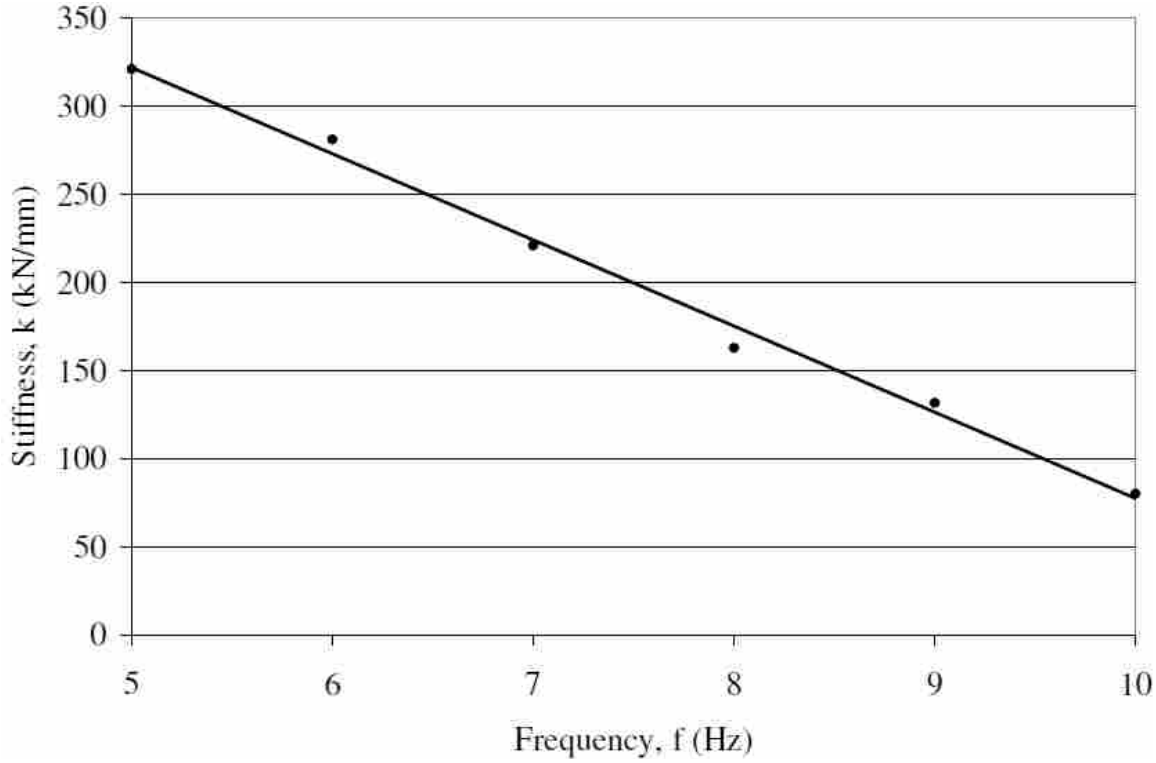

Figure 5-5 Backfill stiffness verses forcing frequency, Shake 8

beginning of dynamic loading. While the pile cap position shift is easily measured, the pressure loss during the time history due to this offset is uncertain. The loss due to residual offset may not forcibly be measured since total force loss is dependent on other mechanisms such as damping and phase lag.

Total residual offset was previously assessed in step two of Section 4.1.1.2.2, filtered displacement. The difference in string potentiometer displacements from beginning to end of each dynamic loading is the residual offset for that loading. For example, the total residual offset during Shake 8 located in Figure 4-12 is 2.32 mm northward. A compilation of the residual offset during dynamic loading at each displacement interval is displayed in Figure 5-6. In this figure, the alternating loading sequence of the pile cap (odd displacement intervals were first cyclically loaded; even

displacement intervals were first dynamically loaded) significantly affects the pile cap offset. For reasons stated previously, the backfill displaced more during dynamic loadings which preceded cyclic loadings than dynamic loadings which followed cyclic loadings at a particular displacement interval. The offset significantly increased between the dynamic loading during the fifth and sixth displacement intervals. Increasing residual offset occurs because the force applied to the backfill increases initially with loading sequence. However, as the passive force develops the change in force begins to decrease. Therefore, after the sixth displacement interval the pile cap offset slowly diminishes (ignoring alternating loading effect).

In subsequent comparisons, the dynamic passive force acting upon the pile cap face will need to be compared to the static force during dynamic loading. Since the static force could not be measured during dynamic loading (due to dynamic effects), it is

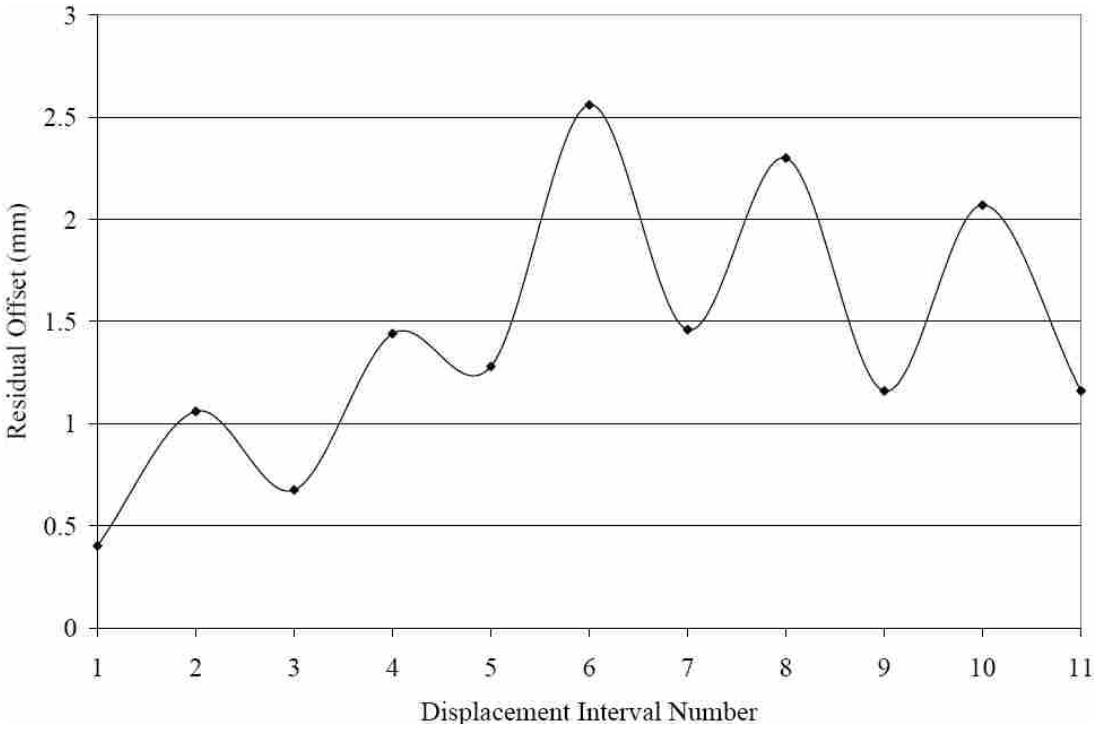

Figure 5-6 Pile cap offset during dynamic loading at each pile cap displacement interval

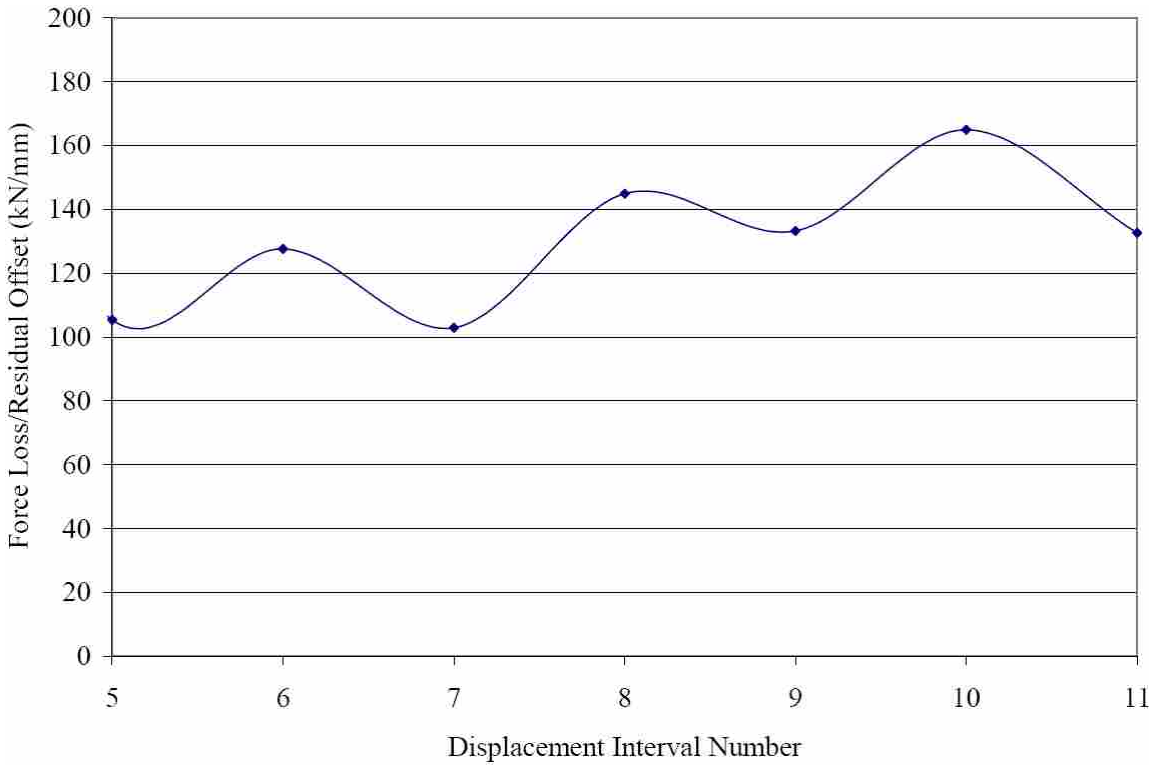

Figure 5-7 Force loss normalized by residual offset at various pile cap displacement intervals

necessary to calculate the static force. Given that residual offset directly affects the developed static force, a parameter of the static force difference between the beginning of the dynamic loading and the ending of dynamic loading normalized by the residual offset throughout dynamic loading will be created. This force loss normalized by residual offset at each pile cap displacement interval is displayed in Figure 5-7. Beginning with the fifth displacement interval, the loss of passive force at the pile cap face due to pile cap offset increases with each displacement interval (ignoring alternating loading effect).

5.3 Phase Angle

The method of analysis for calculating phase angles was previously discussed in Section 4.2.3. This section will analyze backfill response (measured by pressures and

displacements) first through the depth of the backfill at the backfill-pile cap interface and then at varying points across the backfill length.

5.3.1 Through the Depth of the Backfill

The pressure plate measurements during dynamic loading were presented in Chapter 4.1.2. Figure 4-19 illustrated the pressures measured by each of the pressure plates along the pile cap's northern face. A closer look (a 1 second interval) at the pressure plate measurements is displayed Figure 5-8 during Shake 8. This short interval takes a snapshot of the changing pressures at mid-range forcing frequencies (about 6 Hz). Generally, the pressures measured by each pressure plate rise and fall with similar magnitudes and rate changes at similar time periods. This symmetry of motion suggests

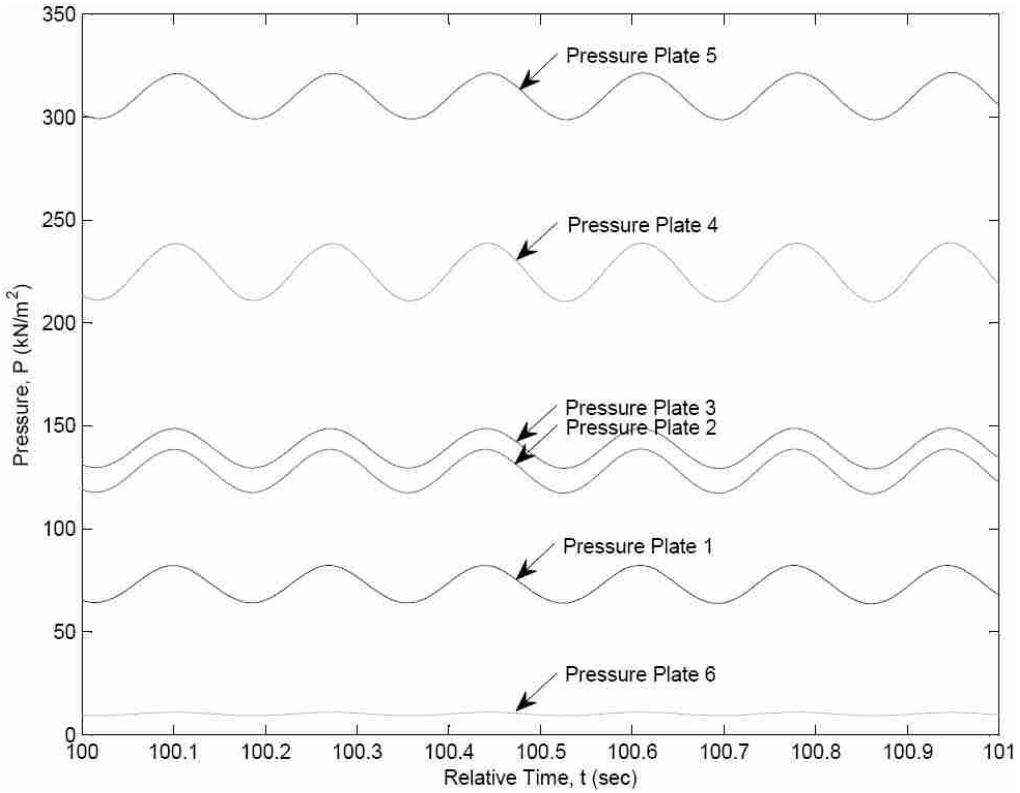

Figure 5-8 Cap pressure time history at 100 seconds or 6 Hz, Shake 8

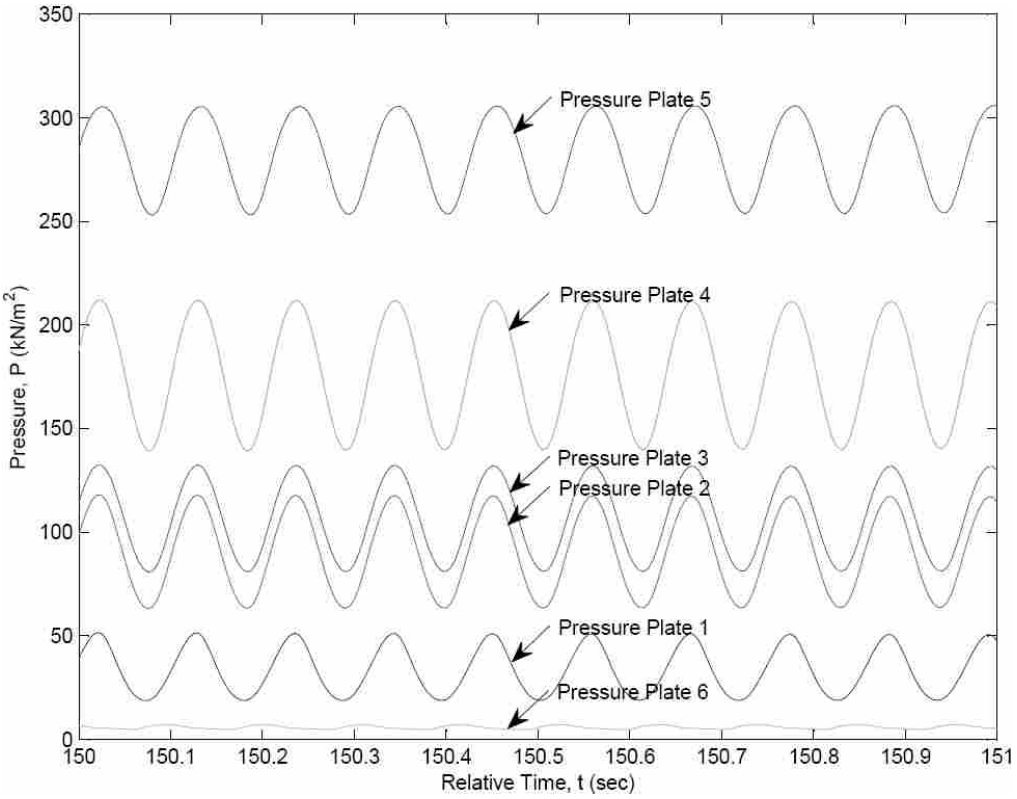

Figure 5-9 Cap pressure time history at 150 seconds or 9.3 Hz (ramp down), Shake 8

that throughout the depth of the backfill at the pile cap-backfill interface, the backfill responds similarly to the load applied.

As the mass shaker ramps down, the backfill still responds uniformly with depth to the pile cap loading. Figure 5-9 captures a snapshot of the pressure time history during the shaker ramp down around 9.3 Hz. This figure shows each of the six pressure plates with maximum and minimum pressures lining up in time from one pressure plate to the next. The pressure plate measurements appear to be in phase with each other. Generally, the pressure plates at every frequency and at every displacement interval throughout testing align with these observations.

5.3.2 Across the Length of the Backfill

The relative movement of the pile cap and the backfill soil mass produce forces on the pile cap face. This displacement-derived force can be treated as a spring. However, the backfill mass itself is not a rigid nor elastic mass. Consequently, absolute backfill displacement decreases with increasing distance from the moving pile cap face, and even movement within the backfill mass may not be in phase at all points. As explained previously, during cyclic loading backfill displacements can be reliably measured by string potentiometers (whereas they cannot during dynamic loading due to vibration effects on the reference frame).

5.3.2.1 Displacement during Cyclic Loading

Figure 5-10 and Figure 5-11, displaying displacements during Series 8 and Series 9, respectively, both show the pile cap moving approximately 0.7 mm forward and then backward throughout cyclic loading. This motion was transferred through the soil where displacement measurements were calculated at points located 0.61, 1.83, and 3.66 m north of the pile cap face. While the displacement magnitudes at each backfill distance vary, the peak displacements at various backfill positions generally align with the pile cap peak displacements. The backfill appears to be generally in-phase with the pile cap. The small irregularities at the beginning and ending of the time histories shown in the figures are artifacts of the data filtering and integration process.

Another notable observation is the relationship of the soil displacements 3.66 m and 1.83 m away from the pile cap. Intuition would say that the closer the soil is to the pile cap the more impact the cap would have on the soil. However, the soil displacements at 3.66 m are greater than those displacements at 1.83 m. One possible

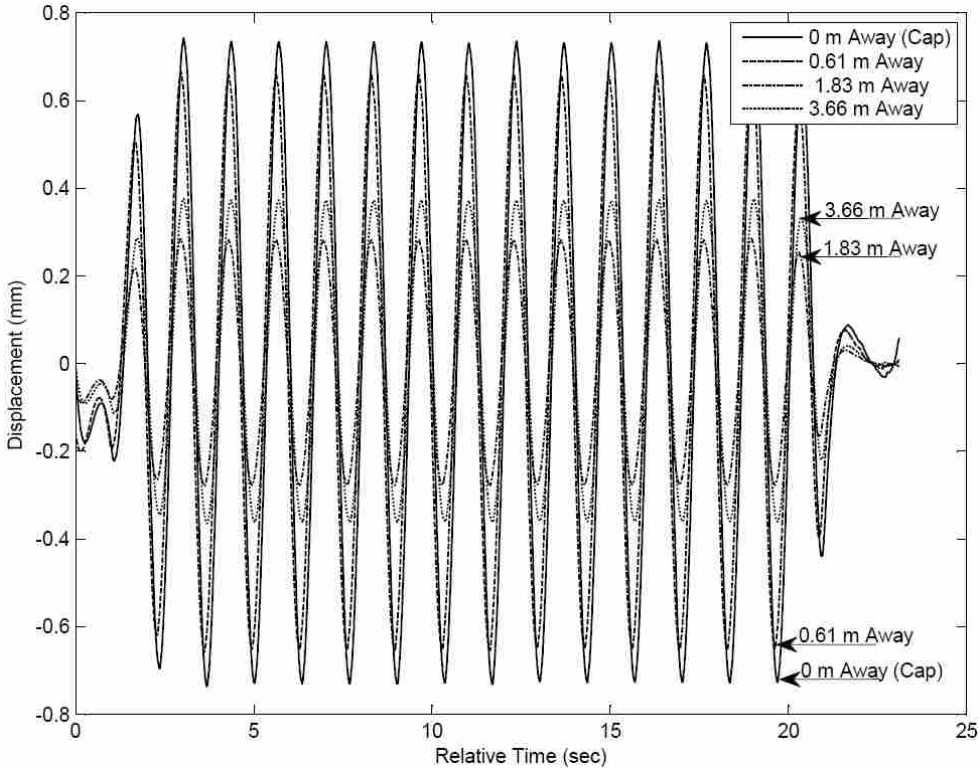

Figure 5-10 Cap and backfill displacement time histories during cyclic loading, Series 8

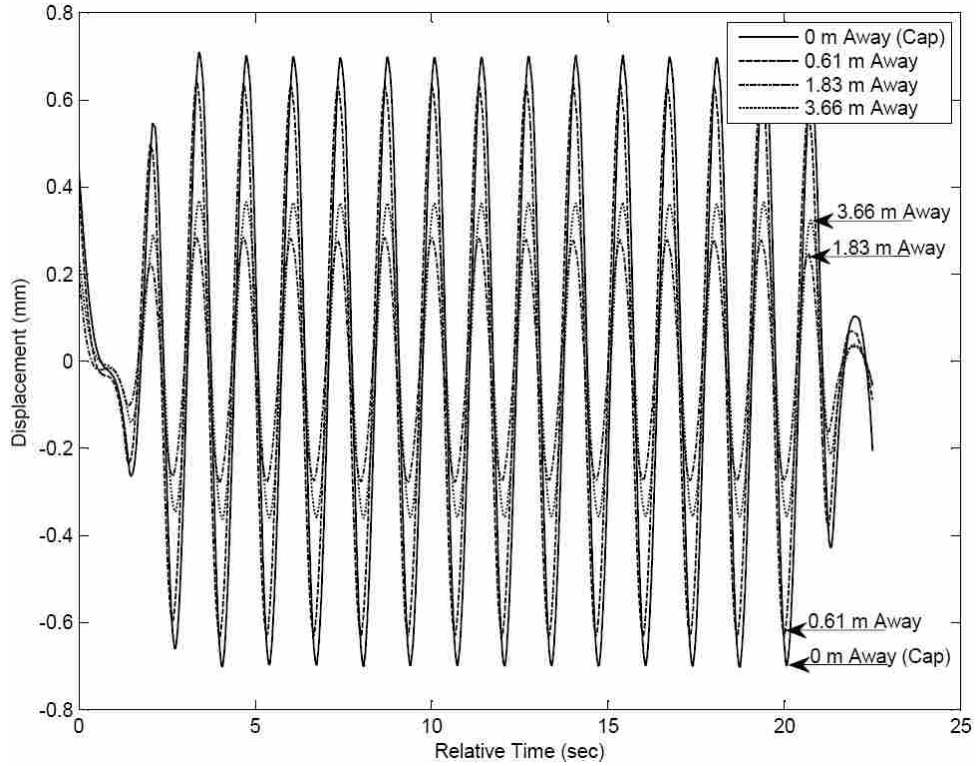

Figure 5-11 Cap and backfill displacement time histories during cyclic loading, Series 9

reason that displacements might be greater further from the pile cap could be 3-D wave interaction effects. During dynamic loading conditions (ie. this response was observed during blasting experimentation) the waves of motion throughout the backfill build upon or counteract each other as they propagate through the backfill. Thus displacement amplitudes are not necessarily related to distance from the pile cap.

5.3.2.2 Displacement during Dynamic Loading

As the mass shaker begins to load the pile cap, the initial backfill displacements peak in-phase with the pile cap displacements. Figure 5-12 and Figure 5-13 show a sample of the displacement amplitudes at the beginning of Shake 8 and Shake 9 (1 Hz forcing frequency); respectively. As the forcing frequency increased, the displacement peaks at the pile cap and the various backfill locations became less and less aligned. Figure 5-14 and Figure 5-15 capture a snap shot of the pile cap and backfill displacements at 100 seconds into the dynamic loading sequence. This time window corresponds with a shaker frequency of 5.8 to 6.0 Hz.

From the figures observed 100 seconds after the start of dynamic loading (at 6 Hz forcing frequency), the backfill was moving out-of-phase in relation to the pile cap movement. Therefore, the phase angle during dynamic loading was determined using methods of analysis discussed in Section 4.2.3. The phase angle of the backfill displacement relative to the displacement of the cap was evaluated 0.61, 1.83, and 3.66 m away from the pile cap. The calculated phase angle changed throughout dynamic loading. As displayed in Figure 5-16, the phase angle analyzed at 0.61 and 3.66 m away from the cap approaches zero at the beginning and ending of loading. However, as the

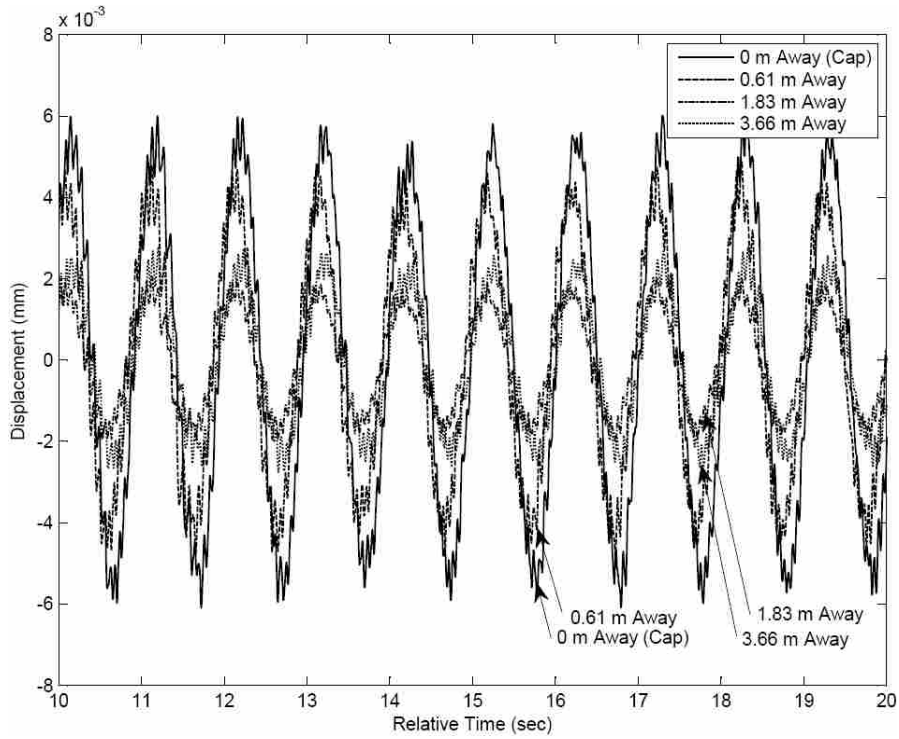

Figure 5-12 Cap and backfill displacement time histories between 10-20 seconds after the start of Shake 8 (at a forcing frequency 1 Hz)

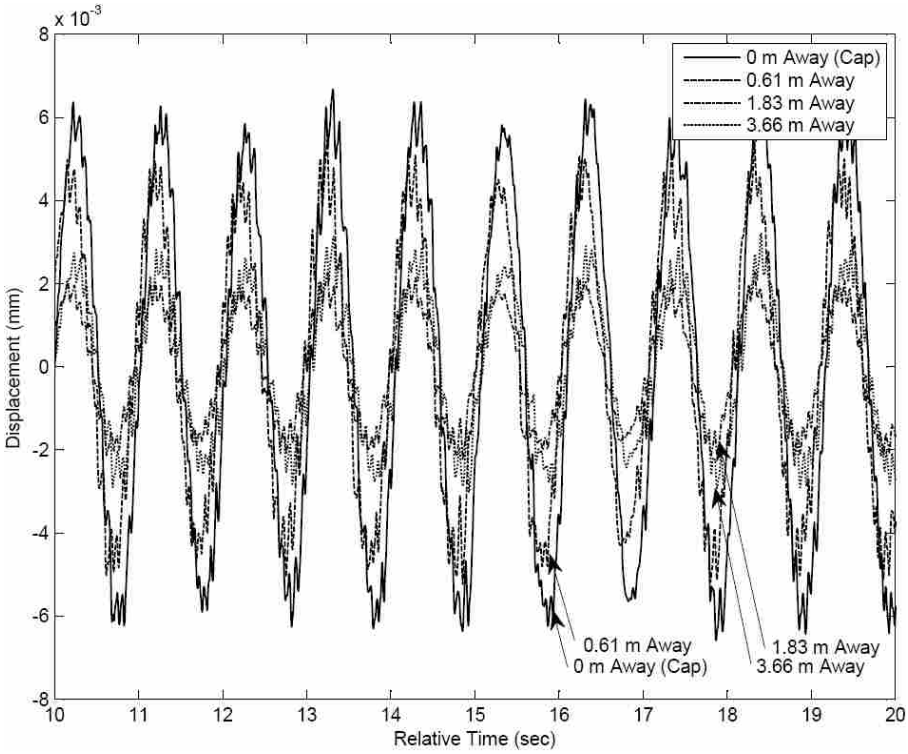

Figure 5-13 Cap and backfill displacement time histories between 10-20 seconds after the start of Shake 9 (at a forcing frequency 1 Hz)

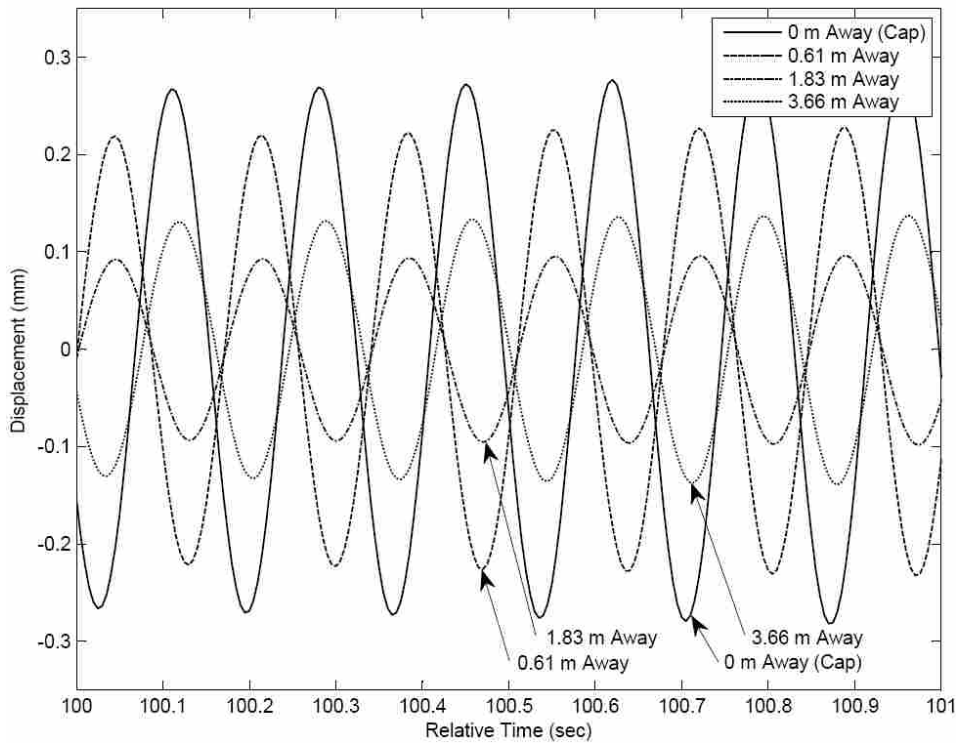

Figure 5-14 Cap and backfill displacement time histories 100 seconds after the start of Shake 8 (at a forcing frequency of 6 Hz)

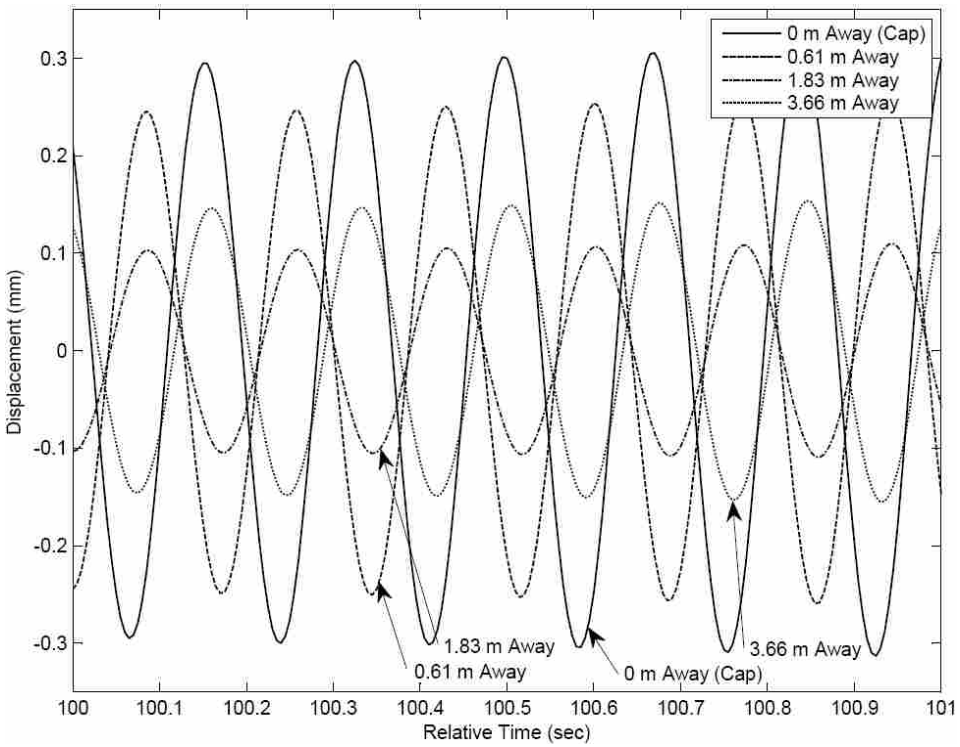

Figure 5-15 Cap and backfill displacement time histories 100 seconds after the start of Shake 9 (at a forcing frequency of 6 Hz)

frequency increases, the pile cap and the backfill movement become less synchronized corresponding to an increasing phase angle.

The pile cap and the backfill are completely out of phase (i.e., 180 degree phase angle) midway through dynamic loading. For both Shake 8 and Shake 9, a 180 degree phase angle occurs at the time and frequency intervals shown in Table 5-1 at various distances from the pile cap. While displacements and phase angles were calculated at 3.66 m away from the pile cap, at this distance the backfill movement was never 180 degrees out of phase from the pile cap movement.

Table 5-1: Time when 180 degree phase angle occurs at 0.61 and 1.83 m away from the pile cap

Shake	Distance (ft)	Time (sec)	Frequency (Hz)
8	2	115.8	7.15
	6	119.7	7.57
9	2	115.9	7.06
	6	118.9	7.52

Table 5-1 highlights that the backfill was completely out-of-phase with the pile cap around 7.5 Hz (120 seconds) at a distance of 1.83 m from the pile cap into the backfill. Interestingly, Cummins calculated the natural frequency of this pile cap-dense sand backfill system as 7.5 Hz (Cummins 2009). This frequency also corresponds to the greatest measured force at the pile cap-backfill interface. At closer distances the calculated phase angle reaches 180 degrees closer to 7 Hz (115 seconds). Other research, such as Tamura and Tokimatsu (2005), have also observed phase lags of 180 degrees when the frequency of the forcing function increased beyond the natural frequency.

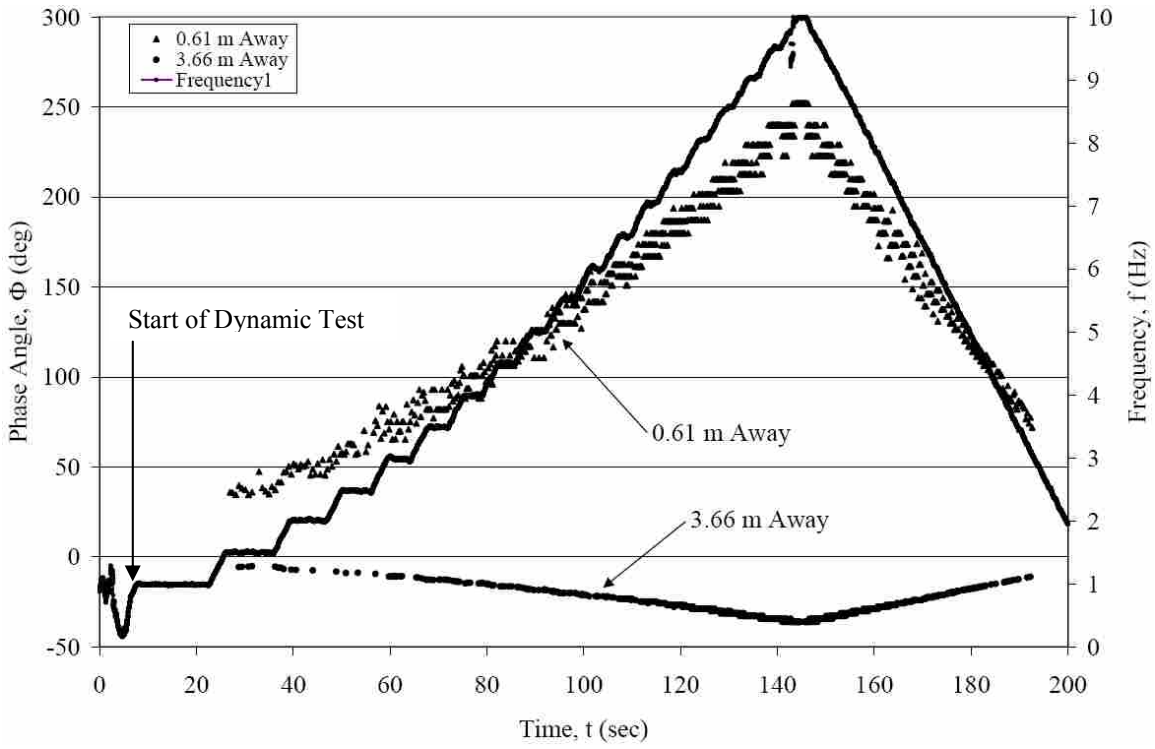

Figure 5-16 Typical phase angles versus time with corresponding frequencies, Shake 8

As the soil and the cap move out-of-phase, pressure between the cap and backfill drastically reduces. The movement of the pile cap and the backfill is modeled in Figure 5-17 and Figure 5-18 through load-displacement loops. Figure 5-17 depicts the pile cap and the backfill moving apart with a black dot representing the exact backfill or pile cap position orbiting the load-displacement loop at a time step of 1/100 second. Figure 5-18 depicts the pile cap and the backfill moving towards each other. Both figures are taken during the Shake 8 at 8 Hz.

In Figure 5-17, the backfill is moving north apparent as the large black dot moves with increasing displacements. The pile cap is moving in the opposite direction – away from the backfill. The partial separation of the pile cap and backfill causes a drastic decrease in the contact force (over 350 kN) over a time period of 0.25 seconds.

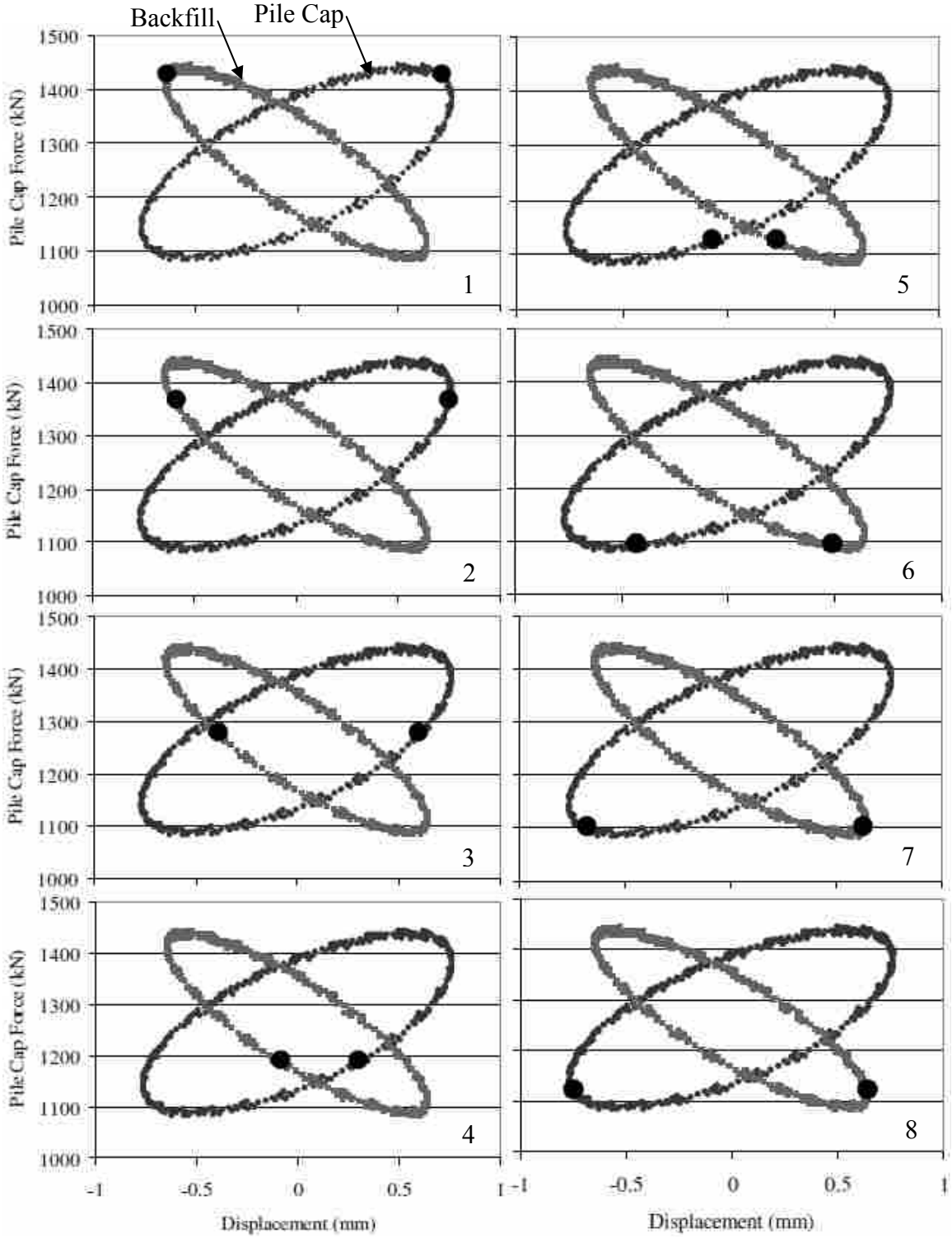

Figure 5-17 Pile cap moving away from the backfill shown with a time step of 0.01 seconds between each frame (1-8)

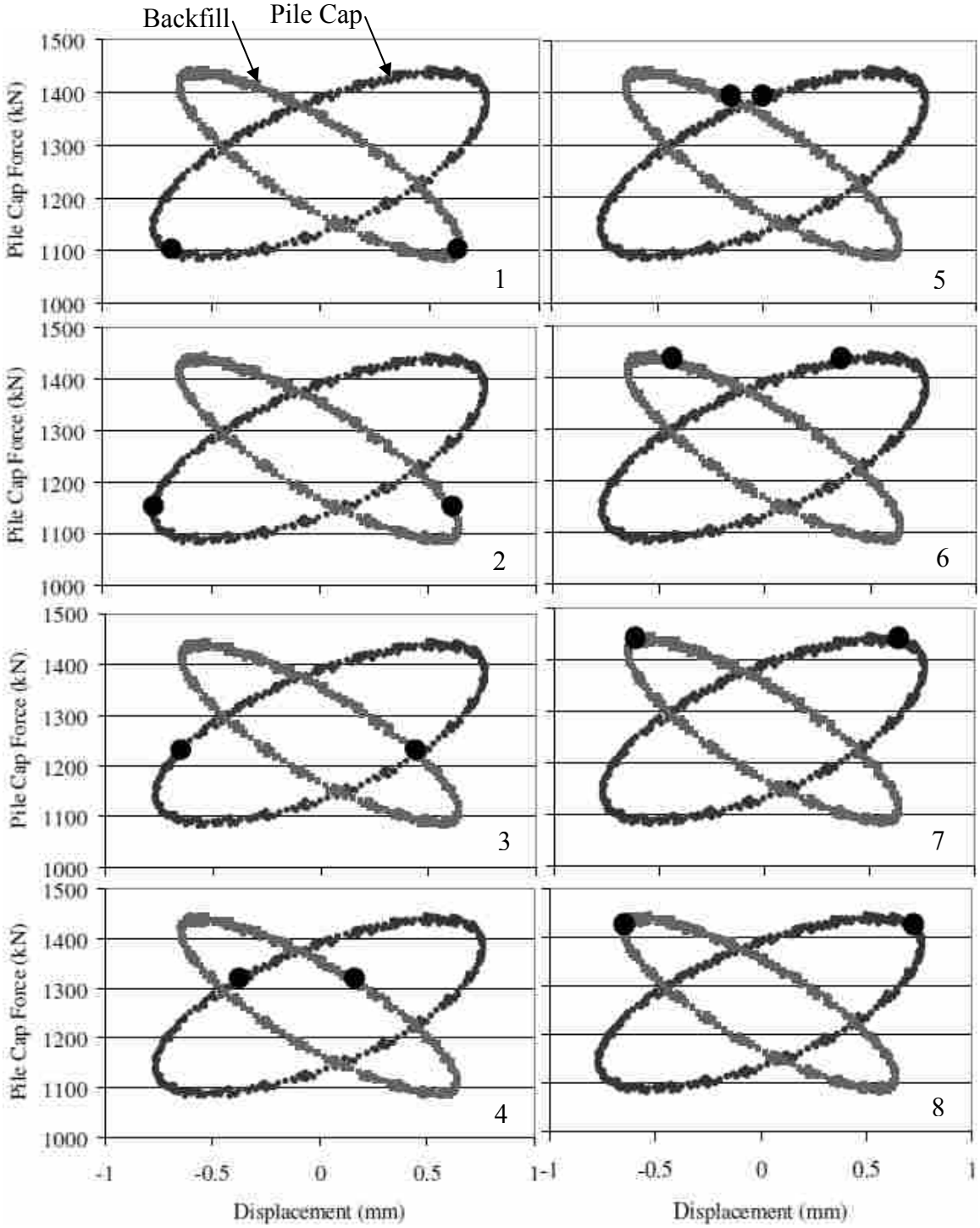

Figure 5-18 Pile cap moving towards the backfill shown with a time step of 0.01 seconds between each frame (1-8)

Figure 5-18 shows the pile cap and the backfill moving towards each other. The pile cap shifts from 0.8 mm south of its position at the beginning of the eighth displacement interval to 0.8 mm north. The backfill moves from just over 0.6 mm north to 0.6 mm south. The backfill does not move the full 0.8 mm that the pile cap displaces. As these entities move closer, the contact force at the interface builds.

5.4 Damping

Calculations for assessing the damping of the system using load-displacement loops were introduced in Section 4.2.4 (examples of load-displacement loops were previously displayed in Figure 5-3 and Figure 5-4). Using the load-displacement loops for the backfill, damping coefficients for the backfill were computed as a function of forcing frequency. The results are shown in Figure 5-19, and it can be seen that the damping coefficient is relatively constant with a value just larger than 3 kN-sec/mm.

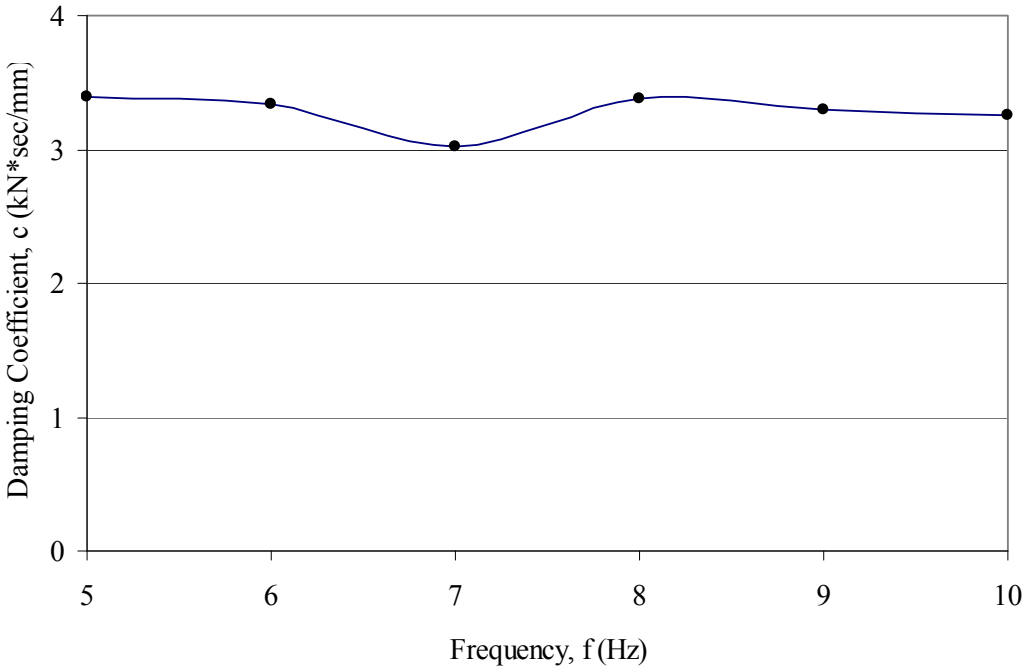

Figure 5-19 Damping coefficient versus frequency, Shake 8

6 Interpretation of Results

The following chapter relies on the analyses contained in the previous chapters. The contact force between the pile cap and the backfill will be examined to identify changes in resistance due to cyclic and dynamic loadings. By isolating losses associated with different mechanisms, the difference between the force under static loading conditions and that under cyclic and dynamic loading conditions can be calculated. The Mononobe-Okabe (M-O) equation is then used with a calibrated pseudo-static seismic coefficient expressed as a faction of peak ground acceleration (PGA) as a means of modeling or predicting cyclic and dynamic losses.

6.1 Identifying Components of Passive Contact Force

Force may be calculated from the simple relationship of stiffness and displacement. A spring with a stiffness of 100 kN/m requires 100 kN to displace the spring 1 m. If the spring was already compressed (i.e., being held in a displaced shape), the initial force causing the compression plus the additional 100 kN to displace the spring an extra meter may be added together to find the total static force. In a like manner, the theoretical pile cap-backfill static contact force is equivalent to the relative displacement amplitude of the pile cap from its initial position prior to the application of cyclic/dynamic loads multiplied by the stiffness of the backfill and then adding the

actuator force initially used to displace the pile cap prior to the application of cyclic/dynamic loads. This may be written as the following equation:

$$F = k \cdot x_{amp} + F_0 \quad \textbf{(6.1)}$$

where:

F =theoretical static force at pile cap-backfill interface

k = backfill soil stiffness

x_{amp} = pile cap displacement amplitude during dynamic loading

F_0 = initial static force at pile cap displacement interval

From this fundamental equation, a theoretical static force on the pile cap face is calculated using the displacement amplitude of the pile cap and the measured static stiffness of the backfill at that pile cap displacement interval.

6.1.1 Cyclic Effect

During cyclic loading, a linear increase in contact force was expected to occur with pile cap displacement such that a higher displacement produces a higher force at the pile cap-backfill interface. However, during cyclic loading, the contact force did not increase as the pile cap displaced further into the backfill with each cycle. The force losses may be attributed to cyclic effects. In other words, if no losses had occurred, the same displacement amplitude should produce the same contact force. As seen in Figure 6-1(a), with repeated actuator cycling, less force is being mobilized with each cycle

despite similar displacement amplitudes. To quantify this force loss caused by cyclic effects, another term was introduced into Equation 6.1. This term, as shown in Equation 6.2, is the product of the force loss per unit of residual offset (calculated in Equation 4.2) and the trendline displacements (prepared in Section 4.1.1.2.2). The following equation estimates contact force accounting for cyclic losses during dynamic loading:

$$F = k \cdot x_{amp} + \left(\frac{F_{offset}}{x_{offset}} \right)_{Total} \cdot x_{offset} + F_0 \qquad \textbf{(6.2)}$$

where:

F = theoretical static force at pile cap-backfill interface

k = backfill soil stiffness

x_{amp} = pile cap displacement amplitude

F_{offset} = force loss per unit of residual offset (a negative value)

x_{offset} = displacement trend during cyclic/dynamic loading

F_0 = initial static force at pile cap displacement interval

These parameters are shown during cyclic actuator loading conditions in Figure 6-1. In Figure 6-1(a), the initial and peak forces are referenced, as is the displacement amplitude. The displacement offset is the distance from the pile cap position corresponding with peak force to the peak displacement during any given cycle. F_{offset} displays the observed force loss associated with cyclic effects. Figure 6-1(b) and Figure 6-1(c) further illustrate the relationship that as displacement offset increases, force offset decreases.

Since force loss during the dynamic shaker loading is in part due to similar cyclic effects, Equation 6.2 can also be used to reasonably approximate cyclic losses during the dynamic shaker loading and thus approximately separate losses due to cyclic loading and losses due to other dynamic mechanisms such as out-of-phase movement of the cap and backfill. The equivalent parameters for Equation 6.2 during dynamic shaker loading are shown in Figure 6-2.

When applied throughout Shake 8 and Shake 10 (displacement intervals which were loaded dynamically first and where passive force appears to have been nearly or fully mobilized along the failure plane), Equation 6.2 produces the results displayed in Figure 6-3 and Figure 6-4, respectively. The contact force at the beginning of Shake 8 is approximately 1425 kN, and at the start of Shake 10 the initial force just above 1600 kN. At the scale shown, individual loading cycles cannot be distinguished by the maximum and minimum forces during each cycle which bound the shaded area formed by all of the load cycles. The force peaks around 7.5 Hz or 118 seconds into Shake 8. Shake 10 also reaches maximum force at 7.5 Hz. Afterward, the contact force decreases as the shaker frequency (and force) continue to ramp up. As the ramp-down of the eccentric mass shaker begins, the maximum and minimum forces during each load cycle begin to converge as the dynamic amplitude decreases, reaching an ending static force of 1092 kN for Shake 8 and 1266 kN for Shake 10.

Both Figure 6-3 and Figure 6-4 display the force decrease due to cyclic effects. The total residual offset in Shake 8 was 2.32 mm which accounted for over 333 kN of total force loss from the beginning to the end of the dynamic loading. During Shake 10, the residual offset was measured at 2.07 mm resulting in 341 kN of total force loss.

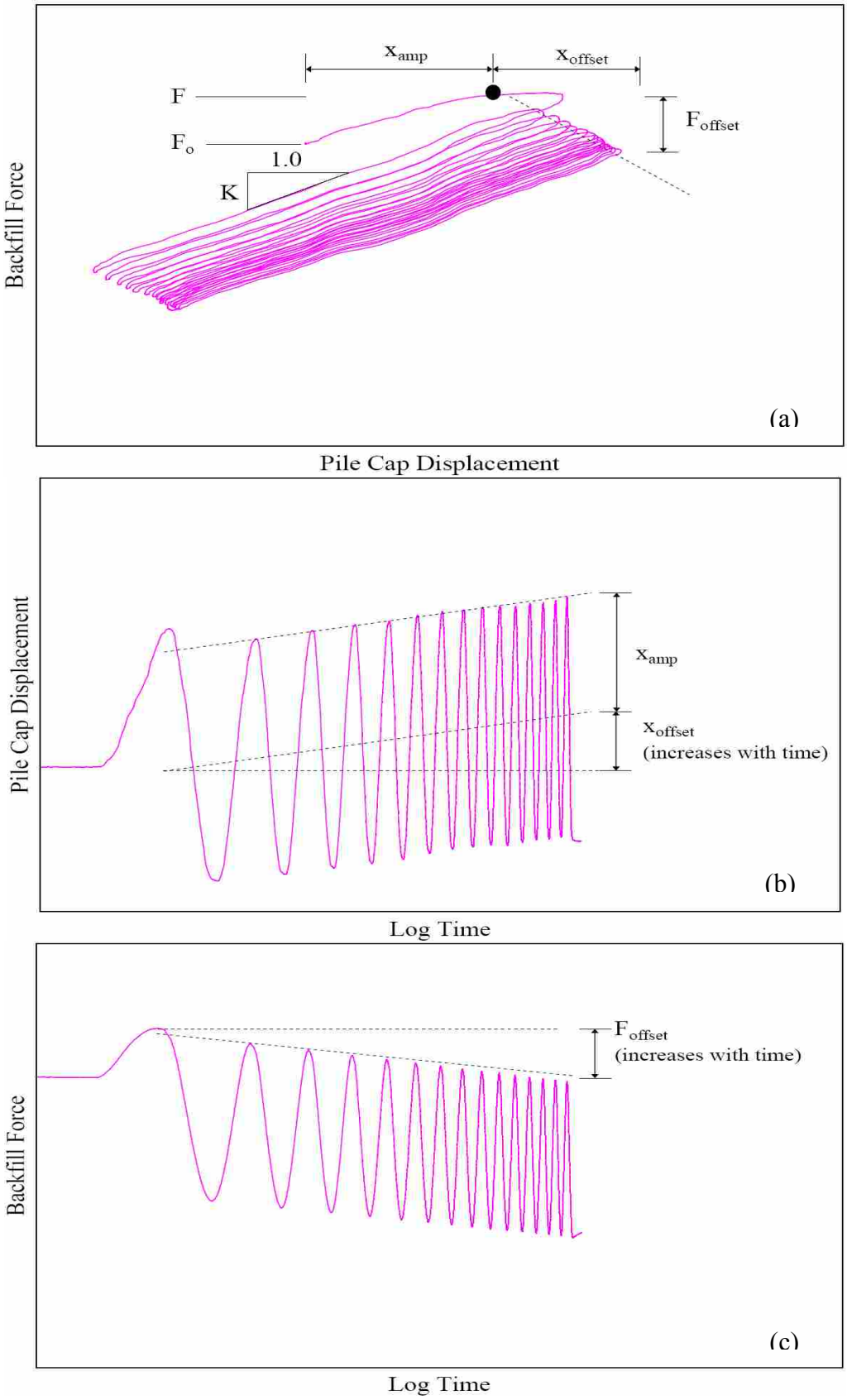

Figure 6-1 Depiction of force and displacement parameters during cyclic loading

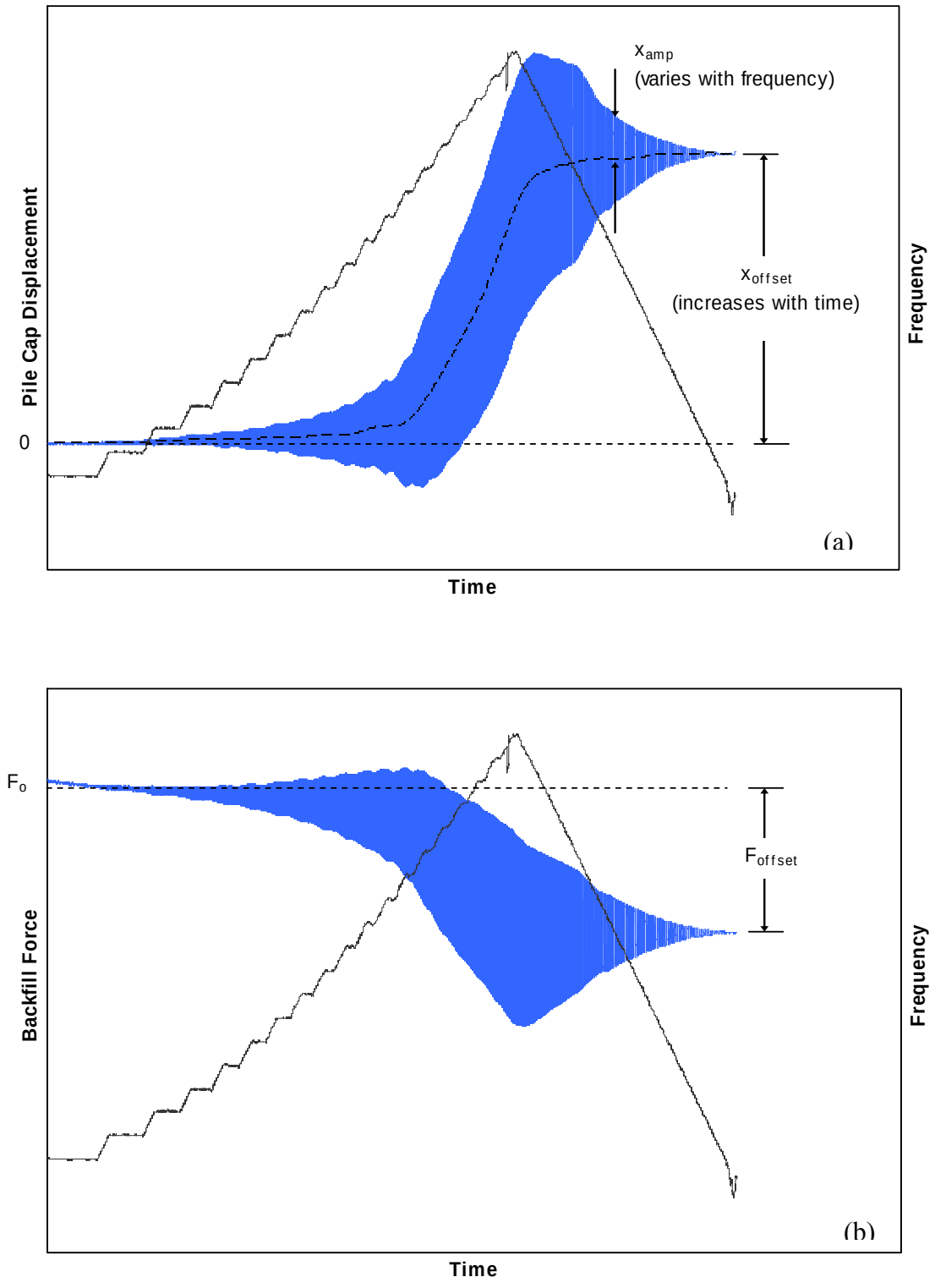

Figure 6-2 Depiction of cyclic parameters during dynamic loading

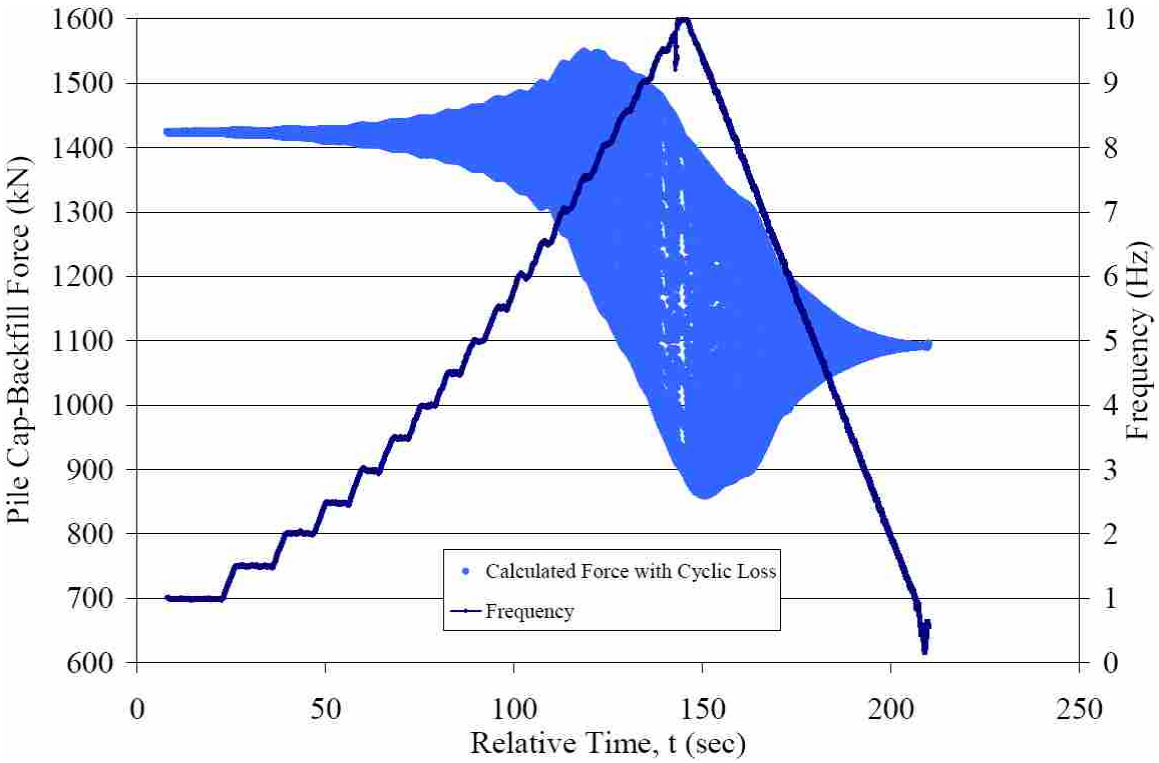

Figure 6-3 Calculated pile cap static force time history, Shake 8

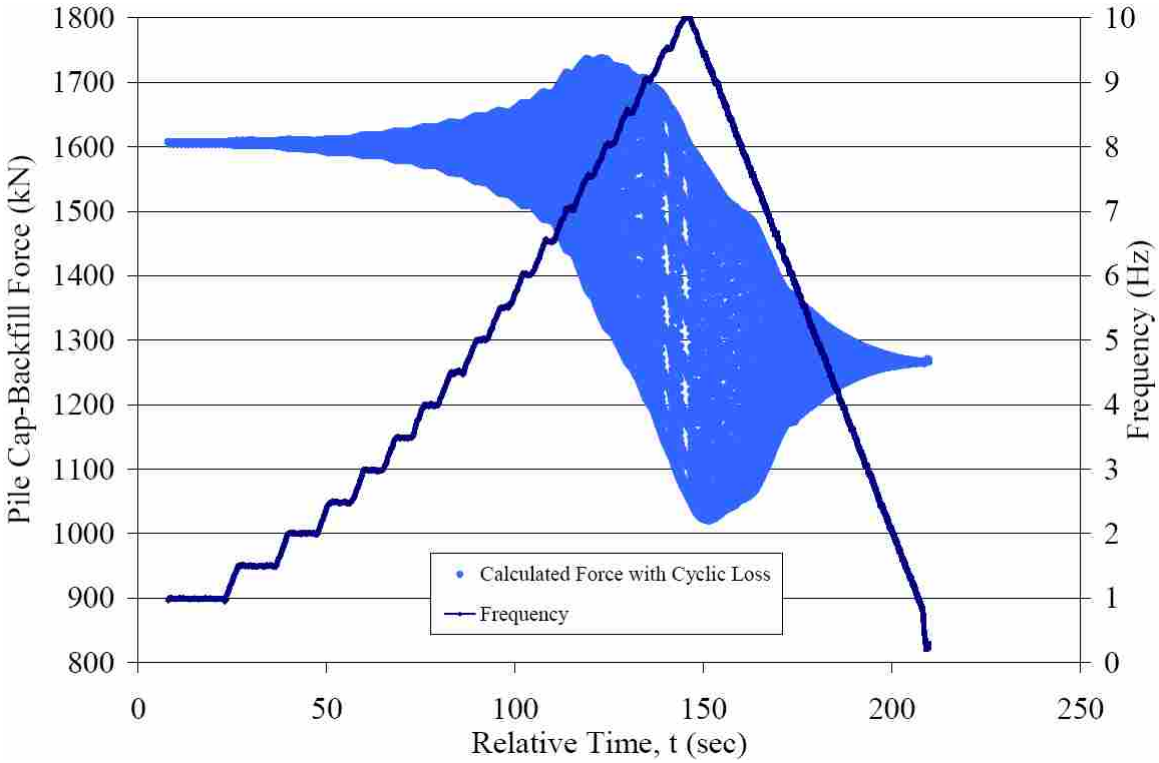

Figure 6-4 Calculated pile cap static force time history, Shake 10

6.1.2 Dynamic Effect

Dynamic effects, in addition to cyclic losses, modified the passive contact force while the shaker was in motion. In general, the results of dynamic loading lowered the maximum and raised the minimum force acting on the pile cap when compared to the contact force with only cyclic effects. Two mechanisms that caused this force alteration are additional changes in backfill stiffness throughout dynamic loading evident at higher forcing frequencies and dynamic motion (out-of-phase pile cap-backfill movement). The method of analysis for both of these mechanisms was addressed in Chapter 4 and the results during dynamic loading were introduced in Chapter 5.

Figure 6-5 and Figure 6-6 relate the calculated static forces from Equation 6.2 to actual measured contact forces. The measured forces come from pressure plate readings at peak pile cap displacements. The difference between the calculated forces with cyclic losses and the measured forces constitute force losses due to dynamic effects.

The forces calculated from Equation 6.2 closely match the measured forces until about 5 Hz. At this point, a separation begins between the calculated forces with cyclic losses and the measured forces at peak displacements. A few previous observations suggest that this gradual separation is most likely caused by reduction of backfill stiffness throughout dynamic loading. First, backfill stiffness reduction during dynamic loading began at approximately 5 Hz which is the same frequency when the separation between forces became noticeable. Likewise, stiffness reduction was gradual and consistent throughout dynamic loading which parallels the gradual separation in forces.

Around 7.5 Hz, the increasing measured force trend suddenly switches direction. At this point, measured forces quickly decrease as the dynamic load continues to

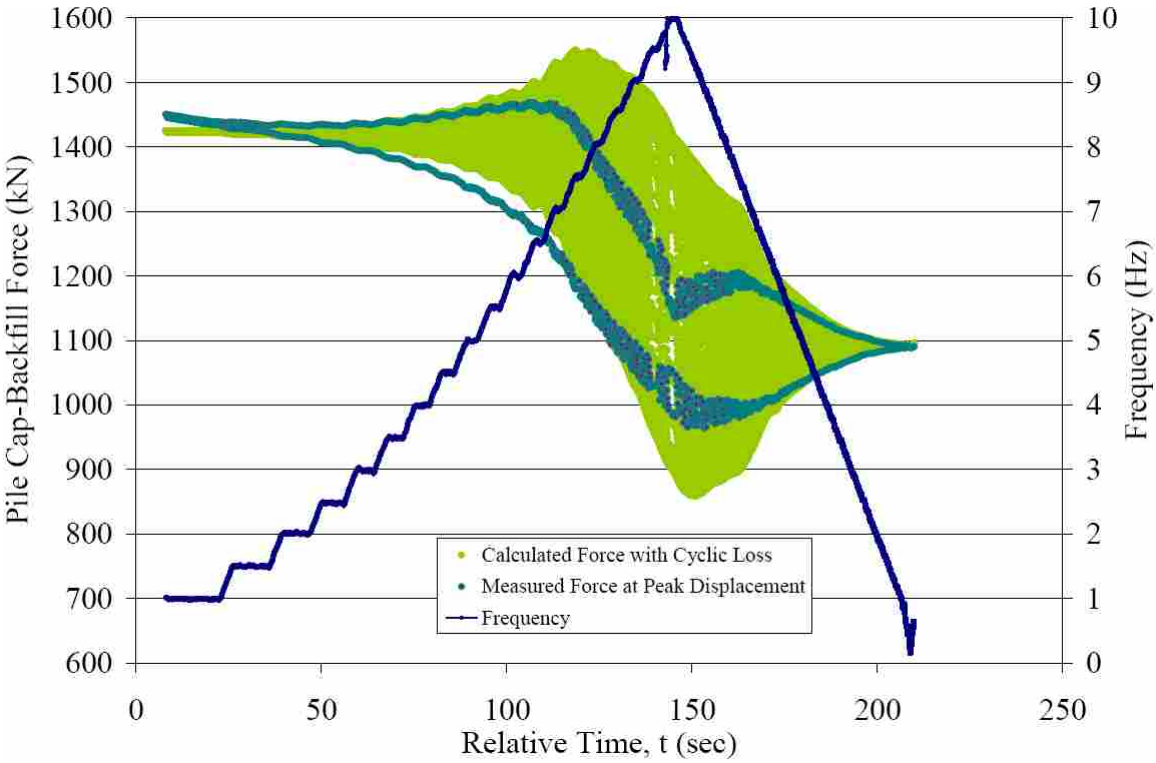

Figure 6-5 Measured dynamic force compared to calculated static force, Shake 8

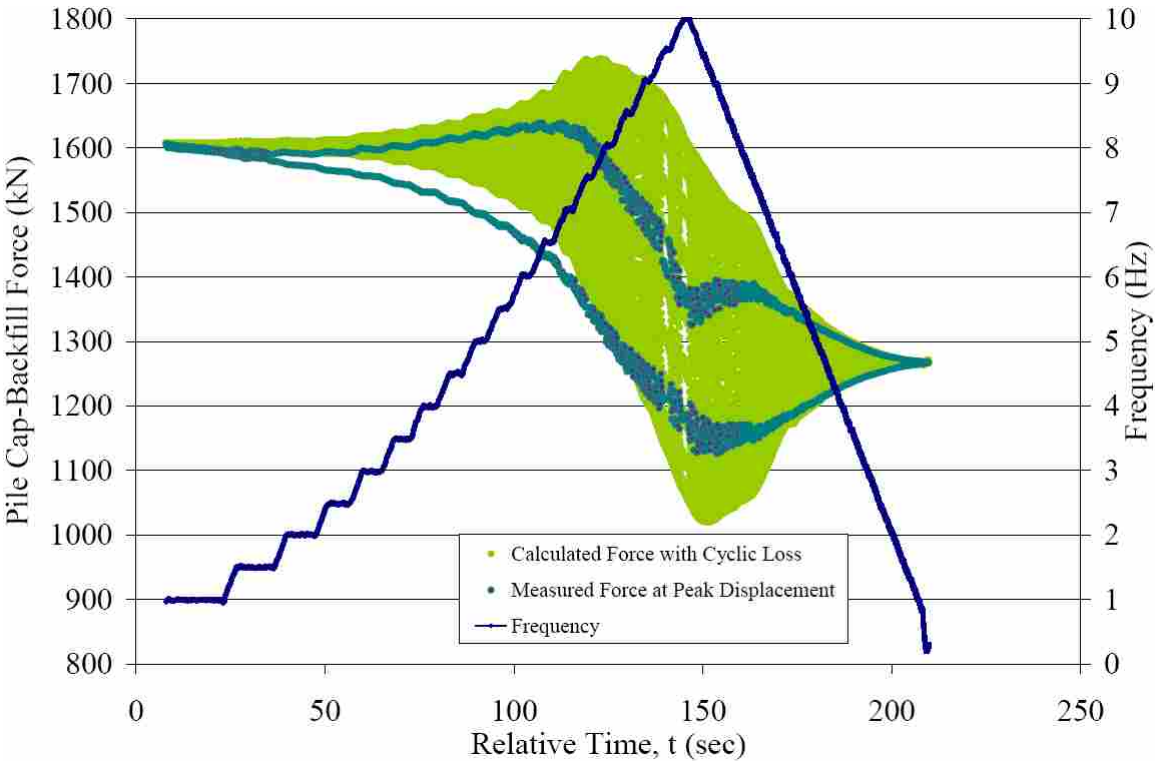

Figure 6-6 Measured dynamic force compared to calculated static force, Shake 10

ramp-up. This sudden shift in the development of passive contact force may be attributed to the dynamic effects of phase lag. Similar effects have been noted by Tokimatsu et al. (2004) in their study of large shaking table tests involving piled foundations. During cyclic loading there was a steady increase and decrease in force which matched the movement of the pile cap into the soil suggesting that the backfill was in-phase with the pile cap. At the beginning of dynamic loading, contact force developed similarly to cyclic conditions. Likewise, the pile cap and the soil were generally in-phase. However, during dynamic loading as the forcing frequency of the mass shaker increased, the soil movement began to lag behind the pile cap movement. When the frequency approached 7.5 Hz, the soil was almost completely out-of-phase with the pile cap. This is the same point that the measured contact force drastically and unexpectedly declines contrary to the calculated force with cyclic losses. As the frequency continues to ramp-up to 10 Hz the separation between the calculated force and actual force widens.

6.1.3 Damping Effect

Damping, another dynamic effect, counteracts a portion of the contact force losses outlined above. Damping, as computed in Section 5.4, increases the passive contact force acting on the pile cap face. This increase is proportional to the increase in frequency (as previously described and depicted as load-displacement loops widen). At greater frequencies, the maximum force separates from the force at maximum displacement (shown in Figure 4-25). The difference between the maximum measured force and the force at maximum displacement is force gain due to damping.

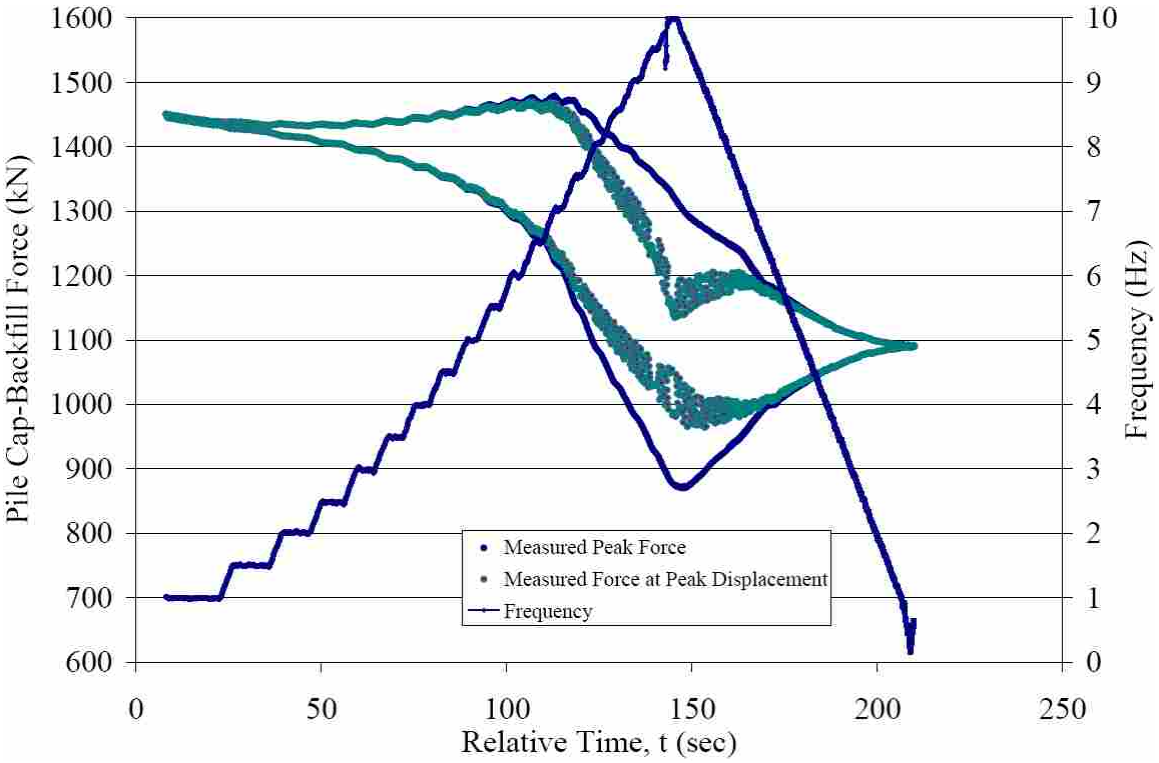

Figure 6-7 Maximum measured force compared to measured force at maximum displacement, Shake 8

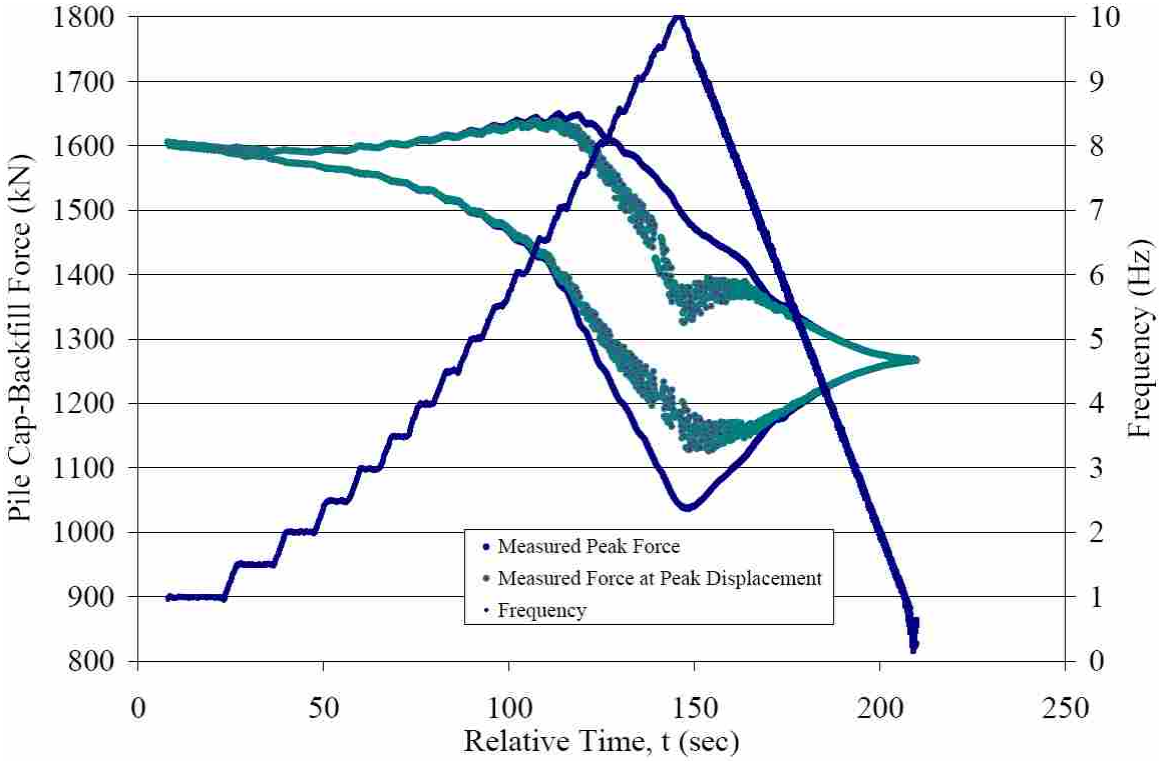

Figure 6-8 Maximum measured force compared to measured force at maximum displacement Shake 10

Figure 6-7 and Figure 6-8 show the maximum measured force and the measured force at maximum displacement for Shake 8 and Shake 10, respectively. Notice that at 10 Hz, approximately 150 seconds, the damping effect (the difference between the two force distributions) is the greatest. This aligns with the damping calculations from load-displacement loops discussed in Section 5.4. Damping is seemingly insignificant at below 7 Hz during both dynamic loading sequences.

6.1.4 Passive Force Loading Comparison

To further illustrate the changes in the pile cap force during dynamic loading, Figure 6-9 and Figure 6-10 overlay the various measured and computed forces. The theoretical static force was first calculated from Equation 6.1. Adding residual offset parameters (Equation 6.2) adjusted this static force to a reasonable estimate of the force including cyclic losses during dynamic loading. The resulting force is referred to as the boundary line because it distinguishes between the losses attributable to cyclic effects (like those observable during the cyclic actuator loading cycles, represented in the figures by Arrow A) and dynamic effects (like those observed during dynamic shaker loading cycles, above and beyond any cyclic effects, represented in the figures by Arrow B). The force measured by pressure plates at maximum displacement represents the static force minus all cyclic and dynamic losses. Also shown in the figures is a line representing the peak measured force measured by pressure plates. This force includes the added damping force; the magnitude of the damping force is represented by Arrow C.

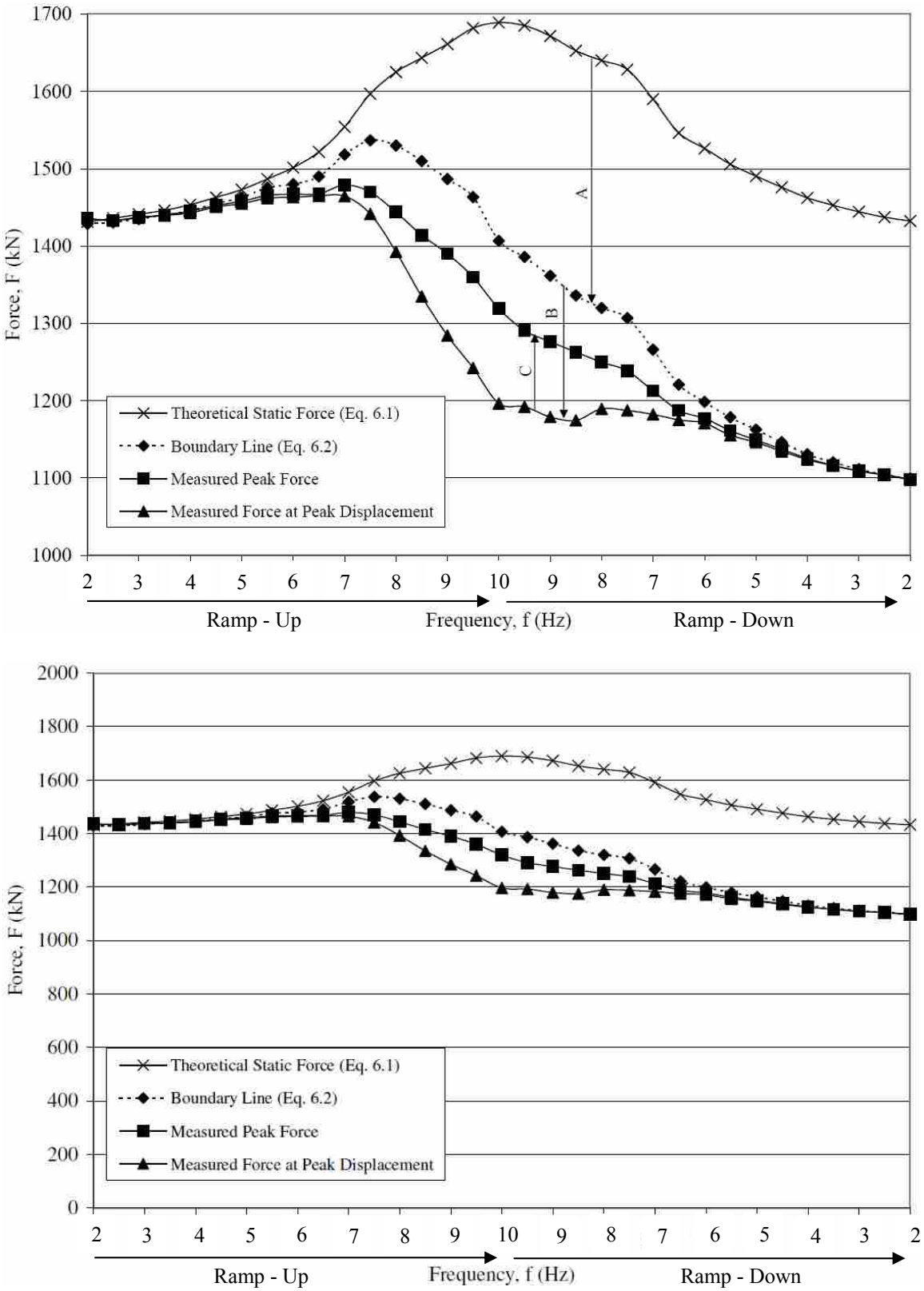

Figure 6-9 Comparison of calculated and measured passive forces on pile cap, Shake 8

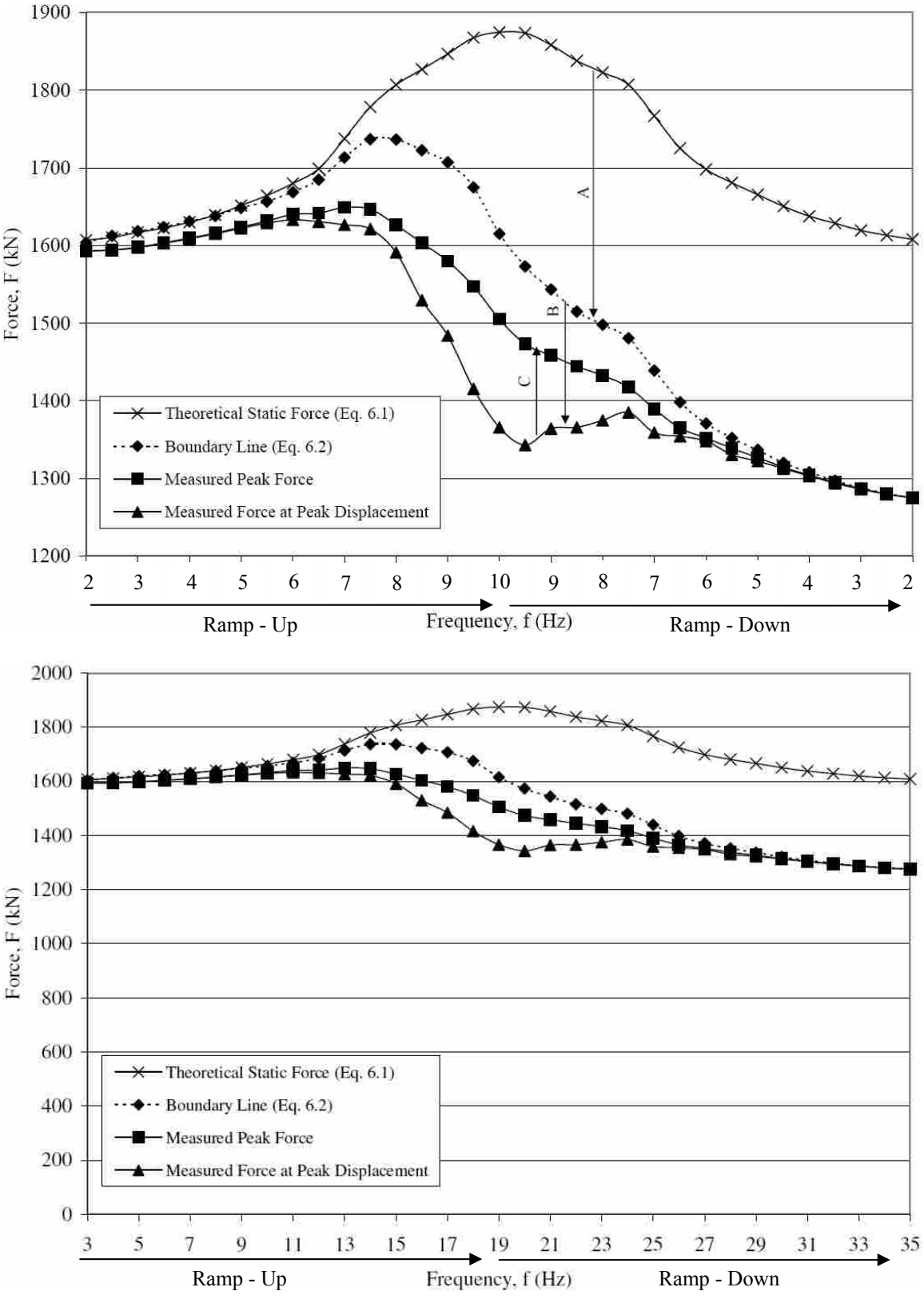

Figure 6-10 Comparison of calculated and measured passive forces on pile cap, Shake 10

For both Shake 8 and Shake 10, the effects of damping at 10 Hz raise the force approximately 10%. The figures for Shake 8 and Shake 10 are quite similar, suggesting a consistency in effects once passive earth forces are nearly or fully mobilized.

6.2 Mononobe-Okabe

The Mononobe-Okabe (M-O) equation is probably the most widely used method to determine the dynamic effects of active and passive earth pressures on a structure. Inherent to this equation are several assumptions which must be satisfied. Some of these assumptions were generally satisfied throughout the entire testing (i.e., homogenous, cohesionless backfill was used for testing). However, other M-O assumptions were only satisfied at certain points during testing. For example, the M-O equation is dependent on fully mobilizing the shear strength of the backfill which occurred after the eighth pile cap displacement interval.

The M-O equation does not explicitly account for dynamic losses due to soil stiffness reduction, phase lag, or damping. Phase lag became apparent when the frequency of the mass shaker increased and the pile cap and the backfill began to move comparatively out-of-phase. The M-O equation is a pseudo-static (or perhaps more correctly a pseudo-dynamic) equation based on static equilibrium relationships and hence does not explicitly account for damping effects which are variable with dynamic loading frequency. While the M-O equation does not explicitly account for non-integral movement between the backfill and retaining structure, backfill stiffness reduction, or damping, the M-O equation computes the lowest passive earth force between the backfill

and the structure by using an inertial force for the backfill failure wedge oriented away from the wall.

Judicial use of the M-O equation can produce accurate results which account for such mechanisms as dynamic loss or damping. One common approach in using the M-O equation is to input only a fraction of the peak ground acceleration (PGA). A value of 0.5 to 0.75 is used in the active case M-O equation, but an appropriate value for the passive case is less certain. To investigate an appropriate PGA factor or multiplier, the M-O inputs were first calibrated such that M-O calculated static forces were equivalent to the static forces calculated from Equation 6.1. Then, the PGA factor was iteratively varied until a good match between the measured forces (at both peak load and peak displacement) and calculated forces from the backfill was determined.

When comparing forces at peak displacements (these forces include dynamic losses comprising of cyclic losses and phase lag), the PGA factors that produce the best match between the M-O equation and measured forces absent any previous cyclic loading varies with frequency as shown in Figure 6-11, but they generally vary between 0.73 and 0.93. Figure 6-11 begins at 6 Hz (the frequency where dynamic effects begin to separate measured forces from estimated static forces), and the peak ground acceleration factors peak at 8.5 Hz forming a gradual crest. While the factors have been optimized to match the measured response, at low frequencies the ground and cap accelerations are quite small. Because of this, the PGA factors are quite sensitive. Even at larger frequencies such as 7.5 Hz during Shake 8, the difference between a PGA factor of 0.8 and 0.9 is slightly under 20 kN, as compared with a passive force of 1600 kN under static

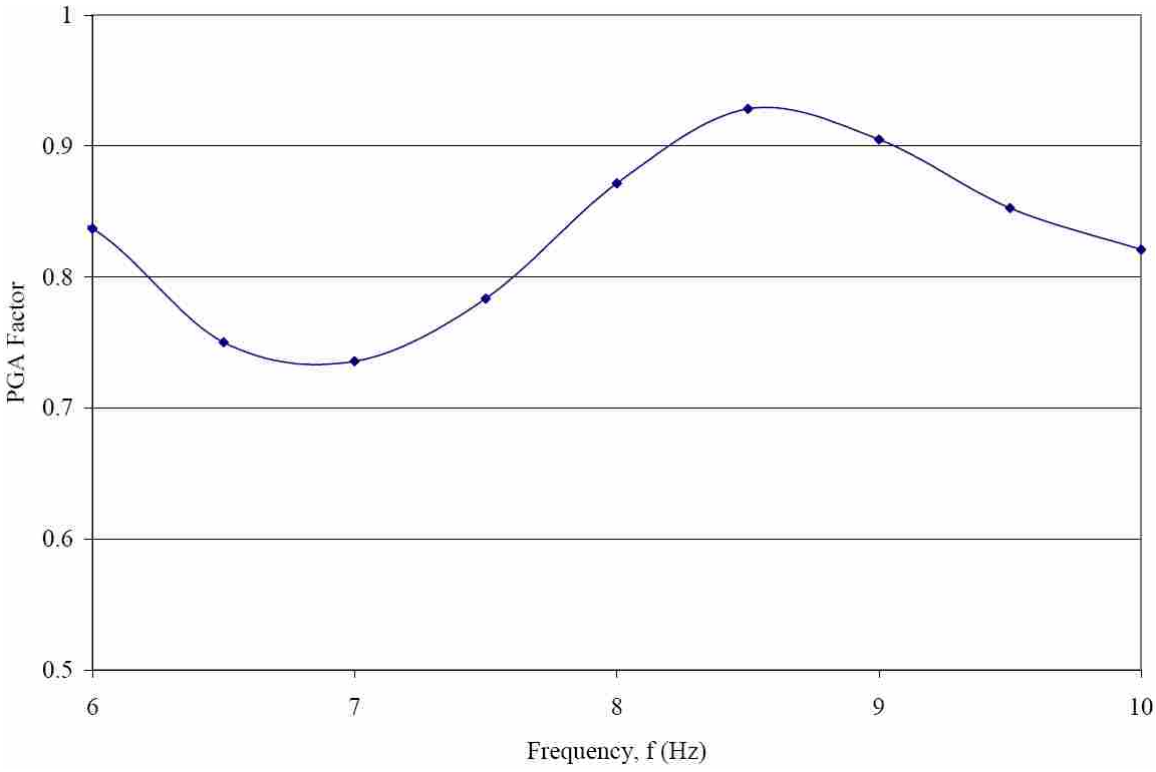

Figure 6-11 PGA factor applied to M-O equation to account for dynamic losses, Shake 8

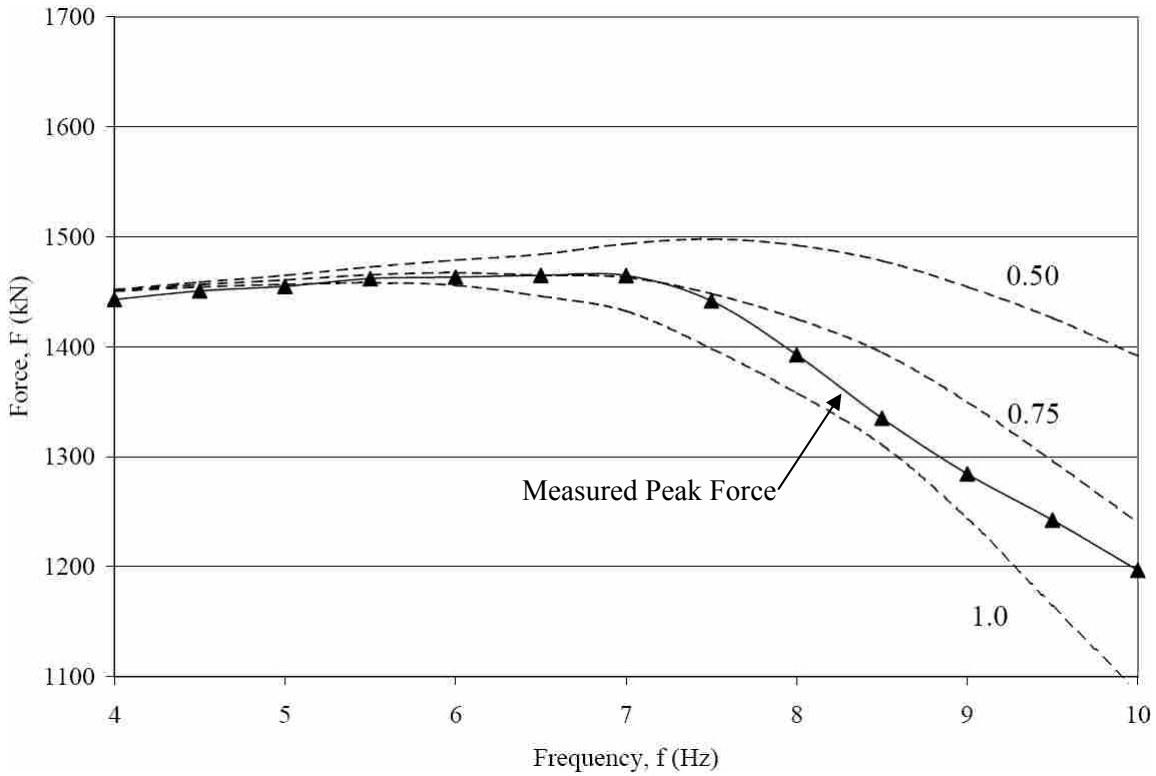

Figure 6-12 Force produced by the M-O equation with various PGA factors, Shake 8

conditions. As shown in Figure 6-12, a PGA factor of 0.84 at 6 Hz provides the best match. A factor of 0.75 to 0.9 appears to consistently provide the best overall match. The maximum PGA used in this analysis was 0.43 g, occurring at a shaker frequency of 10 Hz, while the PGA at 7.5 Hz was 0.16 g.

PGA factors for Shake 10 are displayed in Figure 6-13 for comparison purposes. At lower frequencies, the factor which produces the best match with measured force is somewhat higher than those observed in Shake 8. At higher frequencies (6.5 Hz and above), the PGA factor that produces the closest overall match to measured force is 0.8. These values are generally similar to factors produced in Shake 8. Figure 6-14 compares the measured force with forces computed using the M-O equation at various PGA factors, with values of about 0.75 providing the best match. At lower frequencies, a large difference between PGA factors does not significantly change the calculated force, as was observed previously in the data from Shake 8.

Including increases in resisting force due to damping will reduce the total dynamic losses. Therefore, the PGA factor which will model dynamic loading conditions including the effects of damping should be less than those presented above. Figure 6-15 and Figure 6-17 display the PGA factors which provide the best match to peak force for Shake 8 and Shake 10, respectively. The PGA factor generally ranges between 0.55 and 0.7 at higher forcing frequencies. The corresponding forces that are calculated by various PGA factors including the effects of damping are shown in Figure 6-16 and Figure 6-18 for Shake 8 and Shake 9, respectively. Generally, it appears that the M-O equation may be used to calculate the dynamic passive earth forces considering damping by applying a 0.55 to 0.65 multiplier to the PGA.

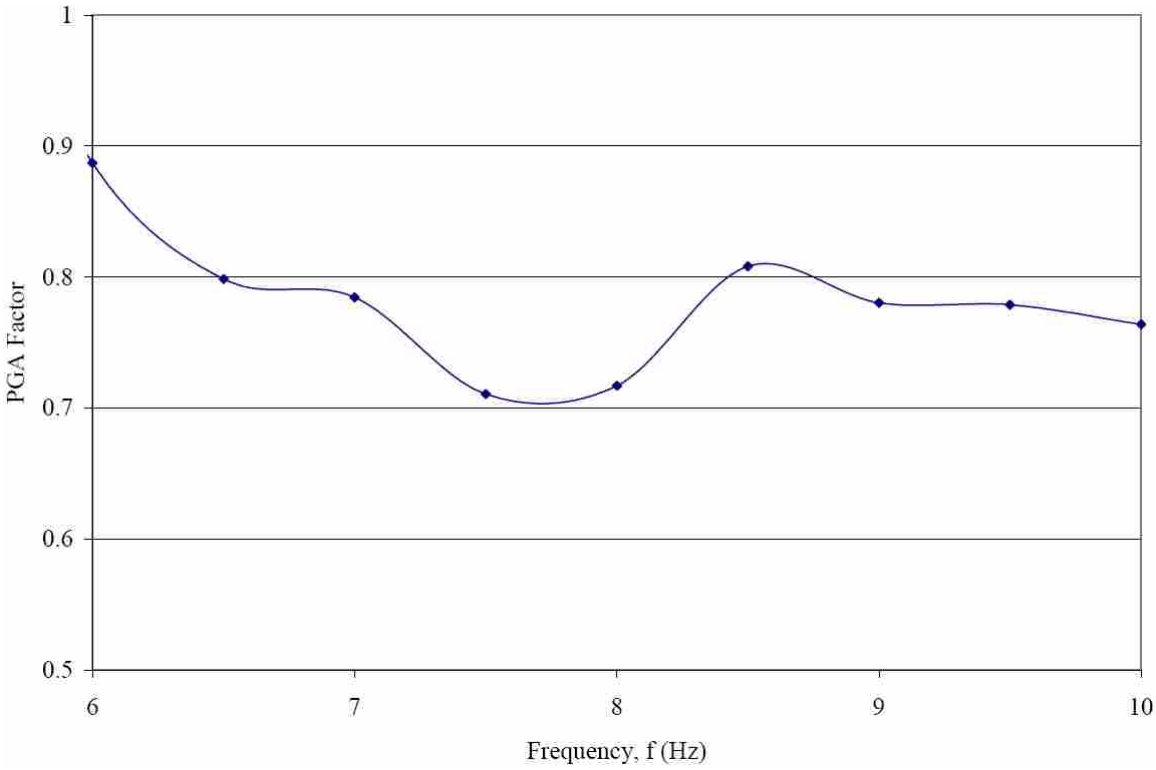

Figure 6-13 PGA factor applied to M-O equation to account for dynamic losses, Shake 10

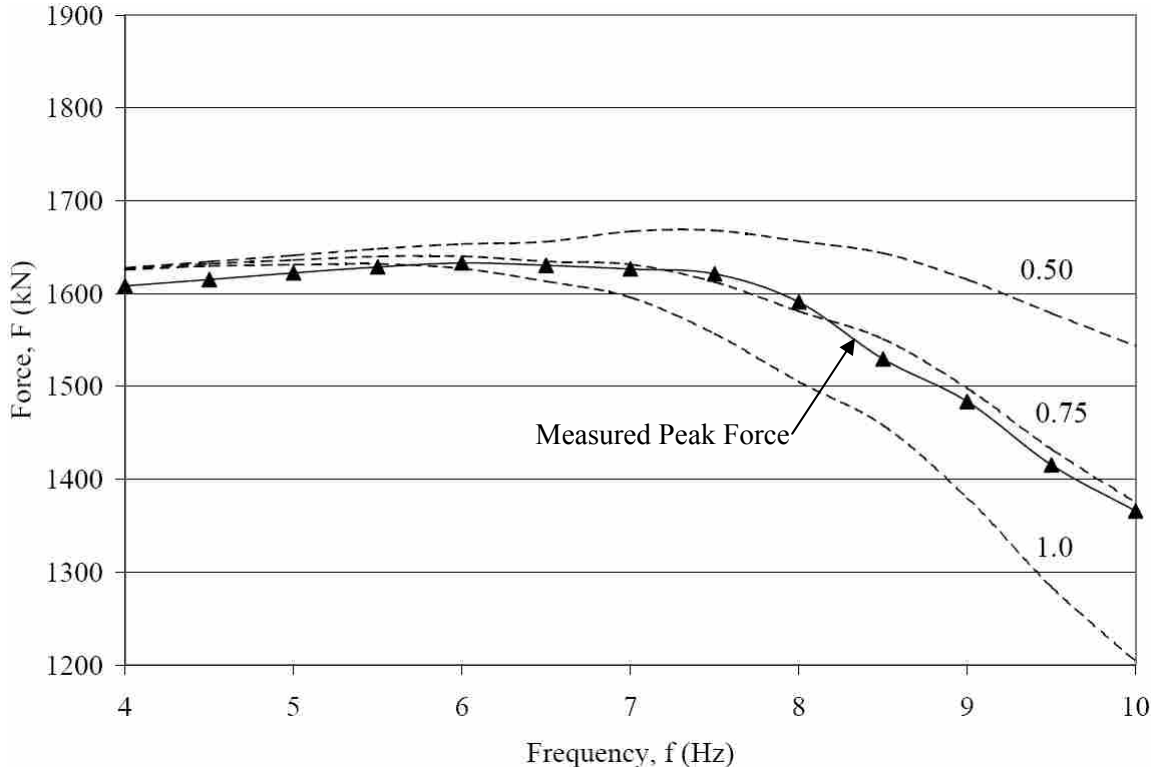

Figure 6-14 Force produced by the M-O equation with various PGA factors, Shake 10

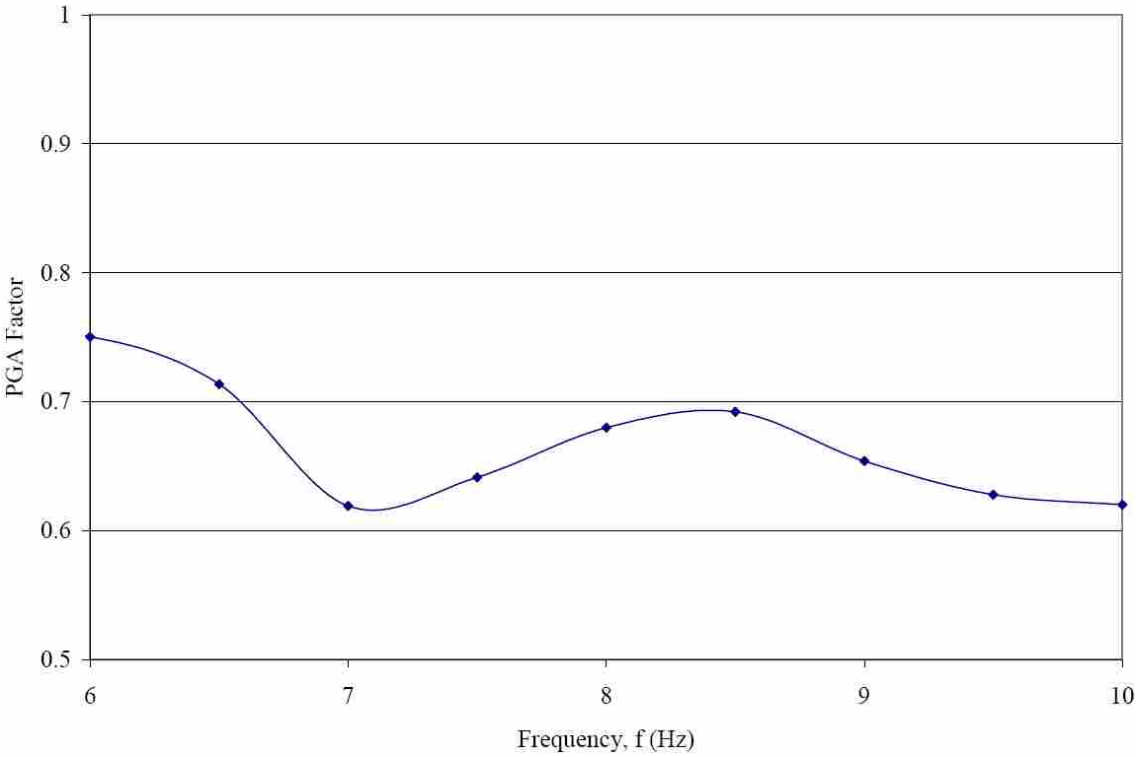

Figure 6-15 PGA factor applied to M-O equation to account for dynamic losses with damping, Shake 8

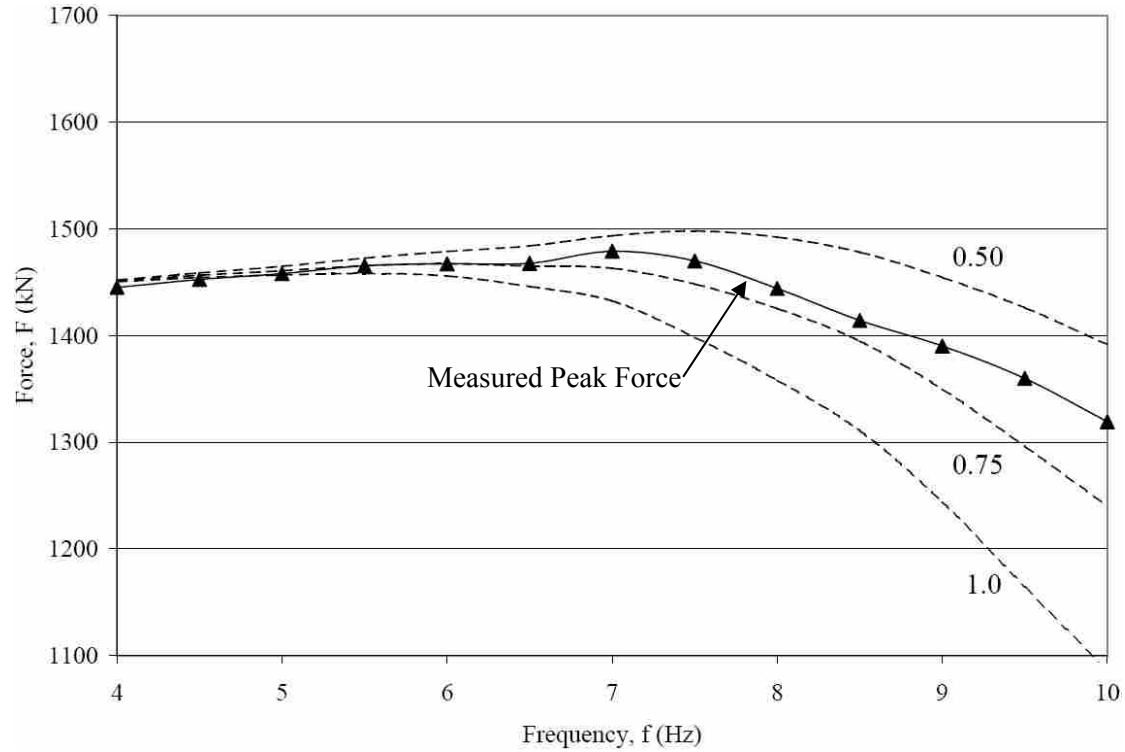

Figure 6-16 Force including damping effects produced by the M-O equation with various PGA factors, Shake 8

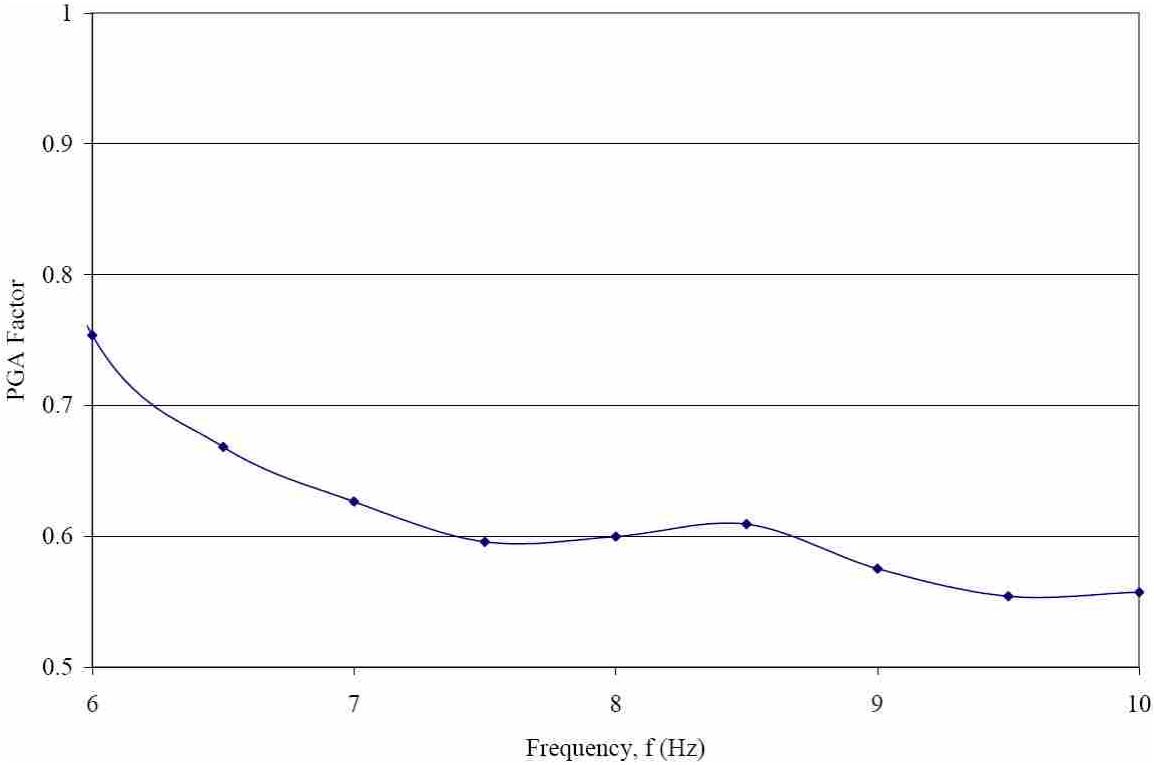

Figure 6-17 PGA factor applied to M-O equation to account for dynamic losses with damping, Shake 10

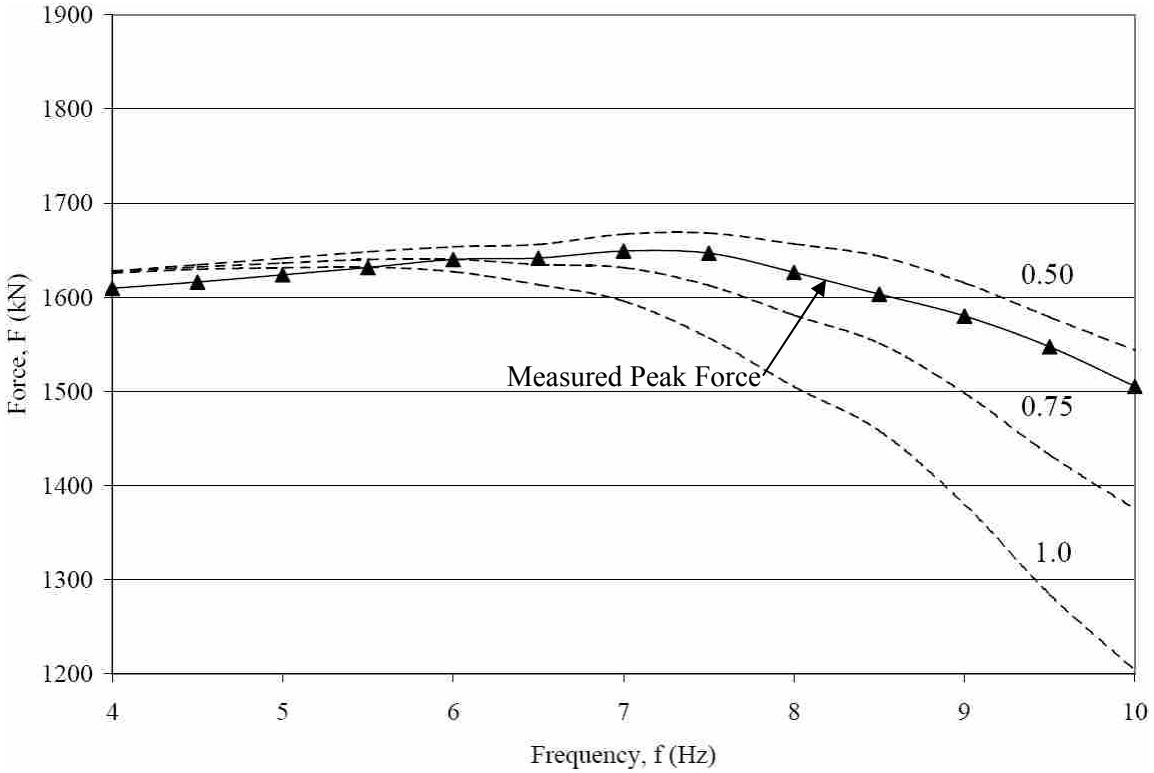

Figure 6-18 Force including damping effects produced by the M-O equation with various PGA factors, Shake 10

7 Conclusion

This thesis analyzed data derived from full scale testing of a pile cap system with a densely compacted sand backfill under static, cyclic, and dynamic loadings. This data was collected on site on May 25, 2007 as part of a larger series of testing. Particular focus has been placed on interpretation of the passive behavior of the backfill based on the soil pressures measured directly by the pressure plates. Based on this work, the following observations, conclusions, and recommendations are presented.

1. Passive earth force develops as the cap is pushed into the backfill. Under slow, cyclic loading, the observed backfill stiffness is relatively constant. Under faster, dynamic loading, the observed backfill stiffness decreases in a relatively linear fashion (with an observed rate of 50 kN/mm for every 1 Hz increase in forcing frequency above 5 Hz).
2. During cyclic and dynamic loading, the pile cap gradually develops a residual offset from its initial position. This offset is accompanied by a reduction in contact force from the backfill. Backfill which had previously experienced cyclic loading at similar displacements exhibited considerably smaller offsets during dynamic loading because of previous loading effects.
3. The pile cap and the backfill appeared to move integrally during static and cyclic loadings. However, during dynamic loading, the backfill exhibited

some out-of-phase movement relative to the pile cap. At 7.5 Hz (the natural frequency of the pile cap-backfill system) the backfill and the pile cap reached a phase angle of 180 degrees suggesting complete out-of-phase movement.

4. Observed losses in contact force were associated with both cyclic (softening due to repeated loading) and dynamic (out-of-phase movement) effects. Force losses due to dynamic loading increased with increasing frequency (which corresponded to larger displacements)
5. Losses due to dynamic loading were offset somewhat by increases in peak force due to damping. Damping effects shift the occurrence of peak force at the pile cap-backfill interface to a point before peak pile cap displacements are reached. The increase in contact force due to damping was observed to be relatively proportional to increasing frequency.
6. Passive earth forces with cyclic/dynamic losses without considering damping can be reasonably estimated using the Mononobe-Okabe (M-O) equation with a 0.75 or 0.8 multiplier applied to the peak ground acceleration (PGA). More specifically, these multipliers ranged between 0.70 and 0.93 during dynamic loadings from 6 Hz to 10 Hz.
7. Passive earth forces with cyclic/dynamic losses including the effect of backfill damping can be reasonably estimated using the Mononobe-Okabe (M-O) equation with a 0.6 multiplier applied to the peak ground acceleration (PGA).

References

Brinch Hansen, J. (1996). "Resistance of a rectangular anchor slab." *Bulletin No. 21*. Danish Geotechnical Institute, Copenhagen, 12-13.

Caltrans (2001). "Seismic design criteria version 1.2." *California Department of Transportation*, Sacramento, California.

Chandrasekaran, S. S. (2009). "Behaviour of pile groups under static, cyclic and dynamic lateral loading in clay." *PhD Dissertation*, Dept. of Civil Engineering, Indian Institute of Technology Madras, Chennai, India.

Christensen, D. S. (2006). "Full scale static lateral load test of a 9 pile group in sand." *MS Thesis*, Dept. of Civil and Environmental Engineering, Brigham Young University, Provo, Utah.

Chopra, A. K. (2001). Dynamics of structures. Upper Saddle River, Prentice Hall, New Jersey.

Cole, R. T. (2003). "Full-scale effects of passive earth pressure on the lateral resistance of pile caps." *PhD Dissertation*, Brigham Young University, Provo, Utah.

Cole, R. T. and Rollins, K. M. (2006). "Passive earth pressure mobilization during cyclic loading." *Journal of Geotechnical and Geoenvironmental Engineering*, ASCE, 132(9), 1154-1164.

Cummins, C. R. (2009). "Behavior of a full-scale pile cap with loosely and densely compacted clean sand backfill under cyclic and dynamic loadings." *MS Thesis*, Dept. of Civil and Environmental Engineering, Brigham Young University, Provo, Utah.

Douglas, D. J. and Davis, E. H. (1964). "The movements of buried footings due to moment and horizontal load and the movement of anchor plates." *Geotechnique*, London, 14(2), 115–132.

Duncan, J. M. and Mokwa, R. L. (2001). "Passive earth pressures: theories and tests." *Journal of. Geotechnical and Geoenvironmental Engineering*, ASCE, 127(3), 248-257

Geokon (2004). "Model 3500/3510 earth pressure cells." Instruction Manual, Geokon Inc.

Jacobsen, L. S. (1939). Described in Appendix D of "The Kentucky Project." Technical Report No. 13, Tennessee Valley Authority, 1951.

Kramer, S. L. (1996). Geotechnical earthquake engineering. Upper Saddle River, Prentice Hall, New Jersey.

Matsuo, H. (1941). "Experimental study on the distribution of earth pressure acting on a vertical wall during earthquakes." *Journal of the Japan Society of Civil Engineers* Japanese Society of Civil Engineers 27(2).

Mononobe, N. and Matsuo, H. (1929). "On the determination of earth pressures during earthquakes." *Proceeding*, World Engineering Congress.

NCHRP (2008). "Seismic analysis and design of retaining walls, buried structures, slopes and embankments." *Report 661*, National Cooperative Highway Research Program, 69-76.

Okabe, S. (1926). "General theory of earth pressures." *Journal of the Japan Society of Civil Engineers*, Japanese Society of Civil Engineers 12(1).

Ostadan, F. and White, W. H. (1997). "Lateral seismic soil pressure – an updated approach." *US-Japanese SSI Workshop*, Bechtel Corporation, San Francisco, California.

Ovesen, N. K. (1964). "Anchor slabs, calculation methods, and model tests." *Bulletin No. 16*, Danish Geotechnical Institute, Copenhagen, 5-39.

Peterson, K. T. (1996). "Static and dynamic lateral load testing a full-scale pile group in clay." *MS Thesis*, Dept. of Civil and Environmental Engineering, Brigham Young University, Provo, Utah.

Richards, R. J. and Elms, D. G. (1979). "Seismic behavior of gravity retaining walls." *Journal of the Geotechnical Engineering Division*, ASCE, 449-465.

Rollins, K. M., King, R., Snyder, J. E., and Johnson, S. R. (2005a). "Full-scale lateral load tests of pile groups and drilled shafts in clay." *Procs. Intl. Conf. on Soil-Structure Interaction, Calculation Methods and Engineering Practice*, Vol. 1, Ulitsky, V. M., Ed., ASV Publishers, Moscow: 287-292.

Rollins, K. M., Snyder, J. L., and Broderick, R. D. (2005b) "Static and dynamic response of a 15 pile group." *Proceedings 16th Intl. Conf. on Soil Mechanics and Geotechnical Engineering*, Rotterdam, Netherlands, 2035-2040.

Runnels, I. K. (2007). "Cyclic and dynamic full-scale testing of a pile cap with loose silty sand backfill." *MS Thesis*, Dept. of Civil and Environmental Engineering, Brigham Young University, Provo, Utah.

Seed, H. B. and Whitman, R. V. (1970). "Design of earth retaining structures for dynamic loads." *1970 Specialty Conference*, Cornell University, Ithaca, New York.

Tamura, S. and Tokimatsu, K. (2005). "Seismic earth pressure acting on embedded footing based on large-scale shaking table tests." *Seismic Performance and Simulation of Pile Foundations in Liquefied and Laterally Spreading Ground (GSP 145)*, ASCE, Davis, California.

Taylor, A. J. (2006). "Full-scale-lateral-load test of a 1.2 m diameter drilled shaft in sand." *MS Thesis*, Dept. of Civil and Environmental Engineering, Brigham Young University, Provo, Utah.

Tokimatsu, K., Suzuki, H., and Sato, M. (2004). "Influence of initial and kinematic components on pile response during earthquakes." *Procs. 11th Intl. Conf. on Soil Dynamics and Earthquake Engineering* and *3rd Intl. Conf. on Earthquake Geotechnical Engineering.* University of California, Berkeley. Doolin, D., Kammerer, A., Nogami, T., Seed, R. B., and Towhata, I., Eds. Vol. 1, 768-775.

U.S. Navy. (1986). *Foundations and Earth Structures - Design Manual 7.2*. Navy Facilities Engineering Command, Alexandria, Va.

Valentine, T. J. (2007). "Dynamic testing of a full-scale pile cap with dense silty sand backfill." *MS Thesis*, Dept. of Civil and Environmental Engineering, Brigham Young University, Provo, Utah.

Whitman, R. V. (1990). "Seismic design and behavior of gravity retaining walls." *Geotechnical Special Publication 25, Design and Performance of Earth Retaining Structures*, ASCE, 817-842.